Data-Driven Prediction for Reliable Mission-Critical Communications

Lechuga, Melisa Maria Lopez

DOI (link to publication from Publisher):
10.54337/aau473636365

Publication date:
2022

Document Version
Publisher's PDF, also known as Version of record

DATA-DRIVEN PREDICTION FOR RELIABLE MISSION-CRITICAL COMMUNICATIONS

BY
MELISA LÓPEZ LECHUGA

DISSERTATION SUBMITTED 2022

AALBORG UNIVERSITY
DENMARK

Data-Driven Prediction for Reliable Mission-Critical Communications

Ph.D. Dissertation

Melisa López Lechuga

Aalborg University
Department of Electronic Systems
Fredrik Bajers Vej 7B
DK-9220 Aalborg

Dissertation submitted:	February 2022
PhD supervisor:	Assoc. Prof. Troels Bundgaard Sørensen Aalborg University
Assistant PhD supervisors:	Prof. Preben Mogensen Aalborg University
	Dr. István Z. Kovács Nokia
	Dr. Jeroen Wigard Nokia
PhD committee:	Associate Professor Jimmy Jessen Nielsen (chairman) Aalborg University, Denmark
	Professor Sofie Pollin The Katholieke Universiteit Leuven (KU Leuven)
	Senior Mobile RAN architect Henrik Lehrmann Christiansen TDC NET
PhD Series:	Technical Faculty of IT and Design, Aalborg University
Department:	Department of Electronic Systems

ISSN (online): 2446-1628
ISBN (online): 978-87-7573-941-7

Published by:
Aalborg University Press
Kroghstræde 3
DK – 9220 Aalborg Ø
Phone: +45 99407140
aauf@forlag.aau.dk
forlag.aau.dk

Printed in Denmark by Rosendahls, 2022

Curriculum Vitae

Melisa López Lechuga

Melisa López Lechuga received her B.Sc. and M.Sc. degrees in telecommunication engineering from Universitat Politecnica de Catalunya (ETSETB-UPC, Barcelona, Spain) in 2016 and 2018, respectively. Since 2018, she pursues her PhD degree at the Electronic Systems Department from Aalborg University (Denmark) in collaboration with Nokia Bell Labs. Her research interests include radio propagation, field measurements, and cellular-based connectivity for mission-critical communications.

Abstract

5G New Radio (NR) technology is expected to provide connectivity to a wide variety of services with different Quality of Service (QoS) requirements. For some applications, Key Performance Indicators (KPIs) such as reliability, latency, or data rate may have stringent targets, which will be challenging to meet with the existing Radio Resource Management (RRM), QoS, and mobility management procedures. These procedures are mostly reactive, i.e., a service degradation is only mitigated once it has already occurred. Having some prior knowledge of the network conditions that the User Equipment (UE) will experience can help avoid a situation that may be critical for the service. Specifically, the service could benefit from a more proactive QoS management in the so-called mission-critical communications, such as Vehicle-To-Everything (V2X) or Unmanned Aerial Vehicles (UAV) using cellular networks. The need for this approach is stated by associations and groups such as the 5G Automotive Association (5GAA) or the Aerial Connectivity Joint Activity (ACJA). Both consider a context where the network can predict changes in the QoS.

A relevant parameter involved in the RRM decisions, as well as for QoS prediction, is the signal level experienced by a UE, typically expressed using the Reference Signal Received Power (RSRP). RSRP is a key metric, as it is used for several procedures such as cell selection and re-selection, or power control. Therefore, estimating the signal level is essential when designing a reliable system. Accurate estimations of the RSRP levels that the UE will experience along the path could provide in-advance information on the expected service availability and reliability conditions. This thesis studies the use of RSRP estimations to predict potential critical areas along the known moving path of a UE using a mission-critical service. The use of ray-tracing or empirical models versus a measurement-based approach for RSRP estimation is analyzed. The Ph.D. project answers research questions such as: How accurate can signal strength be estimated using measurement data? Can measurement data reported by UEs that have previously passed through the same location be used to estimate the signal level that a UE will experience in that same location? Can that estimation be corrected using UE context in-

formation? Can the RSRP estimations be used to predict the expected critical areas along the route? These questions are investigated for the V2X and UAV use cases.

Firstly, a new approach for estimating the serving signal level that a UE will observe along the route is studied. We analyze the achievable accuracy of a data-driven estimation method, consisting of the aggregation of the measurements recorded by multiple UEs in a certain location. The estimation is location-based, i.e., the measurements are aggregated regardless of the cell that is serving the user, such that the estimation is valid for any UE passing through that location. Secondly, we evaluate the accuracy provided by a ray-tracing tool and two empirical models when estimating the signal variations that the user will experience along the route. For that purpose, the estimations are compared to experimental data. The study is done for ground-level and UAV measurement data. Therefore, multiple drive tests and UAV field measurements have been performed during this Ph.D. in urban and rural environments in Denmark. Results show that the data-driven approach improves the estimation error over the traditional techniques studied. This work also investigates how the estimation error can be further reduced by predicting the mean individual offset that each specific UE will observe with respect to the initially estimated value once the UE starts moving along the path. The different results observed for ground compared to airborne predictions are also discussed. Lastly, the work includes an evaluation of how to use the RSRP estimations to calculate the probability that there is a service outage in terms of service availability and reliability. Results show that the data-driven estimation approach allows detecting at least 70 % of the existing critical areas.

Resumé

5G New Radio (NR) teknologien forventes at kunne skabe forbindelse til en lang række services med forskellige krav til Quality of Service (QoS). For visse applikationer er der udfordrende krav til performance indikatorer (KPI'er) såsom pålidelighed, forsinkelse eller datarate, og som derfor bliver en udfordring at imødekomme med de eksisterende procedurer til håndtering af radioresourcer (RRM), QoS, og mobilitet. Disse procedurer er for det meste reaktive, dvs. en serviceforringelse kan først afbødes efter, at den har fundet sted. Et forudgående kendskab til hvilke netværksforhold en terminal (UE) vil komme ud for, kan hjælpe med at undgå en ellers kritisk situation for den benyttede service. Specielt services kategoriseret som missionskritisk kommunikation, eksempelvis Vehicle-To-Everything (V2X) eller Unmanned Aerial Vehicles (UAV) via cellulære netværk, kunne drage fordel af en mere proaktiv QoS håndtering. Behovet for denne tilgang er dokumenteret af sammenslutninger og arbejdsgrupper såsom 5G Automotive Association (5GAA) og Aerial Connectivity Joint Activity (ACJA) der begge tager udgangspunkt i en kontekst, hvor netværket kan forudsige ændringer i QoS.

En relevant parameter, som har betydning for radioresourcehåndtering, såvel som for prædiktion af QoS, er signalniveauet ved terminalen - typisk udtrykt ved Reference Signal Received Power (RSRP). RSRP er en væsentlig performance indikator, da den bliver brugt i mange radiorelaterede procedurer såsom valg og skift af radiocelle, eller justering af sendeeffekten. Det er derfor vigtigt at estimere signalniveauet, når man vil designe et pålideligt system. Præcise estimeringer af RSRP-niveauer, som terminalen oplever langs en given rute, kan give forhåndsinformation om service-tilgængelighed og pålidelighed. Denne afhandling har fokus på brugen af RSRP-estimeringer, til at forudsige eventuelle kritiske områder i brugen af en missionskritisk service, når terminalen bevæger sig langs en given kendt rute. Brugen af ray-tracing (RT) eller empiriske modeller, versus en målebaseret tilgang til estimering af RSRP, analyseres i afhandlingen. Ph.D. projektet besvarer videnskabelige spørgsmål som: Hvor nøjagtigt kan man estimere signalstyrke ved brug af måledata? Kan måledata rapporteret af terminaler, som tidligere har passeret igennem samme lokation, bruges til at estimere det signalniveau,

som en terminal vil opleve i denne samme lokation? Kan denne estimering korrigeres ved at bruge kontekstinformation? Kan RSRP estimeringerne bruges til at forudsige de forventede kritiske områder langs ruten? Disse spørgsmål undersøges for både V2X og UAV brugsscenarier.

Først undersøges en ny tilgang for estimering af det signalniveau, som en terminal observerer langs ruten. Vi analyserer den opnåelige nøjagtighed af en data-drevet estimeringsmetode, som består af en aggregering af målinger fra flere terminaler på en bestemt lokation. Estimeringen er lokationsspecifik, dvs. målingerne aggregeres uden hensyn til den radiocelle, som servicerer brugeren, således at estimeringen er gyldig for en hvilken som helst terminal, der passerer den bestemte lokation. Dernæst evaluerer vi nøjagtigheden af RT og to udvalgte empiriske modeller til estimering af de signalvariationer som terminalen oplever langs ruten, i en sammenligning med eksperimentelle data. Undersøgelsen er udført med eksperimentelle data for V2X og UAV scenarier som er indsamlet gennem adskillige felteksperimenter under kørsel langs vej og flyvning i lav højde i by- og landområder. Resultaterne viser, at den data-drevne tilgang forbedrer estimeringsfejlen i sammenligning med de undersøgte traditionelle teknikker. Afhandlingen undersøger også, hvordan estimeringsfejlene kan reduceres yderligere når terminalen er startet på ruten, ved at prædiktere det terminalspecifikke offset som hver terminal vil opleve i forhold til det overordnede og initialt estimerede signalniveau. Afvigelsen mellem resultater for V2X og UAV scenariet diskuteres i afhandlingen. Endelig indeholder afhandlingen også en evaluering af, hvordan man benytter RSRP estimeringer til at beregne sandsynligheden for, at der et serviceudfald mht. service-tilgængelighed og pålidelighed. Resultater viser, at man ved den data-drevne estimering kan detektere mindst 70 % af de eksisterende kritiske områder.

Contents

Glossary

1G 1st Generation

2G 2nd Generation

3G 3rd Generation

3GPP 3rd Generation Partnership Project

4G 4th Generation

5G 5th Generation

5GAA 5G Automotive Association

ACJA Aerial Connectivity Joint Activity

BLER Block Error Rate

BS Base Station

BVLOS Beyond Visual Line-of-Sight

C2 Command and Control

DL Downlink

DPM Dominant Path Model

eMBB Enhanced Mobile Broadband

FN False Negative

FNR False Negative Rate

FP False Positive

FPR False Positive Rate

GNSS Global Navigation Satellite System

GPS Global Positioning System

GRU Gated Recurrent Unit

HO Handover

IMT-2020 International Mobile Telecommunications for 2020 and beyond

IRT Intelligent Ray Tracing

ITU International Telecommunications Union

KPI Key Performance Indicators

LOS Line-Of-Sight

LSTM Long Short Memory Term

LTE Long Term Evolution

MAE Mean Absolute Error

mcMTC Mission-critical Machine Type Communications

MCS Modulation and Coding Scheme

MDT Minimization of Drive Tests

MIO Mean Individual Offset

ML Machine Learning

mMTC Massive Machine Type Communications

mmW Millimiter Wave

MNOs Mobile Network Operators

MTC Machine Type Communications

NLOS Non-Line-Of-Sight

NN Neural Networks

NR New Radio

NWDAF Network Data Analytics Function

PCI Physical Cell ID

QoS Quality of Service

RAN Radio Access Network

REM Radio Environment Maps

RLF Radio Link Failure

RMSE Root Mean Square Error

RRM Radio Resource Management

RSRP Reference Signal Received Power

RSRQ Reference Signal Received Quality

RSSI Received Signal Strength Indicator

SF Shadow Fading

SIR Signal-To-Interference-Plus-Noise Ratio

SIR Signal-To-Interference Ratio

SNR Signal-To-Noise Ratio

SON Self-Organizing Networks

SS Signal Strength

TN True Negative

TNR True Negative Rate

TP True Positive

TPR True Positive Rate

UAV Unmanned Aerial Vehicles

UE User Equipment

UL Uplink

URLLC Ultra-Reliable Low-Latency Communications

V2I Vehicle-To-Infrastructure

V2N Vehicle-To-Network

V2P Vehicle-To-Pedestrian

V2V Vehicle-To-Vehicle

V2X Vehicle-To-Everything

Thesis Details

Thesis Title:	Quality of Service Enhancements for Reliable Communications for Aerial and Terrestrial Vehicles using Cellular Networks
Ph.D. Student:	Melisa López
Supervisors:	Prof. Troels Bundgaard Sørensen, Aalborg University
Co-supervisors:	Prof. Preben Mogensen, Aalborg University István Z. Kovács, Nokia Jeroen Wigard, Nokia

This PhD thesis is the outcome of three years of research at the Wireless Communication Networks (WCN) section (Department of Electronic Systems, Aalborg University, Denmark) in collaboration with Nokia (Aalborg). The work was carried out in parallel with mandatory courses required to obtain the PhD degree. The papers supporting the work presented in the thesis were published in peer-reviewed journals and conferences.

The main body of the thesis consists of the following articles:

Paper A: M. López, T. B. Sørensen, I. Z. Kovács, J. Wigard and P. Mogensen, "Experimental Evaluation of Data-driven Signal Level Estimation in Cellular Networks", *IEEE 94th Vehicular Technology Conference (VTC2021-Fall)*, September 2021.

Paper B: M. López, T. B. Sørensen, I. Z. Kovács, J. Wigard and P. Mogensen, "Measurement-Based Outage Probability Estimation for Mission-Critical Services," *IEEE Access*, vol. 9, pp. 169395-169408, 2021.

Paper C: M. López, T. B. Sørensen, P. Mogensen, J. Wigard and I. Z. Kovács, "Shadow fading spatial correlation analysis for aerial vehicles: Ray tracing vs. measurements", *IEEE 90th Vehicular Technology Conference (VTC2019-Fall)*, September 2019.

Paper D: M. López, T. B. Sørensen, J. Wigard, I. Z. Kovács and P. Mogensen, "Service Outage Estimation for Unmanned Aerial Vehicles: A Measurement-Based Approach", *IEEE Wireless Commu-*

nications and Networking Conference (WCNC) 2022, **Accepted for publication**.

This thesis has been submitted for assessment in partial fulfilment of the PhD Degree. The thesis is based on the submitted or published papers that are listed above. Parts of the papers are used directly or indirectly in the extended summary of the thesis. As part of the assessment, co-author statements have been made available to the Doctoral School of Engineering and Science at AAU and also to the assessment committee.

Acknowledgements

This thesis is the outcome of more than three years of work that I could not have done alone, so I take this opportunity to thank all the people that have helped me through it.

First, I would like to thank my supervisors for their support and guidance during these years. Having four supervisors was not always easy, but each contributed in his way. I thank Troels B. Sørensen for thoroughly reviewing all my papers and this thesis, which helped produce high-quality material. Jeroen Wigard for always having the right words and helping me build a business point of view for my project; István Z. Kovács for his endless support, knowledge, and good advice; and Preben Mogensen for his critical point of view that always helped me find my way during the project.

I would like to give a special mention to my non-official advisor, Ignacio Rodríguez. Your technical and personal coaching, and the beers in my terrace, have always come at the right time and lifted me up in the low moments. I also thank all my colleagues in AAU and Nokia for providing a friendly working environment and good technical discussions. Special thanks to the international alliance, the funny not-so-technical discussions, the Friday breakfasts, and the multiple lunch breaks talking about everything and nothing at the same time. Also, thanks to Dorthe Sparre for efficiently solving all my questions with a nice smile.

On the personal side, I should thank many people—Majken and Dani, for the sushi and wine nights and for always having my back. Roberto, for encouraging me to pursue this Ph.D. and supporting me in the bad moments. Elisa, for the walks, the ice-creams, the honest conversations, and your contagious joy. Mundo, for all the efforts made to understand what this meant to me and helping me believe in myself, this achievement is partly yours.

I cannot forget my international friends. Living abroad is never easy, but I always managed to find the right people to make Aalborg feel like home (despite the weather). Many of them are still in Denmark, and many others left, but they all contributed to making my time here lovely and enjoyable. Special thanks to María, Mădă, Lisha, Emilio, Marta, David, Pilar, Filipa, and Joăo for all the fun, the trips, the nights out, the board games, the volleyball,

and the endless amount of activities and plans that made all these years much better. Thank you to my friends in Mallorca and Barcelona for supporting me in the distance and constantly reminding me that the sun is always shining even if you cannot see it! A special shout out to Thomas, who never quit sending bad jokes to make my days slightly better.

I would not have made it through this Ph.D. without Enric. Thank you for the insane amount of steps (figurative and literally) that led us where we are today. For acting as my left hemisphere whenever I needed it and letting my right one take over yours every once in a while. For always being my home and my balance. You have been a friend and a partner during the past 12 years and have not disappointed me even once. I love you and your terrible sense of humor.

Last, I would like to thank my family for the unconditional support they have given me in every step I have taken in my life and for making me feel them close even in the distance. Special thanks to my siblings for their annoying way of telling me that I am "the smart one". And to my parents. You two have always given me everything I needed to get where I wanted to be. You all are the best family I could ask for, and I will always be thankful for that.

Melisa López
Aalborg University, February, 2022.

Part I

Thesis Summary

Chapter 1

Introduction

Wireless communications has become essential in our personal and professional lives and currently plays a crucial role in the global economy and development. It was initially designed for human-centric communication purposes: from voice services in the 1st Generation (1G) to data services with increasing data rates in the 2nd Generation (2G), 3rd Generation (3G) and 4th Generation (4G). The rapid advance of technology has motivated the need to support new applications, and cellular communications is the main candidate. The 5th Generation (5G) NR is expected to serve the new emerging use cases which, according to the International Telecommunications Union (ITU) International Mobile Telecommunications for 2020 and beyond (IMT-2020), are grouped in three different categories [1]:

- **Enhanced Mobile Broadband (eMBB):** Includes all the services focusing on human-centric communication. The demand for multi-media content, data, and voice services has only increased over the years. This 5G use case focuses on providing higher data rates, improved performance, and seamless user experience.
- **Ultra-Reliable Low-Latency Communications (URLLC):** Also known as Mission-critical Machine Type Communications (mcMTC) [2], this 5G use case is characterized by the high reliability, low latency, and high availability requirements of the services involved.
- **Massive Machine Type Communications (mMTC):** This use case refers to services with a large number of devices such as sensors or actuators that typically transmit small amounts of non-sensitive data, are low cost, and have low power consumption.

Examples of the three 5G categories can be seen in Fig. 1.1: from voice and data services with increased data rates to smart cities, remote surgery, augmented reality, connected vehicles, drones, and many other applications.

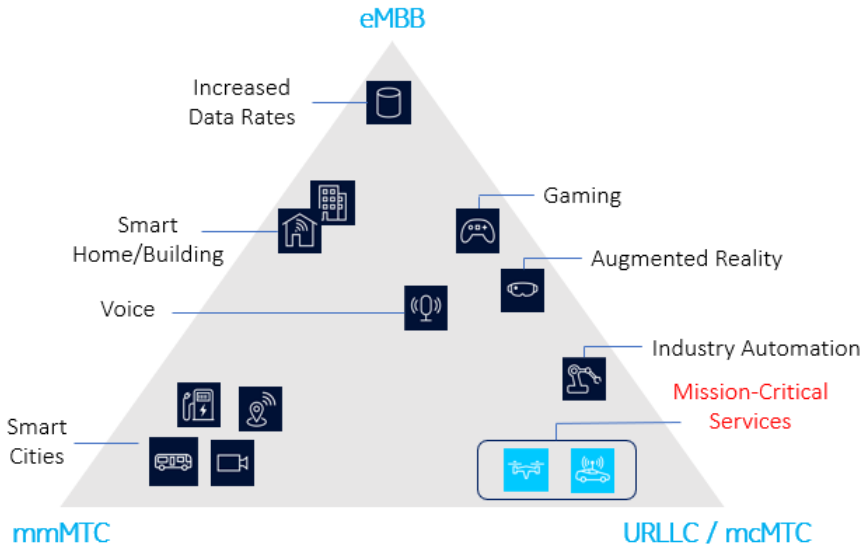

Fig. 1.1: Usage scenarios of IMT-2020 [1].

Manufacturing companies and standard organizations have invested their resources in developing the different cellular telecommunications technologies and have jointly formed the 3rd Generation Partnership Project (3GPP), which provides system description and specifications for each technology and their multiple scenarios and use cases. The following section includes the description, main challenges, and requirements for the specific use cases studied in this thesis.

1 Mission-Critical Communications

The definition of mission-critical communications can be broad, but it all comes down to the same main requirement: high reliability. Seamless and reliable connectivity is essential since a failure may pose a risk to human life [3]. This type of communication was initially meant to provide communication between emergency services such as police, ambulances, or firefighters. Nowadays, the term can apply to many other industries and applications among the increasing number of use cases in the 5G NR. Examples such as remote surgery, real-time automation, connected vehicles, or autonomous robotics, where a communication failure can have severe consequences, show the need for robust and reliable communication at any time.

Within the 5G categories, mission-critical communications is enclosed in the mcMTC, which entails new and completely different needs that were

not a concern in conventional (handheld) communications. Mainly, mission-critical applications are characterized by three requirements:

- **High-reliability:** different definitions can be found in the 3GPP specifications depending on the context. For network layer packer transmissions, it is defined as the percentage of successfully delivered packets within the time constraint required by the target service [4]. For PHY/MAC layer transmissions, it is often evaluated using the Block Error Rate (BLER) i.e., the ratio of failed packets to the total number of transmitted packets [5].
- **High-availability:** as described in [6], availability is the probability that the network can provide service. In [7], the authors claim that it could also be included within the definition of reliability since it indicates the probability of establishing a safe communication link.
- **Low- and Ultra-low latency:** latency typically refers to the time elapsed from the generation of a data packet in the transmitter until it is correctly decoded at the receiver. 3GPP distinguishes between user plane latency, control plane latency [4] and end-to-end latency [8].
- **Scalability:** as explained in [9], the network should be able to dynamically adjust its resources to the number of devices per coverage area and their different service requirements.

The requirements may vary depending on the use case and the service the network aims to provide. There are very stringent use cases such as remote surgery with latency below 1 ms and a BLER of 10^{-9} [10], and use cases with more relaxed requirements such as automation with latency requirement of maximum 100 ms and a 10^{-1} BLER [11]. The constant growth in demand for mcMTC has motivated Mobile Network Operators (MNOs), standardization bodies, and academic researchers to investigate potential solutions to meet these requirements.

This thesis contributes towards the fulfillment of the mission-critical communication requirements, focusing on two use cases: V2X and UAVs. The solutions proposed in Chapter 3 contribute to ensure service availability and service reliability in the studied scenarios. The following sub-sections provide definitions, requirements, and challenges, of the V2X and UAV[1] use cases. A review of potential solutions available in the state-of-the-art is also included.

[1] Also termed Uncrewed Aerial Vehicles or drones.

1.1 Vehicle-To-Everything

Vehicular communications has been considered a key use case within the 5G emerging services [12]. The general V2X term includes Vehicle-To-Infrastructure (V2I), Vehicle-To-Network (V2N), Vehicle-To-Pedestrian (V2P), and Vehicle-To-Vehicle (V2V) communications. Examples of these are self-driving cars, collision avoidance, vehicle traffic optimization, speed regulation, pedestrian safety notifications, or communication with V2X application services [13]. These are safety-critical applications and, therefore, will all have very stringent QoS requirements [14]. In this sub-section, we present the main requirements and challenges and review the recent literature addressing them. The key QoS requirements for the V2X use case and related service applications are [15]:

1. **Support of high radio dynamics.** Not only the UE will be moving at relatively high speeds, but also the surrounding environment will be variant, and the objects around may be in motion. Considering also the spatio-temporal changes in the wireless network, the different Key Performance Indicators (KPI) experienced by the UE will fluctuate rapidly. These fluctuations may implicitly lead to worse QoS performance [16].

2. **Extremely low-latency.** This requirement is meant for cases such as collision avoidance, pedestrian safety notifications, and other situational awareness examples, which are time-critical. End-to-end latency requirements as low as 3 ms are observed for some applications.

3. **High capacity.** The massive number of connected vehicles and the required signaling will lead to a high volume of messages. Among others, efficient resource allocation is required.

4. **High reliability and availability.** These are required especially for safety-critical applications, where reliability and availability of the communication link need to be ensured before and during the service.

5. **Extremely high security and privacy.** There is a need for data and privacy protection since there will be broadcast messages from vehicle to vehicle or from vehicle to network containing the vehicle's speed, location, or other relevant information that can be used to harm the vehicle or the service.

A common assumption for V2X service studies is that the UE's route is known or can be predicted before the service starts, since vehicles can usually provide information on their starting location and final destination. Some studies aim at optimizing the route based on the expected radio conditions. An example is [17], the authors present a real-time route planning model considering the information collected by the network.

Furthermore, as stated by the 5GAA in [18], the service would strongly benefit from predicting the expected changes in QoS. In-advance awareness of potential QoS degradation allows the network to counteract before the degradation occurs, adapting to future conditions and reducing or avoiding completely its consequences.

QoS prediction can be performed at different entities of the communication link:

- **Network-based QoS prediction:** provide predicted QoS notifications based on real-time KPIs available on the network side. The network KPIs are typically averaged over a certain period and therefore cannot observe the rapid fluctuations mentioned above. An example is presented in [19], where the authors discuss the use of machine learning techniques to predict the performance of the network where UE data is not available.

- **UE-based QoS prediction:** The prediction is performed at the UE side and uses real-time KPIs. An example can be seen in [20], where the authors use RSRP and Reference Signal Received Quality (RSRQ) samples available at the UE to perform data rate prediction.

- **Combined approach:** using real-time UE information combined with network data to perform QoS predictions [21].

Relevant prediction-related contributions can be found in the available literature for cellular V2X communications. The authors of [22] propose a statistical learning framework for predicting QoS in V2X. The presented framework combines the prediction of channel model characteristics using contextual information with a statistical learning model to predict QoS. A qualitative performance assessment is included using an example with simulation data. A similar scheme is proposed in [16], where the authors analyze the necessary functions to predict QoS for a certain time horizon using real-time measurements.

Since mobility is one of the main reasons for service degradation due to the Handover (HO) procedure, there are several publications in the literature aiming at predicting HO and mobility-related parameters. An example is [23], where the authors combine a vector auto-regression model and a Gated Recurrent Unit (GRU) to predict user trajectory and use the results to optimize the HO procedure and reduce signaling. Their proposed algorithm reduces HO processing costs by 57 % and transmission costs by 28 %. The authors of [24] propose two prediction schemes for HO prediction based on channel features. They evaluate the performance using simulation data in different scenarios, showing that the proposed schemes reduce the number of unnecessary HOs. Both schemes outperform the existing ones. The first

achieves a prediction success of 99 % using Received Signal Strength Indicator (RSSI) values of all surrounding Base Station (BS)s, and the second shows the same success rate by using Signal-To-Noise Ratio (SNR), RSSI, available bandwidth and UE data rate.

Due to the latency-critical applications, latency is considered a relevant KPI for prediction. In [25], they propose a prediction framework combining Machine Learning (ML) and statistical approaches that uses RSRP, RSRQ, and past latency samples to predict latency. They use measurement data from different locations in an urban environment to show that the proposed approach can reduce the estimation error and the corresponding standard deviation by 45 % and 25 %, respectively, compared to other approaches. The authors of [21] also predict latency inputting measurement data from an urban scenario to a Neural Networks (NN). They propose a classification prediction based on a threshold, and use expected end-to-end delay, speed, Signal-To-Interference-Plus-Noise Ratio (SIR), RSRP, and RSSI to predict whether latency will be below or above the threshold. They show that their approach achieves f1-scores (the harmonic mean of precision and recall [26]) of up to 88%, which they considered insufficient accuracy for safety-related applications.

Those applications in which a minimum throughput is required will benefit from throughput prediction, as it will allow to detect potential service degradation. In [27], the authors show throughput prediction using a random forest algorithm. As inputs, they use UE category and cell frequency band, physical layer radio measurements collected at the UE (RSRP, RSRQ, and RSSI), context information (indoor/outdoor conditions, distance UE-BS, UE speed), and Radio Access Network (RAN) measurements (average cell throughput, BLER, and others). For performance evaluation, they use the median absolute error ratio, which is defined as the absolute value of the difference between the predicted and the actual throughput, divided by the actual throughput. Their algorithm reaches a median absolute error ratio of 0.1. The work presented in [28] uses simulation data to evaluate the use of Long Short Memory Term (LSTM) networks to predict uplink throughput for a time window of 7 s. They input network-related parameters and QoS metrics (location, speed, distance to serving cell, cell load percentage, and observed uplink throughput at time t) to the LSTM network, and obtain an overall Root Mean Square Error (RMSE) of 2.5 Mbps, and 3.5 Mbps at the 7th second.

Other KPIs have been investigated for prediction, depending on the service requirements that the authors are targeting to meet. The authors in [29] conduct a study to predict cellular bandwidth using past throughput samples and lower layer information from real-time experimental data, and propose an ML framework that provides accurate predictions. With a time granularity of 1 s, they show an average prediction error in the range of 3.9% to 19%

in all the studied scenarios (stationary and highway drive test). The work in [30] studies the performance of deep NNs to predict packet loss using V2X throughput as input. Their work is based on simulation data and the proposed model provides accurate results, with RMSE values between 0.02 and 0.5.

The above-presented studies show the wide variety of KPIs that can be predicted to improve the QoS experienced by a user. There are different prediction methods, many of them based on ML, and the accuracy varies depending on the predicted parameter and the approach used. The vast available state of the art shows the need for predictive algorithms for V2X services using cellular networks, where simulated data is commonly used for performance evaluation. In addition, many of them use signal strength as an input to the prediction algorithm, which evidences the relevance of that parameter for QoS prediction. This will be further developed in subsection 1.3, where the importance of RSRP and the benefits of its prediction for mission-critical use cases are motivated.

1.2 Unmanned Aerial Vehicles

The UAV market has experienced a rapid expansion in recent years. New applications such as infrastructure monitoring and inspection, entertainment industry, delivery of goods, or search and rescue motivated the need to provide safe and reliable communication between the UAV and its controller [31]. Establishing a reliable Command and Control (C2) link is essential for the operation of UAVs through cellular networks Beyond Visual Line-of-Sight (BVLOS) since it carries flight-related information that needs to be exchanged between the drone and its controller [32]. We consider as relevant safety-critical applications those where the drone is remotely controlled over cellular networks using the C2 link.

Different requirements are introduced by 3GPP in [33], depending on the service. For the C2 link, data rates up to 100 kb/s and packet error lower than 0.1 % within 50 ms latency are required. For the data link, requirements will depend on the use case, with data rate requirements of up to 50 Mb/s.

The propagation conditions experienced by a UAV will show key differences with respect to the ones observed by a ground user. The main challenges to be considered when addressing the problem of cellular networks for UAV communication can be summarized as follows:

- **Radio visibility conditions:** while ground users typically suffer from obstructions in the propagation path (especially in urban environments) due to the presence of buildings and nearby objects, UAVs experience dominant Line-Of-Sight (LOS) conditions. For flight altitudes near the clutter height, UAVs observe obstructed LOS conditions, with higher

LOS probabilities than in the ground since the signal may interact with, e.g., the roofs of the buildings (LOS probability is not 100 %). For flight altitudes above clutter height, drones experience LOS conditions, where minimal fading is expected since there are no objects in the transmission path [34].

- **Interference:** due to the good propagation conditions observed in the air, the number of visible cells is higher than in the ground. In addition, cellular networks are optimized for ground coverage, with down-tilted BS antennas, which will sometimes cause UAVs to observe strong signal strength from the side lobe of far BSs. This will turn into increased interference, especially in uplink [35], [36].

- **Mobility:** this challenge was also observed in the V2X scenario. However, UAVs show generally higher mobility and degrees of freedom than vehicles. While vehicle mobility can be assumed two-dimensional and following predictable paths (road segments), drone mobility models need to account for the height dimension (3D) [37].

Based on the presented challenges and requirements, there are several studies in the literature focusing on providing a reliable C2 link. According to the ACJA, knowledge of the expected radio conditions and link quality is required before, and during the flight [38]. They propose a two-phase framework: a planning phase and a flight phase. The planning phase assumes the existence of flight corridors and flight path planning for UAV services. The planned flight path's expected coverage should be evaluated in the planning phase, which could be done using coverage maps, propagation models, or other approaches that provide signal level estimations. During the flight phase, the required KPIs for safe operation should be monitored, and real-time data used to predict and react against possible service quality degradation.

The usefulness of predictive mechanisms discussed in the previous subsection also applies for UAVs. There are already some studies addressing prediction-based solutions to provide a reliable UAV communication over cellular networks. Considering the challenges described above and that most of the services have requirements in terms of latency, availability, and reliability, much of the literature focuses on interference mitigation, mobility and RRM management, and channel prediction. Many of them use ML to predict relevant parameters, as pointed out by the authors of [39].

In [40], the authors propose a deep reinforcement learning algorithm that minimizes the interference that UAVs connected to cellular networks cause on ground UEs. The approach allows each UAV connected to the network to decide on the traveled path, transmission power level, and cell association

vector. Using simulation data, they show that the presented method reduces the latency experienced by the UAVs and increases the rate per ground UE.

The authors of [41] address the mobility challenges. They propose a new handover method to support reliable connectivity. Using deep learning, they design a dynamic algorithm that optimizes handover decisions for UAVs. The algorithm is tested using simulation data and shows to reduce the number of handovers at the cost of a slight decrease in signal strength. The UEs report measurement information accordingly to the configuration provided by the RAN. The reporting can be done periodically or event-triggered, as later explained in Chapter 2.

In [42], the authors propose a two-stage online (on-the-fly) framework to predict the achievable Downlink (DL) throughput. They design a recurrent NN architecture where they input past throughput samples along with their corresponding geographic location. Numerical results using simulation data show that their proposed framework outperforms the existing approaches.

The authors of [43] present a ML approach to predict the radio signal strength in urban environments. They propose the combination of measurement data and a 3D map of the area to predict RSRP and use convolutional NNs to learn the relationship between them. The algorithm is tested using data generated by a ray-tracing tool in a simulated urban environment. Results show an average absolute error of 11 dB for a randomly generated trajectory. In [44], they evaluate the performance of random forest and k-nearest neighbors algorithm for path loss prediction of air-to-ground Millimiter Wave (mmW) channels. They use UAV coordinates and altitude, propagation distance, number of buildings within the transmission path, the average height of buildings in the transmission path, percentage of buildings in the square area, and elevation angle as inputs to the algorithm. They evaluate the accuracy of the proposed method by comparing the predictions to data generated using a ray-tracing tool. The proposed method shows an RMSE as low as 1.6 dB. The authors of [45] use artificial NNs to predict the received Signal Strength (SS) experienced by a UAV connected to a cellular network. They input location and elevation from UAV and serving cell, building height, and antenna height to the NN. Their proposed algorithm provides an RMSE of 3 dB for pure LOS conditions.

The available literature shows, also for UAVs, the need for predicting radio metrics and the benefits that it would bring to service reliability. Gathering measurement data is challenging for the UAV case due to flight regulations. Therefore, many of the available studies in the literature use simulation data or ray-tracing generated data. Different radio metrics are chosen for estimation since, depending on the service requirements, it may be more convenient to predict, e.g., throughput than latency. The most commonly estimated radio metric in the available literature is signal strength or path loss since it is essential to evaluate the feasibility of the usage of cellular net-

works to serve drones. The following subsection motivates the importance of RSRP estimation, including some state-of-the-art that supports the presented arguments.

1.3 The need for RSRP Estimation

There are several relevant radio metrics in a cellular network, but the most fundamental is RSRP due to its use for basic procedures. 3GPP defines RSRP, referred to as signal strength or signal level, as the linear average over the power contributions (in W) of the resource elements that carry cell-specific reference signals within the measurement frequency bandwidth measured at and by the UE [46]. It indicates the signal strength perceived by a UE from a certain cell, and it is used for procedures such as cell selection and re-selection, handover, and power control.

The estimation of signal level has been widely investigated as it is key for coverage estimation and network planning. There are traditional methods for signal strength estimation, such as empirical models or ray-tracing, that operators often use to plan and optimize their networks. However, there could be other uses of RSRP estimations that can contribute to improving the QoS experienced by the UEs. An efficient and seamless HO procedure and a proper transmission power management are necessary for optimal operation of the RAN. Experiencing low signal levels due to a lack of coverage or inefficient mobility management can lead to low experienced QoS [21]. Therefore, accurate prediction of RSRP help prevent potential drops in the experienced QoS of a UE.

Since RSRP represents the average cell power, it mainly depends on the users' location, its environment, and corresponding distance to the serving cell [47]. It is not affected by network load or interference. Therefore, one would expect that the RSRP value observed in a particular location is stable in that sense, and it can provide estimations with low time variability.

The authors in [48] use measurement data to study the temporal behaviour of RSRP, RSRQ and throughput in static conditions. While RSRQ and throughput show different values depending on the time of the day due to cell load, noise, and interference variation, RSRP shows long periods of stability. Using static measurements over fifty-six days, they show that RSRP standard deviation gets as low as 0.1 dB with occasional jumps of approximately 1 dB. They explain that these and other RSRP variations are related to rainy days (with wet surfaces reflections) and claim that they can also be due to changes in the environment.

In [49], the authors evaluate signal strength fluctuations at a particular location for vehicular scenarios. They characterize variations for a single user in static periods and a dual-system (two vehicles) in motion in different environments (roads, towns, and cities). For the static periods, they show

fluctuations of up to 2.5 dB in the same location, which they attribute to near environment changes (vehicles or pedestrians moving around the measurement location). The dual-system shows higher variability, with a standard deviation higher than 6 dB for all scenarios.

The RSRP value observed at a certain location is stable compared to other radio metrics, which are impacted by factors such as cell load or interference. On a smaller scale, the received signal strength shows fluctuations due to other effects such as interactions with the environment and the error introduced by the receiver processing (analogue RF and digital baseband). This will be explained in detail in Chapter 2.

2 Objectives of the Thesis

The state-of-the-art presented in the previous section suggests the potential of cellular networks to provide safe communications for mission-critical services. Predictive mechanisms are promising to contribute in meeting the service-specific requirements. This thesis studies the use of RSRP estimation to improve service availability and reliability for autonomous cars and drones connected to cellular networks. The aim is to propose and evaluate a proactive solution that prevents service degradation for these use cases, targeting in-advance detection of what we refer to as *critical areas*. We consider critical areas those locations where the probability of not meeting the requirements for the service under evaluation is high. Using the example scenario shown in Fig. 1.2, the main objective is that the network is aware of which are the critical areas in the route (P_1 to P_4) that a UE moving from source (S) to destination (D) will experience. In-advance detection of these areas would allow, e.g., for more proactive mobility, QoS, and RRM.

Considering the RSRP relevance presented in the previous section, this thesis targets to investigate how to exploit the RSRP measurements that the UEs report to the network for service availability and reliability prediction. The study is performed in scenarios with different propagation conditions such as urban/rural or ground/air.

The presented estimation approach is adapted to the two-stage framework proposed by 5GAA and ACJA. The work is done under the assumption that, in the studied scenarios, it is common to know the possible routes of the UE before the critical service starts, which allows for evaluation of the expected service availability and reliability. This evaluation can only be done in what we refer to as the *pre-service* stage, where we aim to assess the expected availability and reliability in the route before the UE starts the mission-critical service. In this stage, we aim to provide an estimation that is valid for any UE at any time in that location, choosing the appropriate radio metric for that purpose.

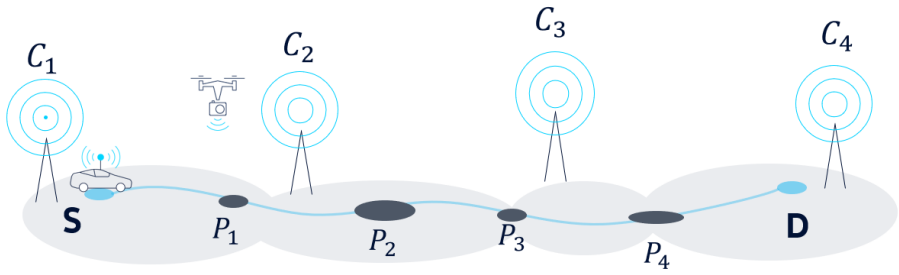

Fig. 1.2: Example of scenario under study. A UE moving along a specific route is able to detect in advance potential critical areas (service degradation points: $P_i, i = 1, ..., 4$).

Mission-critical services will have built-in safety mechanisms for cases where the communication fails. However, it is important to notice that for the network to rely on the signal level estimations, they should have high accuracy requirements since the wrong decision in the mission-critical use case can lead to service degradation. Therefore, we aim to improve the accuracy of the estimations by using UE real-time measurements. Once the UE has started moving along the route, i.e., is using the service, we aim to find a method that corrects the estimation based on UE-specific real-time data. We refer to this as the *on-service* stage, where the estimation is corrected based on the UE and time-specific conditions.

These objectives were used to establish the following hypothesis (H) and research questions (Q), which have been addressed during the Ph.D. study:

H1 UE measurement reports allow for accurate estimation. The experienced signal level in a given location is impacted by factors such as surrounding environment and network deployment. These factors are common to all UEs and remain relatively stationary over time. The impact of these factors is embedded in the measurement reports and can be exploited for signal strength prediction.

Q1 From experimental data, how much variability is observed in the signal strength experienced by different UEs in a specific location? What is the variability of the signal strength observed by different devices with different orientations? How accurate can the signal strength be estimated based on aggregating information? How should information be aggregated?

H2 Exploiting UE conditions (UE type, orientation, etc.) can reduce the uncertainty on individual predictions. Apart from the common factors, signal strength variations are caused by the random nature of the channel and specific UE conditions such as orientation relative to its serving

cell.

Q3 What UE-specific conditions causes significant variations? Can it be used to reduce the estimation error of individual UE predictions?

H4 Differences in the propagation environment between the air (UAV scenario) and the ground (V2X scenario) will require re-adjustments in the estimation approach between the two. The directivity of the UE antenna is more pronounced in the signal strength observed in the air due to dominant LOS conditions. Consequently, the variability of the signal strength at a specific location can be higher due to UEs with different orientations being connected to different serving cells.

Q4 What are the quantifiable differences between UAVs and V2X? How are they useful to improve the prediction?

H5 The measurement-based estimation can provide accurate signal level estimations, which can be used to predict with 95 % accuracy the probability of RSRP dropping below the required availability threshold of the service, i.e., a critical area. Additionally, using the same approach for the estimation of the interfering radio cells (also known as neighbors) RSRP, the expected Signal-To-Interference Ratio (SIR) can be calculated and used to predict the service reliability along the route with the same accuracy.

Q5 How accurate should the signal strength estimation be to detect at least 95 % of the upcoming service availability and reliability critical areas? Can that accuracy be achieved?

3 Research Methodology

The study is developed following a classical research methodology to fulfill the study objectives and answer the research questions presented in Section 2. After the classical problem description, literature review and hypothesis formulation, the following essential steps were identified:

1. **Field Measurements:** Multiple field measurement campaigns are performed over LTE networks, both on the ground (for the V2X scenario) and in the air (for the UAV scenario). The measurement equipment consists of a radio network scanner and four commercial smartphones with a test firmware. In contrast to many of the studies available in the literature, this work is measurement-based. The use of measurements gives realism to the presented results, as real data represents what UEs using mission-critical services such as autonomous vehicles or drones

will experience when moving along a specific route. Urban and rural scenarios are evaluated assuming that these are the most likely for the considered use cases.

2. **Measurement Data Analysis and Modelization:** The data collected during the measurement campaign is processed, structured, and analyzed, which allows identifying data trends, repeatability, and outliers.

3. **Estimation Methods Design:** The trends and values observed in the measurement data analysis step are used to design the estimation methods presented in this thesis. Examples of these methods are the data-driven estimation approach for accurate signal level estimation before the service starts, the UE-specific correction of the estimation using real-time data recorded by the UE, and the service outage probability calculation for critical areas estimation.

4. **Performance Evaluation:** The proposed solutions are evaluated using the data gathered during the measurement campaigns. The data-driven estimation approach is compared to other techniques often used by operators and calibrated using measurement data.

4 Contributions

The main contributions of the Ph.D. study can be summarized as follows:

1. **Proposal of an implementation of the two-stage framework presented by ACJA.**

   This thesis proposes a two-stage framework implementation for mission-critical communications. The framework is initially introduced by [38] for the UAV use case. The implementation presented in this thesis consists of a pre-service and an on-service stage and is valid for all studied scenarios. In the first, the network estimates the potential critical areas for a UE using a specific service and planning to move along a specific route using data-driven RSRP estimations. It occurs before the service starts and can lead to path re-planning in the case of critical areas detection. In the second, the RSRP estimations are corrected for the user moving along the path, and the critical areas predicted during the pre-service stage are fine-tuned based on the corrected estimations. This stage can only occur once the UE is using the service. It can help avoid upcoming critical areas and lead to more proactive management of the mobility and the network resources.

2. **Proposal of a technique that provides accurate cell-agnostic RSRP estimations in the pre-service stage.**

This thesis proposes and evaluates a data-driven approach to estimate the expected RSRP for a mission-critical user planning to move along a specific path. The signal level is estimated using data recorded by UEs that have previously passed through the same path. The proposed data-driven technique provides a cell-agnostic estimation, valid for any user in that same path. The data-driven approach is compared to traditional techniques such as empirical models or ray-tracing, using the recorded measurements to calibrate the predictions. The data-driven technique provides higher estimation accuracy for all studied scenarios.

3. **Proposal of a method for UE-specific corrections of the RSRP estimation in the on-service stage.**

   This thesis proposes and evaluates a method to reduce the estimation error further. By using real-time data recorded by the UE, we propose a statistical method to correct the UE-specific offset, referred to as Mean Individual Offset (MIO). The error samples from the specific UE are used to determine whether they statistically belong to error distributions from UEs that have previously moved along the same path. The method is adjusted to the different propagation conditions of the use cases under study (V2X/UAV), increasing estimation accuracy for both of them.

4. **Evaluation of the use of data-driven approach for critical areas detection in all studied scenarios.**

   This thesis evaluates the use of accurate RSRP estimations for in-advance detection of critical areas. The critical areas are defined in this study in terms of service availability and service reliability. For service availability, an estimation of the probability of RSRP dropping below the necessary threshold to meet the service requirements is proposed considering the RSRP estimation and its corresponding error. In the case of service reliability, the same data-driven estimation is applied first for the neighbors' RSRP. The SIR is then used to identify the critical areas in the path. This contribution verifies the two-stage framework proposed in contribution no. 1.

5. **Performance evaluation using experimental data gathered through different measurement campaigns.**

   The proposed framework and estimation approach are evaluated using experimental data. As shown in previous sections, many of the contributions available in the literature use simulation data, especially for the UAV case. Using experimental data leads to more realistic results, accounting for certain factors that cannot be modeled through simulations.

These contributions are presented in a collection of papers. The scientific findings obtained during this study are presented to the research community through scientific publications, targeting high-impact conferences and journals. Part of this investigation was also a contribution to the European Union Horizon 2020 framework DroC2om project [50]. Additionally, the work was presented and discussed in several Nokia forums. The main contributions and findings are included in the following list of scientific publications:

Paper A: M. López, T. B. Sørensen, I. Z. Kovács, J. Wigard and P. Mogensen, "Experimental Evaluation of Data-driven Signal Level Estimation in Cellular Networks", *IEEE 94th Vehicular Technology Conference (VTC2021-Fall)*, September 2021.

Paper B: M. López, T. B. Sørensen, I. Z. Kovács, J. Wigard and P. Mogensen, "Measurement-Based Outage Probability Estimation for Mission-Critical Services", *IEEE ACCESS*, vol. 9, pp. 169395-169408, 2021.

Paper C: M. López, T. B. Sørensen, P. Mogensen, J. Wigard and I. Z. Kovács, "Shadow fading spatial correlation analysis for aerial vehicles: Ray tracing vs. measurements", *IEEE 90th Vehicular Technology Conference (VTC2019-Fall)*, September 2019.

Paper D: M. López, T. B. Sørensen, J. Wigard, I. Z. Kovács and P. Mogensen, "Service Outage Estimation for Unmanned Aerial Vehicles: A Measurement-Based Approach", *IEEE Wireless Communications and Networking Conference (WCNC) 2022*. **Accepted for publication**.

Additionally, three successful patents were disclosed in relation to the work done on the thesis:

Patent Application 1: I. Z. Kovács, J. Moilanen, W. Zirwas, T. Henttonen, T. Veijalainen, L. U. Garcia, M. M. Butt, M. Centenaro, M. López, "Providing producer node machine learning based assistance", WO2021063500A1, *Published*: April 2021, Nokia Technologies.

Patent Application 2: I. Z. Kovács, A. Feki, A. Pantelidou, M. M. Butt, O. E. Barbu, M. López, "Channel state information values-based estimation of reference signal received power values for wireless networks", WO2021209145A1, *Published*: October 2021, Nokia Technologies.

Patent Application 3: I. Z. Kovács, O. E. Barbu, M. López, "Method of and apparatus for machine learning in a radio network",

WO2021213685A1, *Published*: October 2021, Nokia Technologies.

The data gathered during the different measurement campaigns and the discussions with other researchers has resulted in the following scientific publications related to the studied topic:

- M. Bucur, T. Sørensen, R. Amorim, M. López, I. Z. Kovács, and P. Mogensen. (2019, September). Validation of large-scale propagation characteristics for UAVs within urban environment. *IEEE 90th Vehicular Technology Conference (VTC2019-Fall)*, September 2019.
- B. Sliwa, M. J. Geis, C. Bektas, M. López, P. Mogensen and C. Wietfeld "DRaGon: Mining Latent Radio Channel Information from Geographical Data Leveraging Deep Learning", *IEEE Wireless Communications and Networking Conference (WCNC) 2022*. **Accepted for publication**.

5 Thesis Outline

The thesis is divided into 2 parts. Part I summarizes the main contributions and results obtained during the Ph.D. work, while Part II presents the articles supporting it.

- **Chapter 2:** This chapter provides a brief background on radio propagation and further motivates the choice of signal level as the estimated parameter for critical areas prediction. It presents state of the art on traditional and non-traditional techniques used for signal level estimation, as it is a widely studied topic.
- **Chapter 3:** This chapter includes a description of the proposed signal level estimation method for both the pre-service and the on-service stages in all studied scenarios. It also presents the results of using the data-driven estimations obtained with the proposed method for estimating the expected service availability and reliability. The probability of the UE passing through a critical area is calculated using estimated signal strength. The work presented in this chapter is supported by **Papers A, B, C, and D.**
- **Chapter 4:** Presents the conclusion of the studies conducted during the Ph.D., summarizing the main findings, and discussing the recommendations and suggestions that should be addressed in future work.

References

[1] Series, M, "IMT Vision–Framework and overall objectives of the future development of IMT for 2020 and beyond," *Recommendation ITU*, vol. 2083, p. 0, 2015.

[2] Yilmaz, Osman and Johansson, N, "5G radio access for ultra-reliable and low-latency communications," *Ericsson Research Blog*, vol. 1, 2015.

[3] Zarri, M, "Network 2020: Mission critical communications," tech. rep., GSMA, 2017.

[4] 3GPP, "Service requirements for the 5G system, Stage 1 (Release 15)," Tech. Rep. 22.261 V15.9.0, Sept. 2021.

[5] 3GPP, "User Equipment (UE) conformance specification; Radio transmission and reception (FDD)," Tech. Rep. 34.121-1 V12.5.0, Sept. 2016.

[6] D. Öhmann, M. Simsek, and G. P. Fettweis, "Achieving high availability in wireless networks by an optimal number of Rayleigh-fading links," in *2014 IEEE Globecom Workshops (GC Wkshps)*, pp. 1402–1407, IEEE, 2014.

[7] M. Bennis, M. Debbah, and H. V. Poor, "Ultrareliable and low-latency wireless communication: Tail, risk, and scale," *Proceedings of the IEEE*, vol. 106, no. 10, pp. 1834–1853, 2018.

[8] 3GPP, "Study on latency reduction techniques for LTE (Release 14)," Tech. Rep. 36.881 V14.0.0, June 2016.

[9] H. Alves, G. D. Jo, J. Shin, C. Yeh, N. H. Mahmood, C. Lima, C. Yoon, N. Rahatheva, O.-S. Park, S. Kim, *et al.*, "Beyond 5G URLLC Evolution: New Service Modes and Practical Considerations," *arXiv preprint arXiv:2106.11825*, 2021.

[10] 5GPPP Association, "5G and e-health," Tech. Rep. White Paper, Oct. 2015.

[11] N. A. Mohammed, A. M. Mansoor, and R. B. Ahmad, "Mission-critical machine-type communication: An overview and perspectives towards 5G," *IEEE Access*, vol. 7, pp. 127198–127216, 2019.

[12] Alliance, NGMN, "5G White Paper," *Next generation mobile networks, white paper*, vol. 1, 2015.

[13] M. Boban, A. Kousaridas, K. Manolakis, J. Eichinger, and W. Xu, "Use cases, requirements, and design considerations for 5G V2X," *arXiv preprint arXiv:1712.01754*, 2017.

[14] 3GPP, "Service requirements for enhanced V2X scenarios," Tech. Rep. 22.186 V16.2.0, June 2019.

[15] C. S. I. Cordero, Carlos Director, "Optimizing 5G for V2X - Requirements, Implications and Challenges," in *IEEE VTC Mission-Critical 5G for Vehicle IoT*, IEEE, 2016.

[16] A. Kousaridas, R. P. Manjunath, J. Perdomo, C. Zhou, E. Zielinski, S. Schmitz, and A. Pfadler, "QoS Prediction for 5G Connected and Automated Driving," *IEEE Communications Magazine*, vol. 59, no. 9, pp. 58–64, 2021.

[17] P. Wang, J. Zhang, H. Deng, and M. Zhang, "Real-time urban regional route planning model for connected vehicles based on V2X communication," *Journal of Transport and Land Use*, vol. 13, no. 1, pp. 517–538, 2020.

[18] 5G Automotive Association, " Making 5G proactive and predictive for the automotive industry," Tech. Rep. White Paper, Jan. 2020.

[19] J. Riihijarvi and P. Mahonen, "Machine learning for performance prediction in mobile cellular networks," *IEEE Computational Intelligence Magazine*, vol. 13, no. 1, pp. 51–60, 2018.

[20] R. Falkenberg, K. Heimann, and C. Wietfeld, "Discover your competition in LTE: Client-based passive data rate prediction by machine learning," in *GLOBECOM 2017-2017 IEEE Global Communications Conference*, pp. 1–7, IEEE, 2017.

[21] L. Torres-Figueroa, H. F. Schepker, and J. Jiru, "QoS Evaluation and Prediction for C-V2X Communication in Commercially-Deployed LTE and Mobile Edge Networks," in *2020 IEEE 91st Vehicular Technology Conference (VTC2020-Spring)*, pp. 1–7, IEEE, 2020.

[22] M. A. Gutierrez-Estevez, Z. Utkovski, A. Kousaridas, and C. Zhou, "A Statistical Learning Framework for QoS Prediction in V2X," in *2021 IEEE 4th 5G World Forum (5GWF)*, pp. 441–446, IEEE, 2021.

[23] N. Bahra and S. Pierre, "A Hybrid User Mobility Prediction Approach for Handover Management in Mobile Networks," in *Telecom*, vol. 2, pp. 199–212, Multidisciplinary Digital Publishing Institute, 2021.

[24] K. M. Hosny, M. M. Khashaba, W. I. Khedr, and F. A. Amer, "New vertical handover prediction schemes for LTE-WLAN heterogeneous networks," *PloS one*, vol. 14, no. 4, p. e0215334, 2019.

[25] W. Zhang, M. Feng, M. Krunz, and H. Volos, "Latency Prediction for Delay-sensitive V2X Applications in Mobile Cloud/Edge Computing Systems," in *GLOBECOM 2020-2020 IEEE Global Communications Conference*, pp. 1–6, IEEE, 2020.

[26] T. Fawcett, "An introduction to roc analysis," *Pattern recognition letters*, vol. 27, no. 8, pp. 861–874, 2006.

[27] A. Samba, Y. Busnel, A. Blanc, P. Dooze, and G. Simon, "Instantaneous throughput prediction in cellular networks: Which information is needed?," in *2017 IFIP/IEEE Symposium on Integrated Network and Service Management (IM)*, pp. 624–627, IEEE, 2017.

[28] S. Barmpounakis, L. Magoula, N. Koursioumpas, R. Khalili, J. M. Perdomo, and R. P. Manjunath, "LSTM-based QoS prediction for 5G-enabled Connected and Automated Mobility applications," in *2021 IEEE 4th 5G World Forum (5GWF)*, pp. 436–440, IEEE, 2021.

[29] C. Yue, R. Jin, K. Suh, Y. Qin, B. Wang, and W. Wei, "LinkForecast: cellular link bandwidth prediction in LTE networks," *IEEE Transactions on Mobile Computing*, vol. 17, no. 7, pp. 1582–1594, 2017.

[30] A. R. Abdellah, A. Alshahrani, A. Muthanna, and A. Koucheryavy, "Performance Estimation in V2X Networks Using Deep Learning-Based M-Estimator

Loss Functions in the Presence of Outliers," *Symmetry*, vol. 13, no. 11, p. 2207, 2021.

[31] SESAR Joint Undetaking, ""U-Space Blueprint brochure," Publications Office of the European Union, Luxermbourg," 2017.

[32] M. Neale and D. Colin, "Mobility challenges for unmanned aerial vehicles connected to cellular LTE networks," in *Technology Workshop - Remotely Piloted Aircraft Systems Symposium*, Mar. 2015.

[33] 3GPP, "Study on Enhanced LTE Support for Aerial Vehicles (Release 15)," Tech. Rep. 36.777 V0.3.1, Oct. 2017.

[34] E. Vinogradov, H. Sallouha, S. De Bast, M. M. Azari, and S. Pollin, "Tutorial on UAV: A blue sky view on wireless communication,"

[35] X. Lin, V. Yajnanarayana, S. D. Muruganathan, S. Gao, H. Asplund, H.-L. Maattanen, M. Bergstrom, S. Euler, and Y.-P. E. Wang, "The sky is not the limit: LTE for unmanned aerial vehicles," *IEEE Communications Magazine*, vol. 56, no. 4, pp. 204–210, 2018.

[36] I. Kovacs, R. Amorim, H. C. Nguyen, J. Wigard, and P. Mogensen, "Interference analysis for UAV connectivity over LTE using aerial radio measurements," in *2017 IEEE 86th Vehicular Technology Conference (VTC-Fall)*, pp. 1–6, IEEE, 2017.

[37] J. Stanczak, I. Z. Kovacs, D. Koziol, J. Wigard, R. Amorim, and H. Nguyen, "Mobility challenges for unmanned aerial vehicles connected to cellular lte networks," in *2018 IEEE 87th Vehicular Technology Conference (VTC Spring)*, pp. 1–5, IEEE, 2018.

[38] ACJA, GSMA and GUTMA, "Interface for Data Exchange between MNOs and the UTM Ecosystem: Network Coverage Service Definition, v1.00.," Feb. 2021.

[39] P. S. Bithas, E. T. Michailidis, N. Nomikos, D. Vouyioukas, and A. G. Kanatas, "A survey on machine-learning techniques for UAV-based communications," *Sensors*, vol. 19, no. 23, p. 5170, 2019.

[40] U. Challita, W. Saad, and C. Bettstetter, "Interference management for cellular-connected UAVs: A deep reinforcement learning approach," *IEEE Transactions on Wireless Communications*, vol. 18, no. 4, pp. 2125–2140, 2019.

[41] Y. Chen, X. Lin, T. A. Khan, and M. Mozaffari, "A deep reinforcement learning approach to efficient drone mobility support," *arXiv preprint arXiv:2005.05229*, 2020.

[42] Y. Jiang, K. Nihei, J. Li, H. Yoshida, and D. Kanetomo, "Learning on the fly: An RNN-based online throughput prediction framework for UAV communications," in *2020 IEEE International Conference on Communications Workshops (ICC Workshops)*, pp. 1–7, IEEE, 2020.

[43] E. Krijestorac, S. Hanna, and D. Cabric, "Spatial signal strength prediction using 3d maps and deep learning," in *ICC 2021-IEEE International Conference on Communications*, pp. 1–6, IEEE, 2021.

[44] G. Yang, Y. Zhang, Z. He, J. Wen, Z. Ji, and Y. Li, "Machine-learning-based prediction methods for path loss and delay spread in air-to-ground millimetre-wave channels," *IET Microwaves, Antennas & Propagation*, vol. 13, no. 8, pp. 1113–1121, 2019.

[45] S. K. Goudos, G. V. Tsoulos, G. Athanasiadou, M. C. Batistatos, D. Zarbouti, and K. E. Psannis, "Artificial neural network optimal modeling and optimization of UAV measurements for mobile communications using the L-SHADE algorithm," *IEEE Transactions on Antennas and Propagation*, vol. 67, no. 6, pp. 4022–4031, 2019.

[46] 3GPP, "Physical layer; Measurements (Release 16)," Tech. Rep. 36.214 V16.2.0, Mar. 2021.

[47] C. Ide, R. Falkenberg, D. Kaulbars, and C. Wietfeld, "Empirical analysis of the impact of lte downlink channel indicators on the uplink connectivity," in *2016 IEEE 83rd Vehicular Technology Conference (VTC Spring)*, pp. 1–5, IEEE, 2016.

[48] V. Raida, P. Svoboda, M. Koglbauer, and M. Rupp, "On the Stability of RSRP and Variability of Other KPIs in LTE Downlink-An Open Dataset," in *GLOBECOM 2020-2020 IEEE Global Communications Conference*, pp. 1–6, IEEE, 2020.

[49] M. Toril, V. Wille, S. Luna-Ramírez, M. Fernández-Navarro, and F. Ruiz-Vega, "Characterization of Radio Signal Strength Fluctuations in Road Scenarios for Cellular Vehicular Network Planning in LTE," *IEEE Access*, vol. 9, pp. 33120–33131, 2021.

[50] SESAR Joint Undetaking - Project no. 763601, "Deliverable 5.2. Report of first drone flight campaign.," Dec. 2018.

Chapter 2

Signal Level Estimation

This chapter continues the discussion on the importance of RSRP estimation started in Section 1.3 of Chapter 1. It presents details on the factors that impact RSRP variations and therefore affect the signal strength measured by a UE in a certain location. It also includes a review of the traditional approaches used for channel modeling that are later compared with the proposed data-driven estimation approach. A discussion on well-known fine-tuning methods for estimated signal level is presented, aiming to point out the differences with the work presented in this thesis. A state-of-the-art review of recent techniques for signal strength estimation is also included.

1 Impacting Factors

After briefly discussing the importance of RSRP in Section 1.3, we summarize here the main factors impacting the signal propagating from the transmitter to the receiver. Understanding the physical principles of electromagnetic waves propagation over the air is essential for estimating the received signal strength. The free-space path loss model allows for the calculation of the received power in free-space propagation conditions, which depends mainly on the transmitted power and the distance between the transmitter and the receiver [1]. However, free-space propagation conditions is rarely the case in most wireless propagation scenarios. In practice, any obstacle or change in the radio wave path or environment can cause signal strength variations and will be added to the default distance attenuation. This effect is known as fading, and it is distinguished between [2]:

- **Large-scale Fading:** the attenuation of the signal over large areas, caused by obstacles in the surrounding environment of the propagation path. It is mostly impacted by the terrain shape (hills, mountains) and large

building or objects in the environment present between the transmitter and the receiver. It includes pathloss and shadowing effects, where shadowing is considered the deviation of the received power from its overall mean value, and is statistically modelled using a log-normal distribution [3].

- **Small-scale Fading:** represents the rapid changes in the radio signal over a short period of time (on the order of seconds) [4]. It occurs when the obstacles in the environment cause the signal to be reflected, and multiple versions of the same signal with different delays arrive at the receiver. Factors such as multipath environment, UE speed (Doppler shift at each multipath component), environment dynamics, and transmission bandwidth of the channel affect small-scale fading [5].

Since the work presented in this thesis is based on experimental data, it is important to consider error sources in the UE measurement reports. In practice, the measured RSRP may fluctuate not only due to channel effects but also due to receiver processing.

There are ways of mitigating the impact of these effects for accurate RSRP estimation. A Layer 1 filter is typically applied to overcome measurement inaccuracy due to fast-fading effects. Further averaging to remove fading, measurement noise and measurement/estimation errors is performed at Layer 3 [6]. This is further explained in Section 3 of **Paper B**. However, the random nature of the signal will always limit the accuracy of the signal strength estimation.

Modeling the impact of the different factors or finding a method that estimates the received signal strength as accurately as possible has been the subject of much investigation. The following sections present a review of the traditional and new estimation methods and a summary of the data-driven approach studied in this thesis.

2 Traditional Estimation Approaches

Estimating the signal strength that the user will experience is crucial for the design of a reliable network. Over-estimating the signal power can lead to poor coverage, and under-estimating it can be costly for the MNOs due to unnecessarily dense network deployment. Channel models can be divided into empirical and theoretical. The following sub-sections introduce both types, focusing on the examples that are later used in Chapter 3 for comparison with the proposed data-driven approach.

2.1 Empirical Models

Empirical channel models, often referred to as statistical models, are the result of using measurement data to model the behavior of the radio channel through statistics. The parameters of an empirical model strongly depend on the scenario, as the propagation characteristics of, e.g., urban, suburban, or rural environments are very different. The main problem of this estimation approach is generalization, as it aims at estimating the average behavior of the signal. Despite finding common attributes in a particular propagation scenario, specific signal variations due to, e.g., a building in the path between the transmitter and the receiver in a city can not be captured by a general model for urban scenarios. Therefore, MNOs use correction factors to fine-tune the model and adapt it to the specific area where they are planning to deploy a network.

There are several known empirical models [7], the earliest one being the free-space propagation model [1], which is often used as part of the Friis transmission equation [8]. The two-ray ground reflection model considers the effect of multipath due to ground reflections and assumes that the signal reaches the receiver from two different paths [2]. However, free-space propagation models are not a good representation for scenarios where objects (buildings, vegetation, vehicles, etc.) are in the propagation path. There are specific models for the different scenarios. The most commonly used are meant for urban and rural environments. Examples are the Okumura-Hata model [9], the models proposed by 3GPP [10], the 231 Walfisch-Ikegami model [11] or the guidelines included in ITU-R M.2412 [12] for propagation modeling. The first two are used in this thesis for comparison with the proposed data-driven approach. Therefore, an extended explanation of these models is included:

- **Okumura-Hata**
  This model was built using a large set of signal strength measurements in different scenarios (varying terrain, vegetation, and urban clutter) at multiple frequencies. It is commonly used for network planning, and it has experienced several corrections over the years, adapting the model to the specific propagation conditions of the scenario under study. The Okumura-Hata model used for comparison in this dissertation is defined in Eq. (2.1). The estimated path loss for an urban area is given by:

$$\begin{aligned} PL = {} & 69.55 + 26.16 log_{10}(f_c) - 13.82 log_{10}(h_b) \\ & - \alpha(h_m) + (44.9 - 6.55 log_{10}(h_b)) log_{10}(d) \end{aligned} \quad \text{[dB]} \quad (2.1)$$

  Where the d is the distance between the transmitter and the receiver in km, the carrier frequency f_c is in MHz, the effective transmitter (h_b) and

receiver (h_m) antenna heights are in m and $\alpha(h_m)$ is a correction factor that for small/medium cities such as the one under study in our drive tests is:

$$\alpha(h_m) = (1.1log10(f_c) - 0.7)h_m - (1.56log_{10}(f_c) - 0.8) \quad (2.2)$$

The above equations are a simplified version of the Okumura-Hata model, which does not include the multiple correction factors that may be used when applying the model for planning mobile radio systems. However, they are considered a good representation of the estimation accuracy level that the Okumura-Hata model can provide.

- **3GPP TR 38.901**
  3GPP proposed in [10] a study on channel model for frequencies ranging from 0.5 to 100 GHz. The model is constructed by combining the results from the measurements campaigns performed by many of the different 3GPP partners. It is a common approach for path loss estimation for three scenarios: Rural Macro (RMa), Urban Macro (UMa), and Urban Micro (UMi). Since the comparison with the data-driven approach is only shown for the urban environment case, we include here the equations for the UMa scenario. The equation is different depending on the visibility conditions (LOS/Non-Line-Of-Sight (NLOS)).

  For LOS conditions, the path loss estimation depends on the breakpoint distance d'_{BP}, which is defined as the distance between the transmitter and the receiver where the propagation mode changes. In [10]:

$$d'_{BP} = 4h_{BS}h_{UT}\frac{f_c}{c} \quad \text{[m]} \quad (2.3)$$

  In 2.3, h_{BS} and h_{UT} are the effective antenna heights in m of the BS and the UE, respectively, f_c is the carrier frequency in Hz, and $c = 3.0x10^8$ m/s is the propagation velocity in free space. Two distances are distinguished: two-dimensional d_{2D} distance, and three-dimensional (accounting for height) d_{3D} distance, both between transmitter and receiver. For d_{2D} between a minimum distance of 10 m and d'_{BP}, path loss for LOS conditions is given by:

$$\begin{aligned} PL_{UMa-LOS(1)} &= 28.0 + 22log_{10}(d_{3D}) \\ &\quad + 20log_{10}(f_c) \end{aligned} \quad \text{[dB]} \quad (2.4)$$

  For a d_{2D} distance above d'_{BP} and below 5 km, the LOS path loss estimation becomes:

$$PL_{UMa-LOS(2)} = 28.0 + 40log_{10}(d_{3D}) + 20log_{10}(f_c) - 9log_{10}((d'_{BP})^2 + (h_{BS} - h_{UT})^2) \text{ [dB]} \quad (2.5)$$

As expressed in Eq. (2.6), for NLOS visibility conditions, the path loss estimation will be the maximum between the estimated path loss for LOS conditions and the value obtained using Eq. (2.7).

$$PL_{UMa-NLOS} = max(PL_{UMa-LOS}, PL'_{UMa-NLOS}) \text{ [dB]} \quad (2.6)$$

$$PL'_{UMa-NLOS} = 13.54 + 39.08log_{10}(d_{3D}) + 20log_{10}(f_c) - 0.6(h_{UT} - 1.5) \text{ [dB]} \quad (2.7)$$

As it will be further explained in Chapter 3, for the comparison performed in this thesis, the 3GPP TR 38.901 model has been fine-tuned with the appropriate visibility conditions (LOS/NLOS) based on ray-tracing predictions, corresponding BS heights and an assumed UE height of 1.5 m.

2.2 Ray-Tracing

Ray-tracing is a propagation modeling tool that allows estimating path loss, angle of arrival, and delay spread by modeling electromagnetic waves as rays [13]. It uses physics to calculate the path that a radio signal will follow, considering its interaction with the objects in the propagation environment. It will account for effects such as reflection, diffraction, scattering, as well as the dielectric properties of the surfaces with which the signal is interacting and its carrier frequency. To that end, ray-tracing requires 3D modeling of the propagation scenario:

- Terrain elevation and material properties
- Buildings position, shape, height, and material properties
- Vegetation position, size, and type

Deployment information is also necessary to compute the paths of the rays from the transmitter to the receiver: BS height, BS transmit power, UE height, and carrier frequency. Therefore, very accurate modeling of the propagation scenario is needed for the estimations to provide satisfactory accuracy. This will be further proved in Chapter 3.

One of the main advantages of ray-tracing compared to the empirical models explained in the previous sub-section is that the estimations are specific for the scenario under study. Therefore, the accuracy of the path loss

estimation provided by ray-tracing is expected to be higher, but this comes at the cost of increased complexity and computational load.

In this thesis, the evaluation of ray-tracing is done using the WinProp tool from Altair© [14]. The tool offers different simplifications of full ray-tracing prediction models, and it allows model calibration using experimental data. Two of the prediction models are investigated in this thesis [15]:

- **Intelligent Ray Tracing (IRT):** The received power is calculated by superposing up to hundreds of rays resulting from computing the multiple paths that the signal can travel through. Due to the high number of rays, the computation time of this method is very high.
- **Dominant Path Model (DPM):** In most cases, when using IRT, only 2 or 3 of the computed rays are contributing significantly to the total received power. For that reason, the DPM model focuses on determining the most dominant paths using geometry and calculates path loss using the equation in [15].

Although the accuracy of ray-tracing is acceptable for network planning, it will be shown in Chapter 3 that it is not sufficient for service availability and reliability critical areas estimation.

2.3 Using Drive Tests to Improve the Estimations

The methods introduced above are typically integrated into professional radio planning tools that allow MNOs to perform network planning and optimization. An example is the Atoll tool by Forsk© [16], which is commonly used by operators as it includes a wide variety of empirical propagation models as well as ray-tracing. To improve the estimations after network deployment, operators perform the so-called drive tests. They drive along a specific route using dedicated measurement equipment that provides statistics of the network coverage and performance. Some radio planning tools allow using measurement data to correct and calibrate the estimations and perform network optimization [17].

3GPP introduced in Release 10 a more economic and automatized alternative to drive tests: Minimization of Drive Tests (MDT) [18]. The main idea behind MDT is to exploit the UEs' measurement capabilities to collect real data from a specific area. It enables the UEs to collect periodically (or not, depending on the MDT mode) radio measurements along with their location, even if the UE is in idle state, and report them when in active state [19].

This information serves for radio measurements analysis and statistical data processing. Therefore, MNOs use it for anomaly detection and network capacity and performance optimization, among others. The MDT feature enables the generation of Radio Environment Maps (REM), which is a functionality that provides awareness on the radio environment using geo-located

measurements. A REM is a centralized database that contains information on the surrounding radio environment (device locations, available services, geographical features, etc.), and more intelligent entities may use them to perform network optimization.

There are two major concerns regarding MDT. First, the fact that not all UEs support this feature as it is not mandatory. In practice, MDT can only be used with test devices owned by the operator or an MDT service provider. The second concern is the positioning method that provides the location included in the measurement reports. A poor Global Navigation Satellite System (GNSS) signal or the absence of it, rounding of latitude/longitude values when reported, and generally the inaccuracies of the positioning method can reduce the benefits of MDT reports. For GNSS, which is typically used in MDT, inaccuracies are below 10 m in outdoor environments and recent literature shows methods to improve it [20], leading to positioning errors as low as 5 m [21] in urban scenarios.

MDT is however considered to be a useful approach for sample collection for the data-driven method evaluated in this thesis. The data-driven approach is similar to the REM functionality, as they are both based on the collection of measurement data to estimate the UEs' expected signal strength. One of the main differences is that the estimations provided by REM are cell-specific, whereas the ones provided by the proposed data-driven approach are cell-agnostic. This, and other differences, will be further explained in Chapter 3.

3 New Estimation Approaches

This section summarizes some of the state-of-the-art non-traditional techniques for signal strength prediction. Most of the publications are motivated by improving wireless coverage prediction to reduce network deployment costs. As in this thesis, others aim at high accuracy predictions for reliability assurance purposes.

There are plenty of studies about the use of ML for signal strength prediction. Especially during the past ten years, they have increased since it is generally considered a good solution for predicting QoS-related KPIs. The authors of [22] propose a ML framework to predict the signal strength using crowd-sourced data from urban, suburban, and rural scenarios. They feed features such as context information (e.g., phone model, UE speed, time of the day), RAN configuration parameters (e.g., frequency, transmit power, antenna details, or location of the serving cell), and UE-BS distance to a gradient boosted tree (LightGMB). They predict RSRP and obtain an RMSE of 7.4 dB. The work presented in [23] studies the prediction of RSRP with a method based on path sequence regression. They simulate the transmission

path of the signal, extract the path's features (clutter and antenna heights, distances between UE and BS), and combine them with other antenna information such as transmit power to predict RSRP using NN. Their proposed algorithm reaches an RMSE of 10.3 dB. In [24], the authors also propose a model for feature extraction to estimate signal strength, but they account for more physical and environmental features. They consider in total 18 different features: environmental clutter type (water, vegetation, building, road, and others), frequency, UE-BS angles, BS information, heights and distances, etc. They test their model over measurement data, and achieve an RMSE of 5.1 dB in an urban environment. The studies in [25] design the features for their model based on the Cost 231-Hata empirical model and the geometrical location. They later use feature selection to reduce the number of inputs to the NN used for signal strength prediction, achieving an RMSE of 7.5 dB. In [26], the authors present a deep-learning approach to predict signal strength. They extract the radio environment characteristics from top-view satellite images of the receiver's location and combine that information with expert knowledge. The model is tested over different environments, showing an RMSE of approximately 6 dB.

As observed in the previous section, there are a lot of similarities between the studies aiming to tackle the RSRP prediction problem. It is challenging to find estimation approaches that do not involve ML in recent literature. Many of them use a certain number of features that characterize and impact the signal strength reaching the UE. Some select the features based on empirical models, some use feature selection techniques, and some include images or 3D models containing information about the surrounding environment. The main differences between them are how they obtain the information (measurement or simulation data) and their prediction methods. The data-driven approach presented in the following section relies on the fact that all these features are inherent in the RSRP value measured at the UE.

References

[1] A. Goldsmith, *Wireless communications*. Cambridge university press, 2005.

[2] T. S. Rappaport *et al.*, *Wireless communications: principles and practice*, vol. 2. prentice hall PTR New Jersey, 1996.

[3] M. Gudmundson, "Correlation model for shadow fading in mobile radio systems," *Electronics letters*, vol. 27, no. 23, pp. 2145–2146, 1991.

[4] T. Jiang, D. Chen, C. Ni, and D. Qu, *OQAM/FBMC for future wireless communications: Principles, technologies and applications*. Academic Press, 2017.

[5] B. Sklar, "Rayleigh fading channels in mobile digital communication systems. i. characterization," *IEEE Communications magazine*, vol. 35, no. 7, pp. 90–100, 1997.

[6] M. Anas, F. D. Calabrese, P.-E. Ostling, K. I. Pedersen, and P. E. Mogensen, "Performance analysis of handover measurements and layer 3 filtering for utran lte," in *2007 IEEE 18th International Symposium on Personal, Indoor and Mobile Radio Communications*, pp. 1–5, IEEE, 2007.

[7] O. O. Erunkulu, A. M. Zungeru, C. K. Lebekwe, and J. M. Chuma, "Cellular communications coverage prediction techniques: A survey and comparison," *IEEE Access*, vol. 8, pp. 113052–113077, 2020.

[8] H. T. Friis, "A note on a simple transmission formula," *Proceedings of the IRE*, vol. 34, no. 5, pp. 254–256, 1946.

[9] M. Hata, "Empirical formula for propagation loss in land mobile radio services," *IEEE transactions on Vehicular Technology*, vol. 29, no. 3, pp. 317–325, 1980.

[10] 3GPP, "Study on channel model for frequencies from 0.5 to 100 GHz. (Release 16)," Tech. Rep. 38.901 V16.1.0, Dec. 2019.

[11] J. D. Parsons, *The mobile radio propagation channel*. Wiley, 2000.

[12] M. Series, "Guidelines for evaluation of radio interface technologies for imt-2020," *Report ITU-R M. 2412-0, Tech. Rep.*, 2017.

[13] Z. Yun and M. F. Iskander, "Ray tracing for radio propagation modeling: Principles and applications," *IEEE Access*, vol. 3, pp. 1089–1100, 2015.

[14] R. Hoppe, G. Wölfle, and U. Jakobus, "Wave propagation and radio network planning software winprop added to the electromagnetic solver package feko," in *2017 International Applied Computational Electromagnetics Society Symposium-Italy (ACES)*, pp. 1–2, IEEE, 2017.

[15] R. Wahl and G. Wolfle, "Combined urban and indoor network planning using the dominant path propagation model," in *2006 First European Conference on Antennas and Propagation*, pp. 1–6, IEEE, 2006.

[16] Forsk - Atoll Overview, "Atoll Radio Planning and Optimisation Software," 2021. `https://www.forsk.com/atoll-overview`, Last accessed on 2021-11-30.

[17] Forsk - Atoll Overview, "Measurement-Based Optimization," 2021. `https://www.forsk.com/measurement-based-optimisation`, Last accessed on 2021-11-30.

[18] 3GPP, "Radio measurement collection for Minimization of Drive Tests (MDT); Overall description; Stage 2," Tech. Rep. 37.320 V10.1.0, Mar. 2011.

[19] W. A. Hapsari, A. Umesh, M. Iwamura, M. Tomala, B. Gyula, and B. Sebire, "Minimization of drive tests solution in 3gpp," *IEEE Communications Magazine*, vol. 50, no. 6, pp. 28–36, 2012.

[20] K. Strandjord, P. Axelrad, D. M. Akos, and S. Mohiuddin, "Improved urban navigation with direct positioning and specular matching," in *Proceedings of the 2020 International Technical Meeting of The Institute of Navigation*, pp. 787–800, 2020.

[21] L. Icking, T. Kersten, and S. Schön, "Evaluating the Urban Trench Model For Improved GNSS Positioning in Urban Areas," in *2020 IEEE/ION Position, Location and Navigation Symposium (PLANS)*, pp. 631–638, IEEE, 2020.

[22] A. Ghasemi, "Data-driven prediction of cellular networks coverage: An interpretable machine-learning model," in *2018 IEEE Global Conference on Signal and Information Processing (GlobalSIP)*, pp. 604–608, IEEE, 2018.

[23] C. L. Z. Huang, Y. Wang, M. Liang, J. Hu, and T. Song, "Radio Wave Propagation Prediction Based on Path Sequence Regression," in *2020 IEEE 6th International Conference on Computer and Communications (ICCC)*, pp. 238–242, IEEE, 2020.

[24] Y. Zheng, Z. Liu, R. Huang, J. Wang, W. Xie, and S. Liu, "Feature Extraction in Reference Signal Received Power Prediction Based on Convolution Neural Networks," *IEEE Communications Letters*, 2021.

[25] L. Tao, J. Lu, X. Wang, and L. Qian, "Feature engineering based intelligent wireless propagation model for RSRP prediction," in *IOP Conference Series: Materials Science and Engineering*, vol. 768, p. 042038, IOP Publishing, 2020.

[26] J. Thrane, B. Sliwa, C. Wietfeld, and H. L. Christiansen, "Deep learning-based signal strength prediction using geographical images and expert knowledge," in *GLOBECOM 2020-2020 IEEE Global Communications Conference*, pp. 1–6, IEEE, 2020.

Chapter 3

Data-Driven Estimation Approach

The RSRP estimation approach presented in this dissertation addresses the prediction of the signal level that a UE using mission-critical services will experience along a particular path. Intending to predict service availability and reliability along the route to avoid potential drops, we require highly accurate RSRP estimations at specific locations. For the pre-service stage, we aim at providing estimations that are valid for any UE planning to move along the same path.

The first part of this study included the evaluation of the proposed data-driven approach for signal level estimation and its performance comparison with traditional approaches. The study was done for both use cases under evaluation (V2X and UAVs) and in different environments. This section presents the data-driven approach and summarizes the results presented in **Papers A, B, C, and D**. Additionally to the following explanations, Section 4 of this chapter presents the main findings and a summary each paper.

1 Measurement Campaigns

Collecting measurement data was the first step in this study. We gathered ground and airborne data in urban and rural environments in Denmark. The measurement equipment consisted of a TSME scanner from R&S and four commercial smartphones with QualiPoc© test firmware. These allowed to record L1 and L3 filtered RSRP values and their corresponding Physical Cell ID (PCI) of the serving cell in the case of the phones and the surrounding visible cells in the case of the scanner. For all cases, the measurement equipment was locked to measure in the 1800 MHz band. In the following, a summary

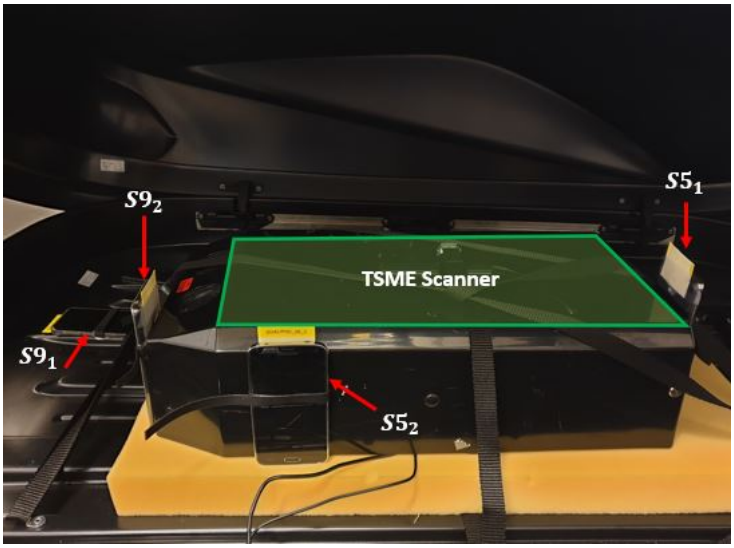

Fig. 3.1: Example of phone configuration in setup A during the drive test campaigns.

of the different measurement campaigns is presented.

1.1 V2X Data Collection

As explained in the following sub-section, the data-driven approach consists of averaging measurements performed by different UEs at the same location. Therefore, the campaign was designed to include as much UE heterogeneity as possible in the collected data. This was achieved through:

- Use of four commercial smartphones from two different models (two Samsung Galaxy S5 and two Samsung Galaxy S9). The two models had different chipsets and antenna implementations, leading to different antenna patterns (as seen in Fig. B.3 from **Paper B**) and measured signal levels.
- Position of the devices in three different configurations (setups A, B, and C in **Papers A and B**), including different orientations and positions inside and outside the car. An example (setup A) is shown if Fig. 3.1. For a better understanding, the reader is referred to Table A.1 and Fig. A.1 in **Paper A**.

The TSME scanner was connected to a paddle antenna in a fixed position and remained in the car top carrier during the measurements. The data recorded by the scanner was used for reference, as explained in **Paper A**. The data was recorded in urban and rural environments in and nearby the city of

Aalborg (Denmark) to evaluate the performance of the data-driven approach in scenarios with completely different shadowing and visibility conditions. For the rural environment, two round-trips of a 14.8 km stretch were driven with each of the three setups. The urban route was a 3.3 km closed loop, and three loops were driven with each setup. Detailed information on this measurement campaign can be found in **Paper A**.

1.2 UAV Data Collection

In this case, two different measurement campaigns were carried out:

- *Campaign A:* With the aim of evaluating ray-tracing performance for the estimation of Shadow Fading (SF) in the air. Measurements from seventeen different streets were collected in the city of Aarhus (Denmark), at 10 m, 15 m, and 30 m heights. In this case, data was recorded using the TSME radio network scanner only, connected to an omnidirectional antenna that was mounted extending about 50 cm above the drone fuselage. Details can be found in Section 2.1 of **Paper C**.
- *Campaign B:* Performed to evaluate the data-driven estimation approach for the UAV use case. The drone flew in a 5 km stretch (two round-trips) in a rural environment nearby Aalborg (Denmark) on two different days. The four smartphone devices were hung from the drone fuselage. Each phone was pointing to one of the four main compass directions to increase UE heterogeneity and include directional antenna effects. Pictures of the measurement setup and other details regarding this measurement campaign can be found in Section 2 of **Paper D**.

2 Data-Driven Estimation

2.1 Pre-Service Stage

This subsection briefly describes the pre-service RSRP estimation approach, which is introduced mainly in **Paper A**. For the pre-service stage, the RSRP values recorded by all the different UEs in a certain location are averaged, as shown in Eq. A.1 in **Paper A**. Data processing and further explanations on how is the data-driven estimation obtained can be found in **Paper A**.

The values recorded by the different UEs in a segment are averaged regardless of the serving cell of the UE recording the value. Therefore, unlike the available literature on signal strength estimation presented in the previous sections, the data-driven approach provides cell-agnostic estimations.

Paper A presents the results obtained when using the data-driven signal strength estimation approach in the pre-service stage for the ground case. Re-

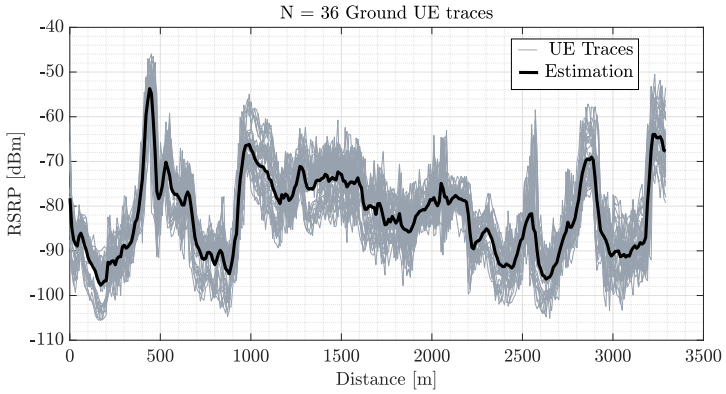

Fig. 3.2: Signal level traces recorded for urban ground measurement campaign; several traces are overlaid. The data-driven estimation (solid black) obtained by averaging the recorded traces is also shown.

sults are shown for urban and rural environments. The urban scenario shows a lower overall estimation error than the rural environment due to propagation conditions. The increased multipath in the urban scenario averages out the effect of the directional antenna patterns of the phones, increasing the *repeatability* of the signal levels observed by the different UEs (as shown in Fig. 3.2) and, therefore, reducing the estimation error. Numerical results are summarized in Table 3.1.

The pre-service estimation method can be applied equally for V2X and UAVs. However, estimations need to be scenario-specific due to the different propagation conditions. Figure 3.3 shows the traces recorded by all UEs in the same stretch of the rural route during the ground and UAV (*Campaign B*) measurement campaigns. The estimation (mean value) of the traces is also shown. The measurements are recorded in the same location but at different heights (approximately 1.5 m in the ground versus 50 m in the air). Due to different propagation conditions and a more pronounced effect of the directional antenna patterns of the phones in the air, the experienced signal levels are completely different between the heights.

The results for the UAV scenario are presented in **Paper D** and summarized in Table 3.1. The overall estimation error is higher than initially expected, as the average SF observed in the air is typically low due to improved LOS conditions. However, as it can be seen in Fig. 3.3, strong variations are observed in the recorded data. Therefore, the *repeatability* of the signal strength recorded by different UEs in the same location is not so pronounced in the air, which increases the estimation error.

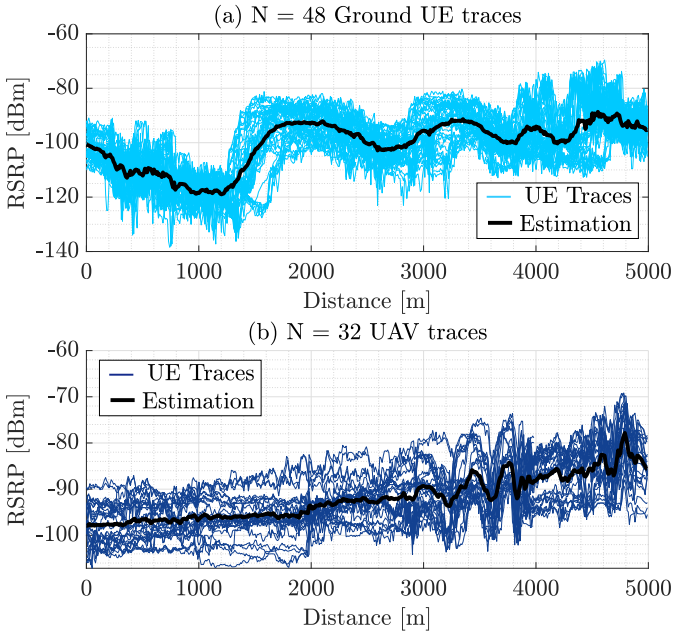

Fig. 3.3: Overlaid signal level traces recorded in the same stretch for ground (a) and drone (b) in the rural scenario. The data-driven estimation (solid black) is also shown for both cases.

Performance Comparison

As explained in Chapter 2, to show the performance improvements provided by the data-driven estimation approach, the results are compared to traditional methods.

For the ground level case, the proposed approach is compared to empirical models (Okumura-Hata and 3GPP TR 38.901) and ray-tracing. Results are introduced in **Paper A**, and the details on how the comparison is performed are explained in **Paper B**. Table B.4 in **Paper B** summarizes the performance of the different estimation approaches, showing that traditional

Table 3.1: Overall estimation error Δ of the pre-service and on-service stage data-driven estimations in all studied scenarios.

	V2X - ***Papers A and B***		**UAV -** ***Paper D***	
	Pre-service [dB]	On-service [dB]	Pre-service [dB]	On-service [dB]
Rural	6.3	5.1	4.8	2.7
Urban	4.9	3.7	-	-

Table 3.2: ***Paper C*** - σ_{SF} of the UAV measurement data recorded in *Campaign A* and the IRT/DPM predictions from the ray-tracing tool.

Height	**Measurements** σ_{SF} [dB]	**IRT** σ_{SF} [dB]	**DPM** σ_{SF} [dB]
Ground Level	6.3	4.3	4.6
10 m	8.4	5.3	5
15 m	6.2	4	3.7
30 m	4.1	2.8	2.8

methods present very high estimation error compared to what is observed with the proposed data-driven approach.

A slightly different approach is followed for the UAV case. The performance of the data-driven, presented in **Paper D**, is shown only for the rural environment and without comparison to traditional approaches. However, **Paper C** studies the feasibility of ray-tracing for predicting the SF experienced by UAVs in an urban scenario. The study is done using measurement data from *Campaign A*, and it compares the observed SF standard deviation σ_{SF} with that predicted by the ray-tracing tool. The results presented in **Paper C** are summarized in Table 3.2. As observed, the ray-tracing tool tends to underestimate σ_{SF} and occasionally shows high inaccuracies when predicting the signal trends along the path. Details can be found in **Paper C**, where it is claimed that this is mostly due to map inaccuracies in the 3D building database. However, ray-tracing inaccuracies remained after the 3D maps were updated, suggesting that this estimation approach is not suitable for QoS prediction purposes.

The data-driven approach also shows high estimation error for the UAV use case. However, the estimation error can be further reduced using real-time data from the UE moving along the route. As it can be observed in Fig. D.5 of **Paper D**, each of the users will observe an offset in the measured RSRP with respect to the estimation provided by the data-driven approach in the pre-service stage. This offset is referred to as Mean Individual Offset (MI0), and it is where the propagation differences between the V2X and the UAV use cases are mostly noticed, as it will be explained in the following subsection.

2.2 On-service Stage

As it is shown in Eq. A.3 in **Paper A**, if known, the Mean Individual Offset (MIO) can be corrected, leading to a decrease in the estimation error. Figures A.5 and A.7 in **Paper A** show the MIO of each UE in the ground level use case for rural and urban environments, respectively. The MIO is consistent for UE traces from phones oriented towards the same direction, suggesting that UE orientation is the main factor impacting the MIO. Considering also that the

signal reaching the receiver will be subject to the effects of the directional antenna patterns of the devices, **Paper B** presents an attempt of compensating for it. Results conclude that the practical challenges of accounting for all possible signal interactions do not provide enough reduction of the estimation error.

Therefore, **Paper B** proposes an alternative method to exploit the consistency of the MIO between UEs in the same orientation, The method is described using the scheme of Fig. B.9, and it consists of comparing current estimation error samples with estimation error distributions observed by previous UEs. **Paper B** presents the tests and corresponding results performed for the ground level case. Fig. B.10 shows a good match between the actual MIO values for each UE trace in the urban environment and the predicted ones using the MIO correction approach. Results are summarized in Table B.6 in **Paper B**, where the achievable estimation error observed in **Paper A** is reached after MIO correction.

While the error is mainly constant in the ground-level use case and can be corrected once for the whole route, it varies in the air. This can be observed in Fig. 3.3, where the different UE traces show very similar trends on the ground but not in the air. The difference is due to a higher impact of the directional antenna patterns in the UAV scenario, characterized by pure LOS conditions. Therefore, the MIO correction needs to be updated every certain distance. Fig. D.3 in **Paper D** shows the scheme of what we refer to as sliding window MIO correction method, and results in Table D.1 show that it can significantly reduce the overall estimation error.

The on-service estimations improve the overall estimation errors for all studied cases. As explained in Chapter 2, these estimations have different uses. The following section presents a potential use studied in this thesis, consisting of estimating the expected service availability and reliability along the route.

3 Outage Probability Estimation

In this thesis, the RSRP estimations are used to estimate the expected service availability and reliability that UEs using mission-critical services will experience. **Papers B and D** present the results for the ground and UAV cases, respectively.

The main objective is to detect those areas in the route where the probability that the service availability and reliability requirements will not be met is high. As previously mentioned, requirements will vary depending on the service. A segment of the grid will be declared critical if the service requirements are not met. For performance evaluation, we compare the recorded critical areas to the estimated ones and use classification metrics. Since we

Table 3.3: Service availability estimation results. Summary for all studied scenarios and estimation approaches.

Scenario	Estimation Approach	TPR [%]	FPR [%]
Rural Ground γ_{RSRP} **= -115** dBm	Data-driven *Pre-service*	85	4
	Data-driven *On-service*	74	3
Urban Ground γ_{RSRP} **= -100** dBm	Okumura-Hata	100	96
	3GPP 38.901	70	38
	Ray-tracing	63	31
	Data-driven *Pre-service*	94	16
	Data-driven *On-service*	99	10
Rural UAV γ_{RSRP} **= -100** dBm	Data-driven *Pre-service*	81	50
	Data-driven *On-service*	88	23

are after the correct estimation of as many critical areas as possible, we aim to maximize the True Positive Rate (TPR). However, we would also like to minimize the False Positive Rate (FPR) to avoid a waste of resources by taking action against non-existent upcoming critical areas.

3.1 Service Availability

Service availability is obtained calculating the probability that the estimated RSRP is below a certain threshold γ_{RSRP}, as show in Eq. B.3 in **Paper B**. It considers the estimated RSRP value $\widehat{RSRP}$ at a segment and the corresponding estimation error distribution $\mathcal{N}(0, \sigma)$.

Results for all studied scenarios are summarized in Table 3.3. We first focus on the performance comparison of the data-driven approach with traditional methods. Based on the RSRP estimation accuracy of the traditional approaches, it is expected that the estimation of the critical areas shows less accurate results. As it is shown if Fig. B.12 in **Paper B**, the empirical methods seem to underestimate the signal. This, and the high RSRP estimation error, causes the availability estimations to declare all segments in the route as critical due to the low estimated RSRP values, confirming that these methods are not suitable for service availability estimations. Even though better results are observed when using ray-tracing estimation, the performance is

still poor. The best results for the pre-service stage in the urban scenario are observed with the data-driven approach.

Secondly, we compare the pre-service stage estimation with the on-service stage estimations. One would expect that, since the overall RSRP estimation error is better in the on-service stage, the service availability estimations would show improved performance compared to the pre-service stage. This is true for the ground urban and the rural UAV scenarios. However, the rural ground scenario, presents a lower percentage of detected critical areas. In the urban ground case, the MIO is constant along the whole route, while in the rural ground case, despite being more stable than in the air, it may vary along the 15 km route. This can cause some inaccuracies in the corrected RSRP estimation, leading to worse performance in the service availability estimations. For the rural UAV, since sliding window MIO is used, the improved RSRP estimations lead to more accurate critical areas detection. Examples of service reliability estimations for ground and UAV cases can be seen in **Papers B and D**, respectively.

3.2 Service Reliability

For service reliability estimations, we first calculate the SIR using RSRP recorded data from the serving and the neighboring cells and an estimation of the load. We calculate SIR for low, medium, and high estimated load values. The SIR traces are compared to recorded Modulation and Coding Scheme (MCS) traces and, as shown in Fig. D.7 in **Paper D**, there is a good match, suggesting that the SIR approximation is correct. For SIR *estimation*, the same calculation approach is followed, but now using the RSRP estimations of the serving cell and the neighboring cells instead, as shown in Eq. B.8 in **Paper B**.

For service reliability critical areas, we calculate, for each segment, the probability that the SIR is below a certain threshold γ_{sir} using Eq. B.3 in **Paper B**. Results for all studied scenarios are summarized in Table 3.4. For all cases, MIO correction results in a decrease of both the TPR and the FPR. As aforementioned, the main objective is detecting the critical areas to avoid potential drops in service reliability. However, high FPR can lead to a misuse of resources, so it is also important to minimize it. On that basis, MIO correction should depend on the service priorities. Service reliability estimations could be further improved by using real load values for each of the neighboring cells involved in the calculation of the SIR. Further details can be found in **Papers B and D**.

Table 3.4: Service reliability estimation results for an average load of 30 %. Summary for all studied scenarios and estimation approaches.

Scenario	**Estimation Approach**	**TPR** [%]	**FPR** [%]
Rural Ground γ_{SIR} **= -3** dB	Data-driven *Pre-service*	72	38
	Data-driven *On-service*	65	28
Urban Ground γ_{SIR} **= -3** dB	Data-driven *Pre-service*	88	41
	Data-driven *On-service*	77	31
Rural UAV γ_{SIR} **= -3** dB	Data-driven *Pre-service*	69	28
	Data-driven *On-service*	67	23

4 Summary of Main Findings

This section outlines the main findings of the Ph.D. study and includes Tables 3.5 to 3.7, which summarize the content of the papers. The main findings of this thesis can be summarized as:

- Use of the data-driven approach provides more accurate RSRP estimations than other approaches available in the literature, as shown in Fig. 3.4.
- UE orientation is the main factor affecting the individual offset observed by a UE.
- Correction of the offset can only be done using real-time data, exploiting the estimation error observed by previous UEs in the route.
- Due to a more pronounced effect of the directional antenna patterns of the UEs, UAV estimations require specific on-service stage corrections.
- The data-driven approach allows detecting at least 70 % of the critical areas of the route, thus not fulfilling the typical 95 % target.

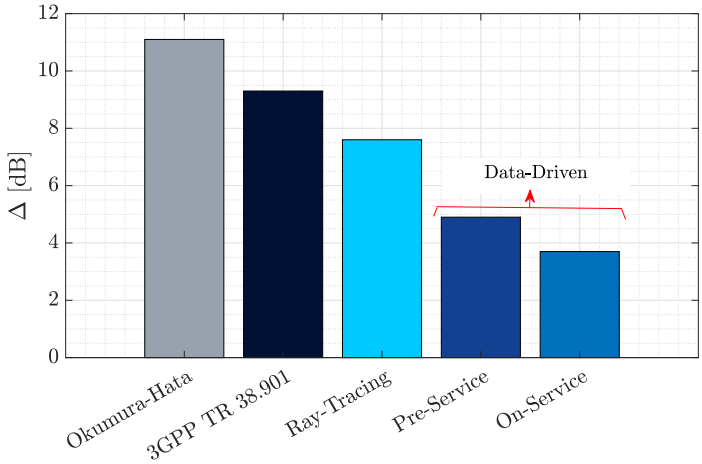

Fig. 3.4: Performance comparison of the data-driven approach (pre-service and on-service) with ray-tracing and empirical methods.

Table 3.5: Paper summary I: use case, measurement campaign, and objectives.

Paper ID	Use Case	Measurement Campaign		Objectives
		TSME Scanner	*Phones*	
A	V2X	Located in the car top carrier, connected to an omnidirectional antenna mounted horizontally.	Different setups (A, B & C). See papers.	- Description of the data-driven estimation approach. - Performance evaluation of the pre-service stage data-driven approach.
B				- Presentation of the two-stage framework concept. - Performance comparison of the data-driven approach with traditional methods. - Description and performance evaluation of the MIO correction method. - Evaluation of critical areas estimation in terms of service availability and reliability.
C	UAV	Hanging from the drone fuselage. Connected to an omnidirectional antenna, mounted 50 cm above the drone fuselage.	Not used	- Feasibility study on the use of ray-tracing for shadow fading prediction using IRT and DPM. - Comparison of measured RSRP trends with traces predicted by the ray-tracing tool.
D		Not used	Phones Drone	- Performance evaluation of the data-driven approach (pre-service and on-service stages). - Description and performance evaluations of the sliding window MIO correction method. - Evaluation of critical areas estimation in terms of service availability and reliability.

Table 3.6: Paper summary II: scenario and numerical results. Δ is the estimation error.

Paper ID	Scenario	Numerical Results Summary
A	Rural *15* km *stretch*	- Pre-service Δ: 6.3 dB - Achievable Δ after MIO correction: 4.9 dB
	Urban *3.3* km *loop*	- Pre-service Δ = 4.9 dB - Achievable Δ after MIO correction: 3.6 dB - Data-driven shows Δ 3 dB better than ray-tracing and up to 6 dB better than empirical.
B	Rural *15* km *stretch*	- Achieved Δ after MIO correction using z-test with real-time data: 5.1 dB - Average on-service stage critical area detection: 70 % - Average on-service stage critical area misdetection: 20 %
	Urban *3.3* km *loop*	- Achieved MIO correction using z-test with real-time data: 3.7 dB. - Average on-service stage critical area detection: 88 % - Average on-service stage critical area misdetection: 21 %
C	Urban *17 streets* *@10* m, *15* m, *30* m	- Predicted σ_{SF} is generally 2 dB below measured σ_{SF}. - Correlation coefficient between predicted trends and measured trends range is from -0.6 to almost 1.
D	Rural *5* km *stretch* *@ 50* m	- Pre-service Δ: 4.8 dB - On-service Δ using sliding window MIO correction: 2.7 dB. - Average on-service stage critical area detection: 78 % - Average on-service stage critical area misdetection: 23.3 %

Table 3.7: Paper summary III: conclusions.

Paper ID	Conclusions Summary
A	- Pre-service data-driven estimations provide accurate RSRP estimations. - Improved performance was observed with respect to other estimation approaches. - Data-driven estimation can be improved if MIO is corrected.
B	- MIO correction cannot be performed in the pre-service stage. - The estimation error can be reduced to the achievable by using error distributions from previous UEs and comparing them with real-time data of the moving UE. - A high percentage of critical areas can be detected, but there is a trade-off with misdetection. - The algorithm does not predict the 95 % target, but it shows the best performance observed in the state if the art.
C	- Ray-tracing can be used to estimate the UAV radio channel if accurate maps of the environment are used.** ***While this is true for overall shadowing predictions, the accuracy is low when predicting specific trends and variations along the UAV path.*
D	- Data-driven approach can be used for RSRP estimation in the UAV case. - Slight modifications are required in the MIO correction method due to a more pronounced effect of the device antenna pattern in the air. - Performance in critical area detection shows similar trends to the ones observed on the ground.

Chapter 4

Conclusions

Cellular networks are used to provide reliable communications for mission-critical services. This use case could benefit from predictive mechanisms (radio conditions, radio resources, traffic, etc.) since predicting a potential service degradation would allow to mitigate it proactively, reducing or avoiding the damage caused by it. This thesis provides an in-depth experimental analysis and develops a framework for predicting service degradation for mission-critical communications in practical V2X and UAV scenarios. The work proposes a two-stage framework: pre-service and on-service. The pre-service stage occurs before the UE uses the service and allows for route planning and optimization. The on-service stage occurs once the service has started and allows for mobility, RRM and QoS management optimization.

Among the different metrics that can be predicted to avoid service degradation, this thesis aims at providing accurate RSRP predictions, primarily due to two reasons. First, RSRP is a metric used for fundamental radio procedures, and in-advance awareness of the UE experienced RSRP values can allow for proactiveness in all of them. Second, the RSRP observed in a specific location is more resilient to load and interference variations than other metrics, allowing to provide an estimation for all UEs at any time of the day in that location.

The first part of this study focuses on signal strength estimation. The proposed estimation approach uses experimental data and aggregates the RSRP values reported from different UEs in a specific location, regardless of their serving cell. The evaluation of the algorithm is done for two scenarios (rural and urban) and use cases (V2X and UAVs) with different propagation conditions. The ground-level urban environment, characterized mainly by NLOS conditions, presents the lowest estimation error with the data-driven approach. The observed *repeatability* of the signal levels in the urban scenario is high due to the increased multipath propagation in this environment. The

signal levels observed by the different phones follow the same trends, which results in lower estimation errors. The rural environment, on the other hand, is mainly characterized by LOS conditions, and the signal levels experienced by UEs in different orientations present slightly different trends in some parts of the route. This is due to a more pronounced effect of the directive antenna patterns of the devices in the rural environment, and causes an increase in the overall estimation error. The effect of the directive antenna patterns is even higher in the air, where there are improved LOS conditions, and different cells are serving the phones in a specific location.

The study compares the performance of the data-driven approach with empirical approaches and ray-tracing estimations. For the ground-level case, the comparison is made for the urban scenario. Results show that the data-driven approach outperforms empirical and ray-tracing methods. In the UAV case, ray-tracing is evaluated for shadow fading prediction only. Results show that ray-tracing typically underestimates the signal variations, resulting in a lower estimated standard deviation of the shadow fading σ_{SF}. The estimation error observed when using traditional approaches suggests that these are not suitable for the purpose of this study, as highly accurate estimations are required.

Each UE presents a mean individual offset (MIO) with respect to the estimated value. The data-driven estimations can be improved in the on-service stage by using real-time data from the UE moving along the route. After evaluation of MIO correction in the pre-service stage, it is concluded that real-time data is needed. On-service correction is performed by comparing the estimation error samples observed by the current UE with error distributions from previous UEs in the same route. A statistical test determines whether the observed samples belong to a certain error distribution. If the test is positive, the mean value of the distribution is used as a correction offset. While at ground level, the MIO can be corrected once for the whole route due to the consistency of the offset, it needs to be updated in the UAV case. The on-service MIO correction reduces the overall estimation error for all studied scenarios, reaching a very low overall estimation error, particularly in the UAV case.

Last, this work studies the estimation of the probability of RSRP or SIR being below a certain threshold, using the signal strength estimations obtained through the data-driven approach. These probabilities are used for in-advance detection of the critical areas in the route. Compared to the probabilities calculated based on the experimental data, results show that the data-driven approach allows for at least 70 % of the critical areas to be detected. Misdetection can reach 40 % for some scenarios. For most of the studied cases, the target of 95 % critical areas detection is not met.

The main key takeaways of the work presented in this thesis can be summarized as follows:

- **A measurement-based estimation can improve the estimation error of ray-tracing by 3 dB and more than 4 dB for empirical methods. Using real-time data can improve user-specific data-driven estimations once the UE is using the service.**
- **Good visibility conditions and lack of obstacles increase the effect of directive antenna patterns in the UE, causing lower *repeatability* and higher estimation error for the presented data-driven approach. This effect is more pronounced in the UAV scenario, with improved visibility conditions.**
- **Despite not meeting the 95 % target, the data-driven provides better performance for RSRP estimations than much of the work available in the literature, and the network may use it for predicting service degradation.**

As part of future work, it would be interesting to investigate the system-level gain provided by estimating a critical area and mitigating it before it occurs. If, e.g., a service reliability drop is estimated due to an SIR drop, the network can activate an interference mitigation mechanism. In the same way, the damage caused by false critical area prediction can be explored. Future work could also be extended with the exploration of different uses of the accurate RSRP data-driven estimations: mobility management (e.g., prepare and execute HO based on the estimations), power control, or other procedures.

Part II

Papers

Paper A

Experimental Evaluation of Data-driven Signal Level Estimation in Cellular Networks

Melisa López, Troels B. Sørensen, István Z. Kovács, Jeroen Wigard and Preben Mogensen

The paper has been published in the
IEEE 94th Vehicular Technology Conference (VTC-Fall 2021)

The layout has been revised.

Abstract

Estimating accurately the signal levels that a user equipment experiences along a movement route is a key step in the process of providing and guaranteeing the required service quality. Obtaining accurate location-specific estimations of the signal level is challenging due to its random variations. In this paper we investigate the use of aggregated measurements from multiple User Equipment (UE) to estimate the serving Reference Signal Received Power (RSRP) that the user will experience along a route. We use Long Term Evolution (LTE) measurements obtained in rural and urban areas from drive tests and analyze the dependence of data variability. Results show that the accuracy of data-driven estimation is impacted significantly by the variability in the underlying data due to UE orientation, UE characteristics and their immediate environment. With compensation for a subset of these effects the standard deviation of the estimation error can be lowered from an overall approximately 8 dB down to 4 dB.

1 Introduction

The need of accurate estimations and/or predictions of the Key Performance Indicators (KPI) involved in a wireless communications system is becoming more obvious with the wide variety of services and real-time applications that the upcoming 5G New Radio (NR) is aiming to provide. Some applications, such as the critical type of communications as e.g., Vehicle-To-Everything (V2X) [1] or Unmanned Aerial Vehicles (UAV) [2], will have strict latency and/or reliability demands in order to meet the required Quality of Service (QoS).

Estimating accurately the signal levels that would be experienced by aUser Equipment (UE) along a route allows to evaluate the service availability and reliability with certain accuracy, e.g. Signal-To-Interference-Plus-Noise Ratio (SIR) along the route before the UE starts using the service. This can be specifically useful for the mentioned critical services, where reliability planning ahead is involved.

There are different approaches to estimate signal strength. Traditional empirical and statistical models are inferred from measurements and aim for the generalization of the estimation in a specific environment, which compromises their location-specific accuracy [3]. An alternative method for signal strength estimation are deterministic models such as ray tracing or other physical-based models. These methods provide more accurate estimations but are computationally complex and require detailed modelling of the environment [4].

Another option for estimating signal strength is using a data-driven approach. It is specified in [5] that the network may require the UE to provide

radio measurements such as its Reference Signal Received Power (RSRP) associated with the corresponding location information. This feature, known as Minimization of Drive Tests (MDT), was standardized as part of 3rd Generation Partnership Project (3GPP) Release-10 specifications for Long Term Evolution (LTE), and it is typically used by network operators for optimization purposes. Data-driven RSRP estimation could be performed using radio measurements that could be easily acquired exploiting the MDT feature. The RSRP estimations obtained would be location-specific. A drawback of this approach, as we will explore in this paper, is the impact from device heterogeneity due to antenna patterns and coupling effects, device orientation and placement, and how they interact and compare with the variability caused by the random nature of the wireless propagation channel. Other potential inaccuracies introduced by MDT such as positioning and quantization errors or scarcity of user reports are discussed in [6].

In our experimental evaluation we have limited the number of different devices to two specific UE models, but included these in many different configurations within our measurement setup. The two models have been verified to have significantly different radiation patterns, but are calibrated to remove average measurement offsets. Any offset in our analysis will therefore result from the mentioned heterogeneity effects, which cause the real variability in the data. Implementation (chipset) specific measurement offsets will occur in reality but are degenerate to those effects. In addition, we have performed measurements in two different environments – urban and rural – to see the impact of any interaction between propagation environment and devices. This methodology attempts to include a similar range of diversity as if we had included several different UE models in our analysis. RSRP measurements have been collected over several measurement drive tests in an LTE network in Denmark. For data aggregation we use the geometric average of the collected RSRP data. The specific contribution in our work is the identification of factors that significantly impact the accuracy of the data driven approach and therefore should be accounted for when processing measurements obtained from MDT. Not only do such corrections significantly improve the accuracy of the data driven approach, but it also gives a clear performance improvement over the alternative use of ray-tracing.

Several approaches have been proposed in the recent years to improve accuracy in the signal level estimation, most of them using machine learning techniques. In [7] the authors use a neural network to estimate path loss, and achieve an estimation error of 6-7 dB standard deviation depending on the frequency. The authors of [8] propose the use of a convolutional neural network and satellite images to estimate path loss, achieving a Root Mean Square Error (RMSE) between 6 dB and 9 dB with standard deviations of up to 6 dB depending on the scenario used for testing the model. In [9] they propose a feed-forward neural network to predict path loss. Using field

measurements from different environments, they achieve an RMSE of 6.3 dB.

These studies provide better accuracy than traditional approaches. They rely mainly on regression or learning techniques and require training and testing over different environments. Differently from the existing literature, the work in this paper is a simple approach that provides a realistic estimation of the actual signal levels experienced by the user at a specific location without additional features in the network.

The rest of the paper is organized as follows: Section 2 shows the measurement campaign details. Data processing and estimation procedures are shown in Section 3 and Section 4 presents the obtained results. Conclusions are presented in Section 5.

2 Measurement Campaign

A drive test was carried out using four commercial smartphone devices with Rohde&Schwarz QualiPoc firmware and a TSME professional radio scanner[1]. The use of mobile devices with specific measurement capability limits the number of available device models. However it considerably eases the data collection and ensures a consistent, calibrated and regular measurement update rate as a basis for our analysis. The scanner was connected to a reference paddle antenna in a fixed position. The reference antenna was mounted horizontally outside and on top of the car with its main lobe extending to both sides of the car. It served to check the repeatability between measurements e.g. impact of changing network and environment conditions (fast fading, load/interference, etc.).

With respect to the smartphone devices, we used two different models from the same vendor: two Samsung Galaxy S5 ($S5_1$, $S5_2$) and two Samsung Galaxy S9 ($S9_1$, $S9_2$) and positioned them in a total of 8 different orientations. We drove several times along two different scenarios in different directions to ensure as much variance (in terms of received signal levels in the different phones) as possible in our data.

All phones and scanner were locked to measure a 20 MHz LTE carrier in the 1800 MHz band. The phones had a sampling rate of 500 ms and were forced to be in active mode during the whole test. Each recorded measurement from the phones consisted in the RSRP of the serving cell and its corresponding Physical Cell ID (PCI). Differently, the scanner provided the RSRP and corresponding PCI of all the visible cells in the 1800 MHz frequency band. Location of the devices was tracked during the test using GPS. The instantaneous RSRP measurements recorded by the phones and the scanner are subject to L1 and L3 filtering. As explained later in Section 3, they are

[1]QualiPoc and TSME ©Rohde & Schwarz more information can be found at https://www.rohde-schwarz.com

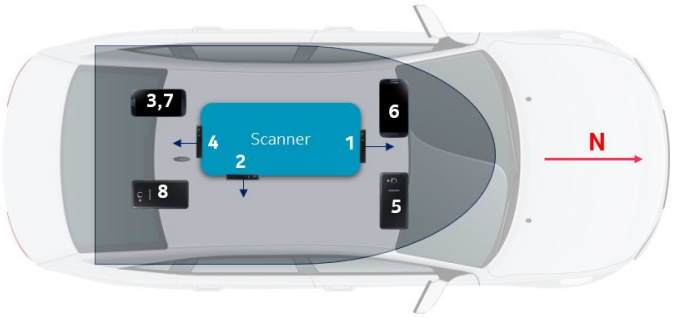

Fig. A.1: Phones-Scanner positions in the car top carrier. *Phone ID* in Table A.1.

Table A.1: Measurement Setups Description

ID	Phone	Setup	Position	Orientation
1	$S5_1$	A	Standing	N
2	$S5_2$		Standing	E
3	$S9_1$		Laying	Up
4	$S9_2$		Standing	S
5	$S5_1$	B	Laying	Down
6	$S5_2$		Laying	Up
7	$S9_1$		Laying	Up
8	$S9_2$		Laying	Down
9	$S5_1$	C	Front Seat	E
10	$S5_2$		Glove Compartment	Up
11	$S9_1$		Back Seat	Up
12	$S9_2$		Trunk	Up

also spatially averaged, which reduces the fast fading effects and measurement errors [10]. According to our calibration test, this reduces the RSRP measurement error of the estimation to below ± 1 dB in all cases.

The measurements were performed using three setups (A, B and C) where the phones had different orientations. The orientation and position for each phone in every setup is included in Table A.1, where the north reference is the front of the car. The reader can locate in Fig. A.1 the ID numbers from Table A.1 for better understanding. For setups A and B, the phones and the scanner were mounted (laying or standing) in a car top carrier, while for setup C the phones were moved inside the car, keeping the scanner in the top carrier.

The measurement campaign was conducted in rural and urban scenarios nearby and in the city of Aalborg (Denmark, Sept. 2020). The measurement route for the rural environment consisted of two round-trips in a 14.8 km stretch from point X to point Y, whereas in the urban scenario the car drove

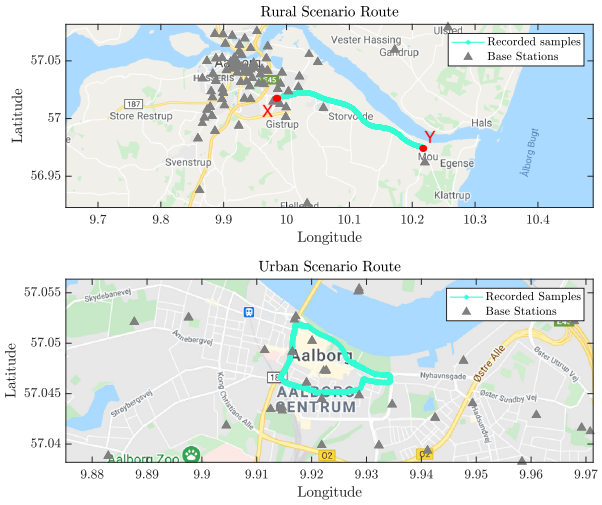

Fig. A.2: Measurement Areas.

three times along a 3.3 km loop (see Fig. A.2). An average driving speed of 65 km/h was kept in the rural case, while it was 22 km/h in the urban scenario. The averageBase Station (BS) height in the LTE networks is 29 m and 24.7 m for the rural and urban scenarios, respectively. BS heights ranging from 20 m to 39 m and down-tilts between 3 and 6 degrees are observed in the rural case while the urban scenario presents heights between 10 m and 58 m, and down-tilts within 0 and 10 degrees. The rural radio environment is mostly characterized by LOS conditions. The urban scenario is a city center, where the average height of the buildings is approximately 15 m and conditions are dominantly Non-Line-Of-Sight (NLOS). In both cases, the terrain profile is flat and on average 5 m above sea level.

3 Data Processing

The reference estimation is obtained by averaging signals recorded by multiple UEs that have previously passed through a certain route. We use the RSRP measurements recorded by all the different phones to obtain a statistical estimation of the average signal level that any user will experience in a specific location. The metric chosen for data aggregation is the geometrical mean.

Each measurement route was split in a *distance grid* of J segments of 10 m as shown in Fig. A.3. For each UE and run/loop, the measurement trace of the serving cell recorded by that UE was located in the distance grid, av-

eraging (also using geometrical mean) all the data points located within the same 10 m segment. This further reduced the fast fading effects and measurement errors aforementioned. The number of samples recorded by each phone in one segment depends on the driving speed: for the rural scenario we observed 1-2 samples per segment, while for urban case, 4-5 samples per segment were recorded. For cases where a handover occurred in the middle of the grid segment, we used only the samples related to the serving cell with the highest number of recorded samples within that 10 m segment.

For each segment in the distance grid we have available a set of values corresponding to measurements recorded by multiple UEs in the different runs or loops. Regardless which cells are serving those UEs the measurements are aggregated to one average signal level estimate. The main reason for this approach is data sparsity as we will discuss in the results section. Aggregating all values provides a continuous and more reliable estimate of network availability along that route. Furthermore, aggregating serving cell measurements irrespective from the serving PCI is a reasonable approach if we aim to estimate the expected average signal level in a segment, since the cell selection/re-selection procedures tend to equalize the measured signals, minimizing the effect of distance between the UE and the corresponding serving BS. The aggregation process is illustrated in Fig. A.3, where each segment in the distance grid, from seg_1 to seg_J, has an estimated value which is obtained using the geometric average from all the values in the corresponding segment from UE_1 to UE_N, regardless which cell these users are connected to. The **RSRP estimation** for that location (10 m segment) is the mean, in logarithmic scale (dBm units), of that set of values.

$$\widehat{RSRP}_{seg_j} = \frac{1}{N}\sum_{i=1}^{N} RSRP_{i,seg_j} \tag{A.1}$$

where $\widehat{RSRP}_{seg_j}$ is the RSRP estimated value in the grid segment j, and $i = 1, ..., N$ indexes the collected values in that location (10 m grid segment). N is different for each environment:

- Rural: 4 phones, 3 setups, 4 runs (two round-trips) gives N = 48 recorded values for the mean. With a stretch length of 14.8 km, Number of segments is 1480.
- Urban: 4 phones, 3 setups, 3 loops gives N = 36 recorded values for the mean. With a stretch length of 3.3 km, Number of segments is 330. Only one driving direction was measured due to traffic restrictions.

The radio network scanner data was used as a reference, so that measurements on the same serving cell PCIs as the phones were extracted in each case. The same averaging process over the 10 m *distance grid* was applied to

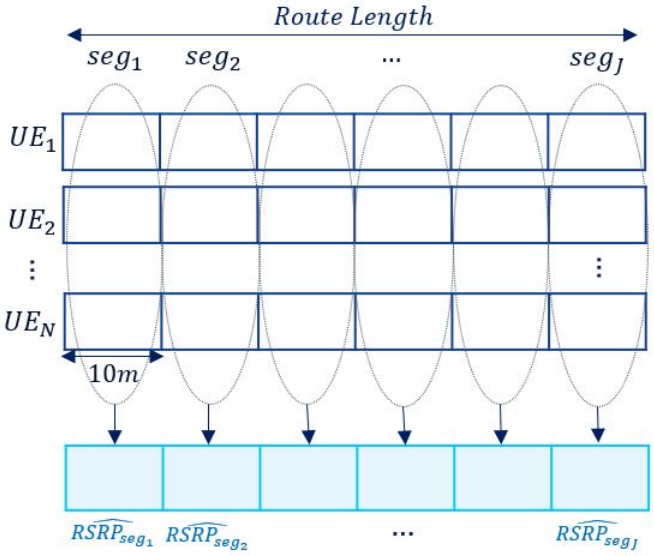

Fig. A.3: Measurement averaging and distance grid scheme. Estimations (blue lowest row) are built using measurements from multiple UEs (white upper rows).

this data, and an estimation for each UE based on scanner data was obtained for each grid segment. An average of 5 and 8 samples per segment was used for the rural and urban environments, respectively.

To evaluate the accuracy of the RSRP estimation, we calculate for every segment of the grid the difference between the estimated value and each of the measured values used to obtain the estimation at that grid segment. The estimation error Δ (in dB) for a UE i in a grid segment j is defined as:

$$\Delta_{UE_i,seg_j} = RSRP_{UE_i,seg_j} - \widehat{RSRP}_{seg_j} \tag{A.2}$$

where $RSRP_{UE_i,seg_j}$ is the actual measured value by a certain UE i in grid segment j and $\widehat{RSRP}_{seg_j}$ is the estimated value for grid segment j. The error is calculated for each of the N available UEs ($i = 1, ..., N$) used to estimate the average signal level at segment j.

To evaluate the estimation accuracy over all samples we use the mean and standard deviation of the estimation error in Eq. A.2. We aim to obtain an error distribution with a σ as low as possible as this would indicate that the difference between the estimation and the actual values of the individual phones is low in expectation regardless the UE and its driving direction or orientation. The distribution of the estimation error, as shown further in Section 4, is generally well behaved for all the analyzed cases, having a symmetric uni-modal characteristic with good approximation to a Gaussian

distribution. It therefore motivates our choice of the mean aggregation function based on the logarithmic signal values since mode, median and mean degenerates to the same case.

Furthermore, instead of evaluating the distribution of the estimation error for all phones, the mean μ and standard deviation σ of the estimation error is shown for each individual UE and run separately (as later shown in Fig. A.5). This allows to observe the mean individual offset of each phone with respect to the overall mean value (estimation). We also evaluate the effect that removing the phone individual offset has in the overall standard deviation by subtracting, for each of the phones, their corresponding mean value μ. The estimation error (in dB) is in this case calculated as:

$$\Delta'_{UE_i,seg_j} = RSRP_{UE_i,seg_j} - \mu_{\Delta_{UE_i}} - \widehat{RSRP}_{seg_j} \tag{A.3}$$

where $\mu_{\Delta_{UE_i}}$ is the mean value of the estimation error for UE_i over the full measurement run.

4 Results

The results presented in this section show how the estimation error in the data-driven estimations is impacted by:

- *Environment effects*: Shown by presenting separately the rural and urban scenarios.
- *UE directional antenna pattern effects*: We present results for devices with different orientations and compare them to the scanner reference measurements.
- *UE driving direction*: Results for rural environment compare estimation error when using a single estimation based on the combined directions with the case where different estimations are used for the two directions.
- *UE Conditions*: Such as e.g. whether the UE is inside or outside the car.

4.1 Rural Environment

Two approaches are followed for the analysis of this environment. First, we evaluate the results obtained when using the $N = 48$ available values to calculate the estimation at each grid segment. Later, we evaluate the two different driving directions separately, i.e. $N = 24$ recorded values are used to calculate the estimation. Therefore, for the latter case, there are two estimations for each grid segment, one for each direction.

A summary of the overall standard deviation for all the studied cases before and after correction of the individual phone offsets can be found in Table A.2. The mean of the distributions of the estimation error is zero regardless the data used for the estimation (combined/separate directions) or the source of it (phones /scanner) due to normalization.

We use the scanner results as a reference considering that its position is fixed for all runs in all setups. The scanner shows a standard deviation of 5.1 dB for combined directions and 4.1 dB and 3.6 dB for the separate directions analysis. This illustrates that the moving direction of the UE will affect its experienced signal level. Cells serving the UEs are mostly different when driving in opposite directions, which is assumed to be one of the causes for the standard deviation of the estimation error to increase when combining directions. For the scanner measurements, variability due to orientation and position is mostly eliminated, but measurements from different cells are combined. Furthermore, in reality there is a small difference in the reference antenna pattern between the two sides of the car, due to the antenna itself and the impact of the car structure. The inherent measurement process will also lead to slightly different results for the two directions due to the temporal evolution of the signals, the impact of interference in the measurement, etc. In general, much of this variability cannot be removed from any measurement.

The phones present a standard deviation of 6.3 dB for combined directions, as observed in Fig. A.4-a, whereas if the two directions are treated separately, the standard deviation is barely reduced to 6 dB (X to Y direction, as shown in Fig. A.4-b) and 5.5 dB (Y to X direction). These values are higher than the ones observed for the scanner, and we assume that this is mainly due to the different UE antenna orientations and placement.

In Fig. A.5 we evaluate the estimation error over the full route for each individual UE in the separate directions analysis. The estimation error is calculated with respect to the corresponding estimated average for each direction (X-Y or Y-X). It can be seen that μ is generally stable between different runs for the same phone and direction. However, different means are observed for each phone, which suggests that the effective antenna patterns and placement have an effect on the received signal. This difference is especially noticeable for setup C, which shows a negative mean for all phones due to the car body blockage. This suggests that the overall standard deviation of the error could be reduced by identifying if the phone is inside or outside the car. The standard deviation shows values varying from 3 dB to 6 dB. These are, for some cases, not consistent between opposite directions. The overall scanner standard deviation is 3.8 dB (average from the two separate directions).

We correct the phone individual offsets as per Fig. A.5 using Eq. A.3. The results show that standard deviation is further reduced to 4.3 dB (as shown

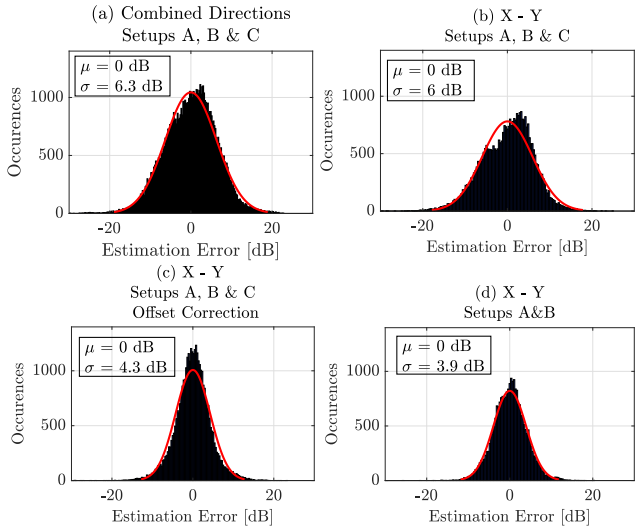

Fig. A.4: Rural Δ distributions for the different compensations applied.

Table A.2: Rural Environment - Std. Dev. Results

	Combined Directions		**Separate Directions @Phones**		**Separate Directions @Scanner**	
	Phones	**Scanner**	**X-Y**	**Y-X**	**X-Y**	**Y-X**
σ [dB] **Before Offset Correction**	6.3	5.1	6	5.5	4.1	3.6
σ [dB] **After Offset Correction**	4.9		4.3	4		

in Fig. A.4-c) in the X to Y direction and 4 dB in the Y to X direction after individual offset correction. These values, as observed in Table A.2, are much closer to the ones obtained with the scanner data. Similar improvements can be obtained by identifying the phones located in the car top carrier i.e., only setups A and B included in the mean value calculation. It is shown in Fig. A.4-d that the estimation error in that case is reduced to 3.9 dB in the X to Y direction and 4.2 dB in the Y to X direction i.e., the error decreases on average 1.7 dB with respect to Fig. A.4-b.

4.2 Urban Environment

The same analysis as previously shown for the rural environment was performed for the urban scenario. Results for this case are summarized in Table A.3. For scanner data an overall standard deviation of 3.3 dB is observed. The phones, on the other hand, show an overall standard deviation of 4.9 dB, cf. Fig. A.6-a. In this scenario, we further compare the results with two ref-

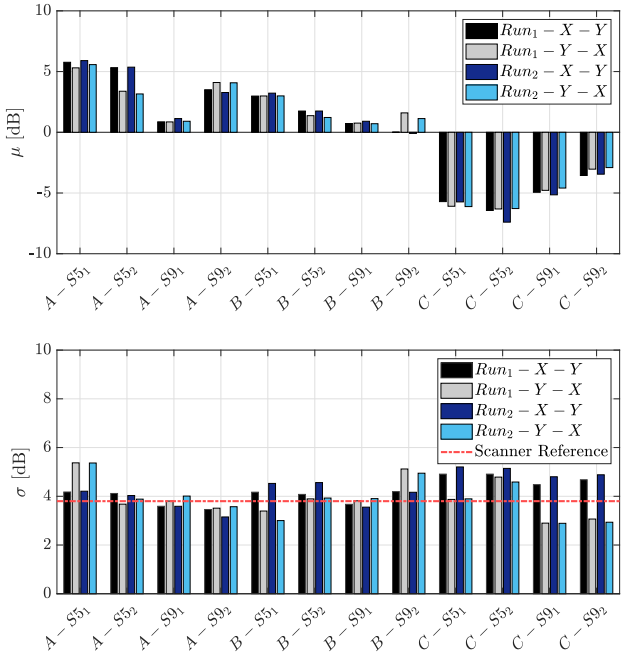

Fig. A.5: Rural environment phone-individual estimation error statistics before mean offset correction.

erence methods. First, we show the results for ray-tracing estimations, which provide a σ of 7.6 dB after calibrating the Dominant Path Model (DPM) [11] with our measurement data. Secondly, the UMa TR38.901 model [12] is used for comparison. The estimations for this model are tuned to Line-Of-Sight (LOS)/NLOS conditions based on ray tracing predictions, and it shows a σ of 9.3 dB when calibrating parameters to this specific scenario. These results illustrate that the data-driven estimation approach can provide much higher accuracy than the traditional methods, as the estimation is obtained using real data from previous UEs passing by that exact same location.

In Fig. A.7 we show the individual analysis for each phone. As it was observed in the rural case, the mean offset for each of the phones is different but stable between different loops for the same phone, and standard deviation varies between 2 dB and 5 dB. Different results are also observed between setups A-B and setup C. We remove the offset for each of the phones individually, and show in Fig. A.6-b the overall standard deviation, which is reduced to 3.6 dB, closer to the scanner reference. Approximately the same effect is observed when excluding setup C from the estimation, which as

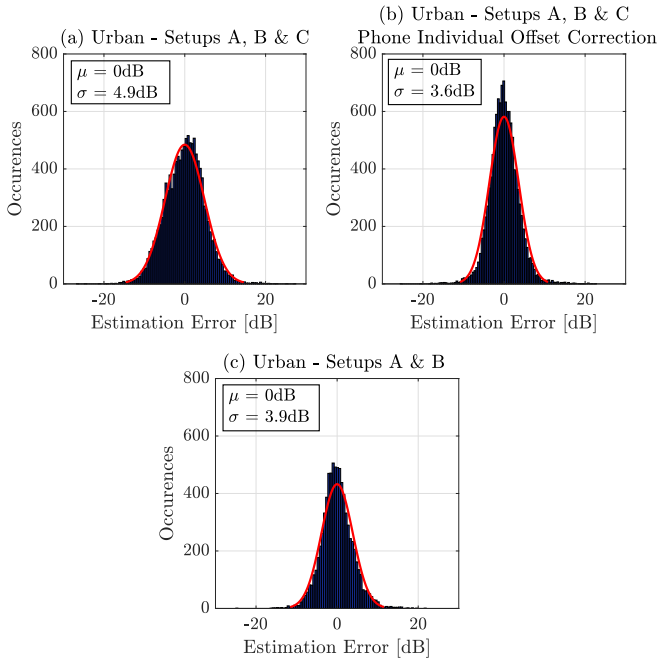

Fig. A.6: Urban Δ distributions for the different compensations applied.

Table A.3: Urban Environment - Std. Dev. Results

	Phones	**Scanner**	**Ray-tracing Reference**	**3GPP 38.901 UMa Reference**
σ [dB] **Before Offset Correction**	4.9	3.3	7.6	9.3
σ [dB] **After Offset Correction**	3.6			

shown in Fig. A.6-c, shows a standard deviation of 3.9 dB.

In the urban scenario propagation mechanisms differ, primarily by the increased multi path propagation compared to the rural environment. Therefore, the impact of UE directional characteristic as we saw for the rural, will be less pronounced and lead to reduced standard deviation.

5 Discussion and Conclusion

Initially we made a choice to aggregate measurements over a segment regardless the serving cell PCI. The choice was mainly in consideration of data sparsity since with cell specific data aggregation it would be difficult to col-

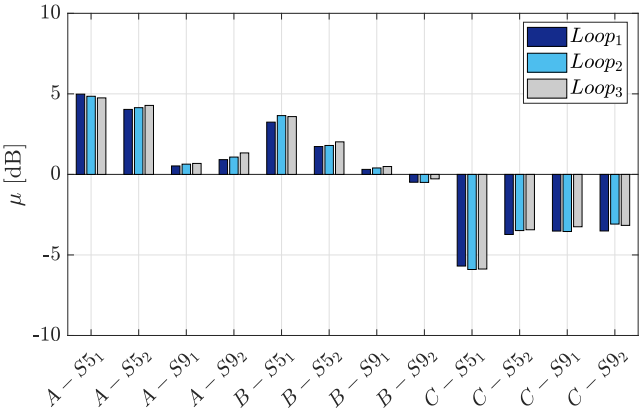

Fig. A.7: Urban environment phone-individual estimation error statistics before mean offset correction

Table A.4: PCI Overlap % in Rural and Urban Scenarios

	Urban	**Rural Same Driving Directions**	**Rural Opposite Driving Directions**
Avg. PCI Overlap [%]	80.3	69.6	53.7

lect a sufficient number of samples to obtain a reliable estimate for each and every grid segment along a route. The main reason for this is that the UEs are not likely to have the same serving cells in a particular segment. Table A.4 shows the summary analysis of the average percentage of grid segments along the route in which the serving cell is the same for different UEs, which we refer to as PCI overlap percentage. The urban scenario is clearly showing the highest average PCI overlap percentage. For the rural environment, the percentage is clearly higher when driving in the same direction than when the opposite directions are analyzed. As one can imagine, the price to pay when mixing measurements irrespective of the serving cell is that more variation is included which in turn leads to higher estimation error. This relates very well to our results, e.g. highest PCI overlap is observed in the urban environment where lowest estimation error is observed, and for the rural case higher PCI overlap is observed between UEs driving in the same direction which also shows lower estimation error than when different directions are combined. There are many factors one could speculate impacting these results, e.g. the distance to the serving cell or the absence or presence of LOS condition. We have investigated most of these factors in an attempt to reduce the estimation error, but have found no clear relation yet.

The main benefit of our chosen data aggregation for the data driven estimation approach is its simplicity and that estimation errors of approximately 3.5 to 4 dB are possible by identifying a few main impacting factors. They can be accounted for by similarly simple means, i.e. having knowledge of the driving direction, as well as approximate location, and being able to remove the UE individual offset resulting from UE placement, orientation and immediate environment conditions. Information on the driving direction reduces the overall standard estimation error by almost 3 dB on average, and another additional 1.5 dB reduction results when accounting for the individual offsets. The estimation of individual offsets is for future work, but a range of methods are available such as based on adaptive filtering or statistical inference.

As we have illustrated by comparison with the use of ray tracing and statistical estimation methods, the data driven approach has the potential to considerably improve the estimation accuracy.

References

[1] 5G Automotive Association, " Making 5G proactive and predictive for the automotive industry," Tech. Rep. White Paper, Jan. 2020.

[2] Vodafone and Ericsson, "Vodafone and Ericsson trial automated flight paths for connected drones," *Press Release, Mobile Europe*.

[3] O. O. Erunkulu, A. M. Zungeru, C. K. Lebekwe, and J. M. Chuma, "Cellular communications coverage prediction techniques: A survey and comparison," *IEEE Access*, vol. 8, pp. 113 052–113 077, 2020.

[4] Z. Yun and M. F. Iskander, "Ray tracing for radio propagation modeling: Principles and applications," *IEEE Access*, vol. 3, pp. 1089–1100, 2015.

[5] 3GPP, "Radio measurement collection for Minimization of Drive Tests (MDT); Overall description; Stage 2," Tech. Rep. 37.320 V10.1.0, Mar. 2011.

[6] H. N. Qureshi, A. Imran, and A. Abu-Dayya, "Enhanced MDT-based performance estimation for AI driven optimization in future cellular networks," *IEEE Access*, vol. 8, pp. 161 406–161 426, 2020.

[7] M. Ayadi, A. B. Zineb, and S. Tabbane, "A UHF path loss model using learning machine for heterogeneous networks," *IEEE Transactions on Antennas and Propagation*, vol. 65, no. 7, pp. 3675–3683, 2017.

[8] J. Thrane, B. Sliwa, C. Wietfeld, and H. L. Christiansen, "Deep learning-based signal strength prediction using geographical images and expert

knowledge," in *GLOBECOM 2020-2020 IEEE Global Communications Conference*. IEEE, 2020, pp. 1–6.

[9] S. I. Popoola, E. Adetiba, A. A. Atayero, N. Faruk, and C. T. Calafate, "Optimal model for path loss predictions using feed-forward neural networks," *Cogent Engineering*, vol. 5, no. 1, p. 1444345, 2018.

[10] 3GPP, "Requirements for support of radio resource management (Release 17)," Tech. Rep. 36.133 V17.3.0, Sep. 2021.

[11] R. Wahl, G. Wölfle, P. Wertz, P. Wildbolz, and F. Landstorfer, "Dominant path prediction model for urban scenarios," *14th IST Mobile and Wireless Communications Summit, Dresden (Germany)*, 2005.

[12] 3GPP, "Study on channel model for frequencies from 0.5 to 100 GHz. (Release 16)," Tech. Rep. 38.901 V16.1.0, Dec. 2019.

Paper B

Measurement-Based Outage Probability Estimation for Mission-Critical Services

Melisa López, Troels B. Sørensen, István Z. Kovács, Jeroen Wigard and Preben Mogensen

The paper has published in the
IEE Access, 2021.

The layout has been revised.

Abstract

An accurate estimation of the service quality that the user will experience along a route can be extremely useful for mission-critical services. Based on availability and reliability estimations, it can provide the network with in-advance information on the potential critical areas along the route. If such estimation is based on empirical/statistical or site-specific estimations, both of which are typically used for cellular network planning, it will lead to significant uncertainty in the estimation, as we demonstrate in this paper. Instead, if estimations are based on previously collected measurements, the uncertainty can be significantly reduced. In this paper, we analyze the achievable accuracy of such a data-driven estimation which aggregates measurements from multiple User Equipment (UE) moving along the same route by averaging the measured signal levels over a route segment. We evaluate the estimation error for both empirical/statistical, site-specific and data-driven estimations for measurements collected in urban areas. Based on the demonstrated advantage of data-driven estimation, and the relevance of including context information that we proved in a previous paper, we discuss and analyze how the estimation error can be reduced even further by predicting the Mean Individual Offset (MIO) that each specific UE will observe with respect to the average. To this end, we propose and evaluate a technique for MIO correction that relies on observing a time series of signal level samples when the UE starts a mission-critical service. By observing 100-300 m *of real-time samples along the route results show that the overall estimation error can be reduced from 5-6* dB *to 4* dB *using MIO correction. Finally, using the obtained results, we illustrate how the signal level estimations can be used to estimate the outage probability along the planned route.*

1 Introduction

5G New Radio (NR) technology is expected to provide connectivity to a wide variety of services with different Quality of Service (QoS) requirements. For some applications, Key Performance Indicators (KPI) such as reliability, latency, or data rate may have stringent targets which will be challenging to meet with the existing Radio Resource Management (RRM), QoS, and mobility management procedures in Long Term Evolution (LTE) [1]. These procedures are mostly reactive, i.e. actions against a drop in the signal level or the QoS are taken after the drop has already occurred. Having prior knowledge of the network conditions that the User Equipment (UE) will experience can help to avoid a situation that can be critical for the service requirements to be met. Therefore, recently proposed solutions have adopted predictive algorithms and aim for more proactive management of the network resources [2, 3].

The service could strongly benefit from proactive QoS management in the

so-called mission-critical communications, such as Unmanned Aerial Vehicles (UAV) or Vehicle-To-Everything (V2X) over cellular networks. The need for this approach is stated by the 5G Automotive Association (5GAA) in [4] where they present the concept of *predictive QoS*, which consists of in-advance notifications from the network to the UE about predicted changes in the QoS. Furthermore, the Aerial Connectivity Joint Activity (ACJA) presents a two-phase operational context for UAVs in [5]. They propose a planning phase where there is the need to determine RF conditions for the planned path and a flight phase where constant monitoring of the requirements is performed and used for predictive mechanisms based on real-time radio KPIs. A similar framework could be expected for autonomous driving in the V2X context.

A relevant parameter for RRM decisions, as well as for QoS prediction, is the signal level experienced by a UE, typically expressed using the Reference Signal Received Power (RSRP) [6]. RSRP is a key measure used for several procedures such as cell selection and re-selection, handover, and power control. Therefore, the estimation of the signal level perceived by a UE in a certain area is essential in the process of designing a reliable system. Accurate estimations of RSRP levels that the UE will experience along the path could provide in-advance information on the expected service availability and reliability conditions.

There are well-known techniques for planning and estimating the signal level using empirical or deterministic propagation models. However, as it will be shown in this article, despite the ability of these traditional techniques to characterize the signal level in a particular environment, their accuracy along specific paths is too low for predictive QoS purposes.

1.1 Contributions

In [7] a data-driven approach for serving cell signal level estimation was presented. The approach aggregates measurements from UEs in the same location and uses their average as an estimation for that location. The technique is shown to achieve an overall estimation error of 5-6 dB, which can be further reduced to 4 dB if the Mean Individual Offset (MIO) of a specific user with respect to the estimation is corrected. The novel contributions included in this article are the following:

- Quantify the advantage of data-driven estimations over statistical and deterministic techniques. We use two empirical models as well as the estimations provided by a ray-tracing tool to show the improved performance of our approach.
- Propose and evaluate an MIO estimation and correction technique that shows an advantage over the use of context information, using real-time measurements of the UE moving along the path.

- Present a framework that estimates areas with a high probability of signal and service degradation that the UE will experience along a route.

1.2 Related Work

Different KPIs can be used to estimate the QoS and outage probability depending on the service requirements. However, RSRP is one of the most critical parameters when designing a cellular network. Furthermore, the authors in [8] show that, unlike other KPIs such as Reference Signal Received Quality (RSRQ) or throughput, RSRP remains stable for long periods and can be modeled as time-invariant. This stability motivates the choice of RSRP, as it ensures that the estimation is valid for any time of the day.

Estimating the propagation conditions is a widely studied topic in the literature. Empirical models are a practical approach where measurements are used to develop statistical models of the channel and estimate path loss for a particular type of environment. Although there are different models for the different propagation scenarios, their accuracy in a specific location is compromised by the generalization of the model. For the urban environment, there are well-known empirical path loss models such as COST-231 Walfisch-Ikegami [9], and Okumura-Hata [10]. On the other hand, geometric models rely on physics to compute the dominant and secondary paths of the radio waves propagating through a specific propagation environment. This approach is generally more accurate than the empirical techniques but more computationally complex. A common implementation of this estimation technique is ray-tracing [11].

The computational cost of ray-tracing, and the lack of accuracy of stochastic models, led to the study of new approaches. In recent literature, there has been extensive work on signal level estimation. The authors in [12] characterize the fluctuations of signal strength using a large measurement dataset in roads and cities. They conclude that, for static periods, the RSRP shows fluctuations between 1.8 and 2.2 dB, increasing up to 6 dB when considering mobility. In [13], the authors propose a two-step algorithm (clustering and k-nearest neighbor) to predict an RSRP map using UE measurement reports and show a Mean Absolute Error (MAE) of 3.5 dB.

More complex approaches based on Machine Learning (ML) techniques can also be found in the literature. The work in [14] fuses crow-sourced measurements from LTE users with other context information to build a predictive model that provides a Root Mean Square Error (RMSE) of 7.4 dB. In [15] the authors present a deep learning approach where they use satellite images to extract the features of the receiver's surrounding environment, obtaining a prediction RMSE of approximately 6 dB. The authors in [16] use a feed-forward Neural Networks (NN) for path loss estimation showing an RMSE of 6.3 dB when testing the algorithm over measurements from differ-

ent scenarios. The work in [17] uses a NN for path loss estimation at different frequencies, resulting in a minimum observed RMSE value of 6 dB. The authors of [18] present path loss prediction using artificial NNs, achieving an RMSE of 7 dB.

The proposed technique in [7] is simple. It exploits UE measurement reports for signal level estimation, providing reasonably improved accuracy compared to the existing traditional and non-traditional techniques, especially after using the techniques presented in this article to correct the MIO of the UE. Unlike the literature mentioned above, the technique in [7] is location-specific, i.e., it provides an estimation of the signal level that the UE will experience in a particular location, regardless of which Base Station (BS) the UE will connect to along the route. The RSRP estimations are used in this article to estimate the outage probability that a particular mission-critical UE will experience along a specific route. This type of estimation is not available in the current literature to the best of the authors' knowledge.

The rest of the article is organized as follows. Section 2 presents our vision on service availability and reliability provisioning for mission-critical communications. In Section 3 we explain how we have obtained the measurements for the analysis in this article, while Section 4 shows a summary of the data-driven estimation approach and results presented in [7] as well as a comparison with the traditional signal level estimation techniques. Section 5 shows results for MIO correction in the pre-service and on-service stages. In Section 6 we exemplify how these estimations can be used to provide information on the outage probability along the route and compare the estimation results with recorded values. Section 7 concludes the paper with a summary of the findings.

2 Service Reliability Provisioning

The mission-critical communication services will most likely require reliability assurance mechanisms within the cellular network. In this context, we build upon the same architecture as specified for QoS sustainability analytics [19], where the Network Data Analytics Function (NWDAF) can notify an external (third-party) application server when QoS degrades over a path of interest.

The Radio Access Network (RAN) is composed of radio cells in the network and handles all radio interface protocols ensuring a minimum QoS can be delivered to the UEs. The core network configures the RAN cells, the analytics function (e.g., NWDAF), and establishes signaling links to the application server for the specific mission-critical service. The application server is assumed to be able to communicate directly with the application layer in the UE.

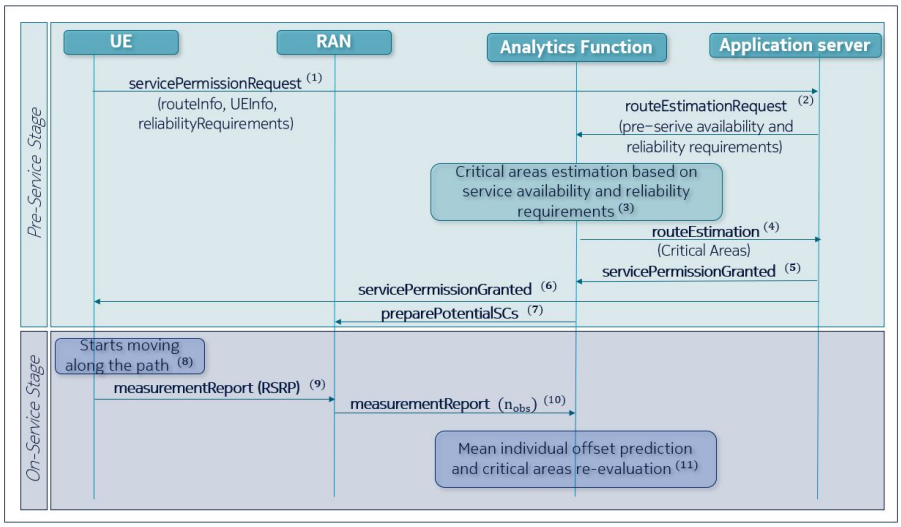

Fig. B.1: Service availability/reliability provisioning scheme.

In our case, following the structure presented in [5], we further consider a two-stage framework for the addressed mission-critical communication services: a "pre-service" and an "on-service" stage, as it is shown in Fig. B.1. The following explanations can be linked to Fig. B.1 through notation $^{(\#)}$.

In the pre-service stage, the application server determines that a UE intends to move along a certain route (e.g., UAV flight or V2X drive)$^{(1)}$ and provides information about the planned movement path to the analytics function$^{(2)}$, which then performs route quality estimations$^{(3)}$. For the route quality estimations, the analytics function can use the measurement-based RSRP estimations, e.g., from all other UEs moving along the same path combined potentially with historical measurement data. The service availability estimation is obtained by considering serving cell RSRP estimations and a certain connectivity threshold. For service reliability, Signal-To-Interference Ratio (SIR) estimations (assuming interference-limited scenarios) can be obtained based on the RSRP reports for the serving and the strongest neighboring cells and compared with the minimum service requirements. RSRP and SIR are used to estimate QoS metrics such as service availability and service reliability, which help to identify the potential critical communication areas along the planned route of the UE. Next, the analytics function replies to the application server with the corresponding route quality estimations$^{(4)}$, and the application server communicates the decision to the UE application e.g., permission to start the mission along the route. Assuming the answer is positive, the application server informs the analytics function$^{(5)}$ and the UE application$^{(6)}$. The analytics function can optionally trigger the proce-

dure to perform more proactive management of the radio resources along the planned movement path of the UE (e.g., prepare potential serving cells)(7).

The "on-service" stage is triggered when the UE starts moving along the planned path(8). Once the UE service is started, the UE reports the measured RSRP values to the RAN(9), which forwards them to the analytics function(10). The analytics function uses these measurement reports to predict the RSRP MIOs for a certain time horizon(11). This allows a more accurate estimation of the service availability and reliability along the route. This information would allow the RAN to take action with regard to critical areas, e.g., activate multi-connectivity or apply interference mitigation techniques before SIR becomes too low, etc. Furthermore, the information could be forwarded to the application server, which could potentially revisit its decision.

3 Measurement Campaign

3.1 Measurement Setup

An extensive LTE measurement campaign was carried out in order to evaluate the data-driven approach. This campaign aimed to collect RSRP measurements recorded by multiple UEs in a specific route.

Four commercial phones with a test firmware (QualiPoc©) and a professional radio network scanner (R&S TSME) [20] were used during this measurement campaign. Using a specific firmware to measure the radio KPIs ensured that the recorded data was consistent, calibrated, and reliable. However, it also limited the number of mobile devices and the available vendors that could be used for the campaign. Two Samsung Galaxy S5 ($S5_1, S5_2$) and two Samsung Galaxy S9 ($S9_1, S9_2$) measured several times the same route in multiple positions and orientations. In this article, we used three different setups (referred to as A, B, and C) to obtain as much UE heterogeneity as possible in terms of experienced signal levels along the route, i.e., to increase variation in the aggregated measurements. Further information on the position and orientation of each of the phones in the different setups can be found in Table B.1. The scanner antenna remained in a car-top carrier during the whole measurement campaign, and so did the phones for setups A and B, as shown in Fig. B.2. During the recording with setup C, the phones were located inside the car. As it will be further explained in Section 4, the recorded data by each of the UEs is averaged to obtain an estimation.

The antenna patterns of the phones were measured using a multi-probe antenna measurement system [21]. Fig. B.3 shows the measured antenna patterns for each of the four phones. As it can be observed, the patterns are similar between the same phone model but significantly different when comparing the S5 and S9 models. As expected, none of them is omnidirectional.

Table B.1: Measurement setups information. The IDs can be used as a reference to identify the phones placement in Fig. B.2.

ID	Phone	Setup	Position	Orientation
1	$S5_1$	A	Standing	F
2	$S5_2$		Standing	L
3	$S9_1$		Laying	Up
4	$S9_2$		Standing	B
5	$S5_1$	B	Laying	Down
6	$S5_2$		Laying	Up
7	$S9_1$		Laying	Up
8	$S9_2$		Laying	Down
9	$S5_1$	C	Front Seat	L
10	$S5_2$		Glove Compartment	Up
11	$S9_1$		Back Seat	Up
12	$S9_2$		Trunk	Up

The different shapes and orientations of the multiple phones will introduce variation within the traces used to build the serving cell RSRP estimation.

A reference paddle antenna was connected to the radio network scanner and mounted in a fixed position with its main lobe extending towards both sides of the car. This reference was used to exclude the effects of the directional patterns of the phones, allowing us to observe the influence of factors that are inherent to the measurement process, such as changes in the network and/or environment conditions.

In our experimental investigations the UE heterogeneity is achieved through:

- Use of two device models with different chipsets and device antenna implementation (type, placement on the frame, coupling to the frame, etc.), which impact the signal levels observed when the devices are moving.
- Position of the mobile devices with their corresponding directional antenna patterns in different orientations outside the car.
- Location of the mobile devices inside the car in one of the setups, such that the effect of the car body blocking the received signal is also included in the aggregated measurements.

As it is shown in [7], to evaluate the accuracy of the estimation in different environments, data was collected in two scenarios distinguished by completely different characteristics: rural and urban. For the rural case, the car drove 2 round-trips along a 14.8 km stretch with each of the 3 setups, recording RSRP measurements for the two different driving directions. In the urban environment, the route was a 3.3 km loop through which the car

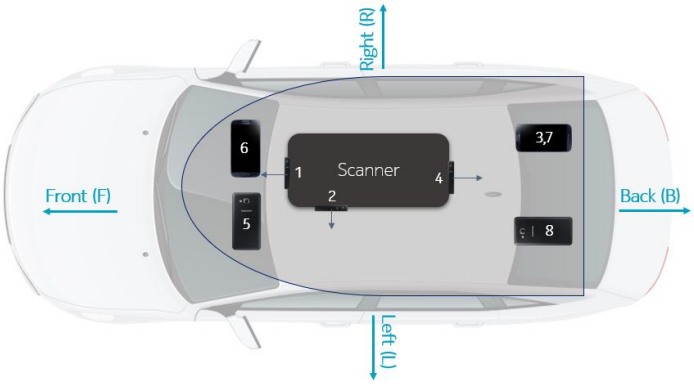

Fig. B.2: Phones placement and orientation in setups A&B in the car top carrier. The numbers in this figure can be mapped to descriptions in Table B.1. The radio network scanner is also shown in the center of the car top carrier. For setup C, the phones were located inside the car.

Table B.2: Relevant measurement campaign information.

	Rural	**Urban**
Carrier Frequency	1800 MHz	
Carrier Bandwidth	20 MHz	
RSRP Sampling Rate	500 ms	
Route Length	14.8 km	3 3km
Avg. Driving Speed	65 km/h	22 km/h
Avg. Recorded Samples/10 m	5	8
Coverage	Sparse	Dense
Visibility	Mainly LOS	Mainly NLOS

drove 3 times with each of the setups in one direction only due to traffic restrictions. Other relevant information regarding the measurement campaign for the corresponding scenarios can be found in Table B.2. For further details, the reader is referred to [7].

3.2 RSRP Recording

The LTE RAN typically configures the UE to report these measurements periodic or event-triggered. The Minimization of Drive Tests (MDT) feature first introduced in Rel-10 [22], allows operators to configure their UEs to report measurements with a specific periodicity to evaluate or improve network performance. This feature could be particularly useful for data gathering in the data-driven estimation approach.

This experiment uses the measurements recorded by the different devices, which go through the L1 and L3 filtering mentioned above. The measure-

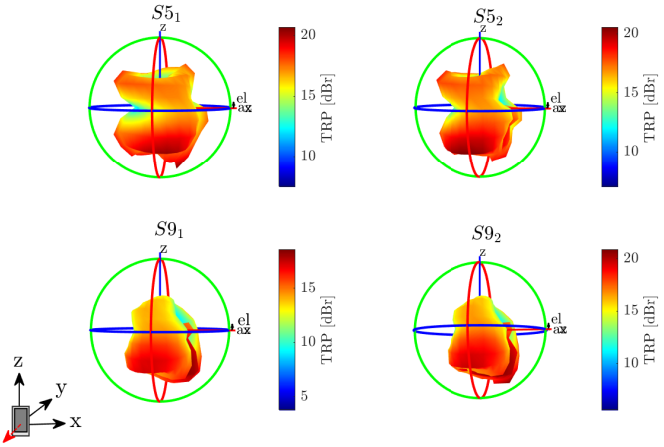

Fig. B.3: Total Radiated Power (TRP) in dBr (relative) of the measured antenna patterns from the different test phones. The position of the phones in the multi-probe antenna measurement system was along the z-axis with their front (screen) facing against y-axis.

ments are obtained with a sampling rate of 500 ms, as shown in Table B.2. To evaluate the variability of the measured RSRP, we performed a static over-the-air test of 6 minutes duration, where all phones were connected to the same serving cell and pointed towards the same orientation. The observed signal levels for the four phones are shown in Fig. B.4. The mean μ and standard deviation σ of the measurements collected during the static test are also included in the figure. Different mean values are observed between the different phones, which further confirms the UE heterogeneity mentioned in Section 3.1. It can also be seen that all mobile devices show a standard deviation of approximately 1 dB, generally lower than the results observed in [12] due to a stable environment during the test (no cars or moving objects surrounding). The static test affirms that RSRP recordings are stable and not significantly impacted by noise in the measurement acquisition. In practice, devices will show an offset between them due to implementation differences. In our analysis, this is degenerate to the offsets caused by the position and orientation of the phones/devices, i.e., a static mean offset.

4 Data-Driven Estimation Technique

Considering the previous work in [7], this section summarizes how the recorded data is used to obtain the estimations. Using Fig. B.5 as a reference, we explain how the estimation is built based on the values recorded by different UEs moving along the same route.

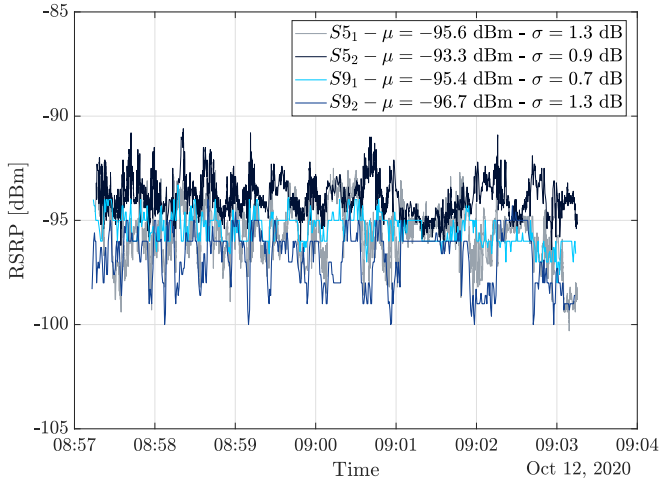

Fig. B.4: Static test of measurement acquisition evaluation. The phones were in the same position and orientation, all connected to the same serving cell.

The routes of the two environments are split in a distance grid of J segments of 10 m length. This means that e.g., for the urban environment, the 3.3 km are split in $J = 330$ segments of 10 m. The serving cell traces recorded by each of the UEs in every run or loop are located in the corresponding distance grid. If UE_1 is taken as an example, it may correspond to e.g., the trace recorded in the urban environment by mobile device $S5_1$ in $Setup_A$ and $Loop_1$. Then UE_2 would correspond to the trace recorded by the same device, same setup, but $Loop_2$. The process would continue until the N traces are located in the distance grid, where N results from the following:

- Urban: 4 available phone devices in 3 different setups, where 3 loops of the route were driven. This results in a total of $N = 36$ recorded serving cell traces used to estimate the average signal level experienced by a UE driving along that urban route.
- Rural: 4 available phone devices in 3 different configurations or setups, where 4 runs (2 in each direction) of the route were driven. This results in a total of $N = 48$ recorded serving cell traces used to estimate the average signal level experienced by a UE driving along that same rural route.

When a serving cell trace is located in the distance grid, multiple recorded samples are observed within a 10 m segment. The average number of samples recorded per segment depends on the driving speed and can be found in Table B.2. As it is shown in Fig. B.5, all the samples within the same grid

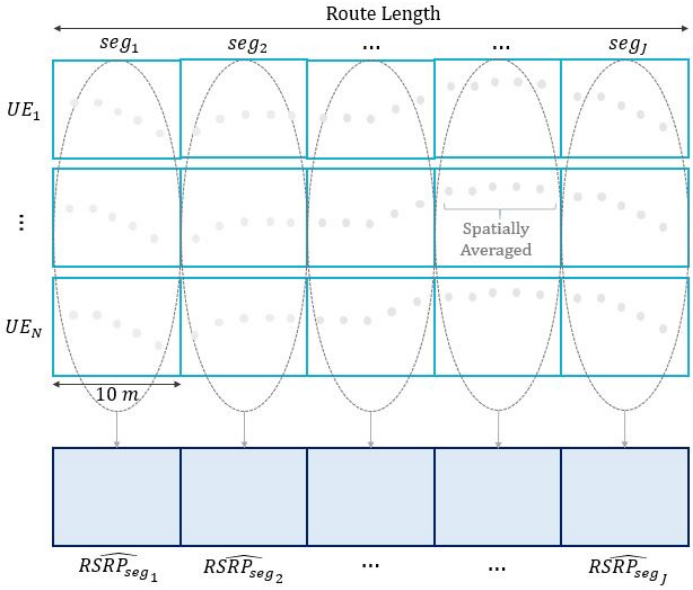

Fig. B.5: Data processing scheme. The different UE traces are located in a distance grid and averaged to obtain the estimation.

segment are spatially averaged. This further averages fast fading effects previously mentioned in Section 3.2 the selected 10 m segments fulfill the Lee criteria ($40\lambda = 6.6$ m) [23].

Once the N traces are organized in the distance grid, they are averaged to obtain an estimation. This is done on a segment basis, i.e. for each segment $j = 1, ..., J$ the values from all UEs $i = 1, ..., N$ are averaged, providing as a result an estimated value for each corresponding segment. The estimated RSRP value at a segment j is defined as the geometric average:

$$\widehat{RSRP_{seg_j}} = \frac{1}{N} \sum_{i=1}^{N} RSRP_{i,seg_j} \qquad \text{[dBm]} \quad \text{(B.1)}$$

where N takes the values defined above and $RSRP_{i,seg_j}$ is the RSRP value recorded by UE_i in segment j.

The RSRP measurements recorded by the UEs in a certain segment will be aggregated regardless of the cell that they are connected to. The main motivation behind this is that we aim to estimate the average signal level that any UE in that location would experience.

When aggregating measurements from different serving cells, it could be expected that UE-BS distance impacts the estimation error. The estimation error, shown in Fig. B.6 and defined in Eq. (B.2), does not seem to be impacted by the UE-BS distance. This can be partially due to the cell selection

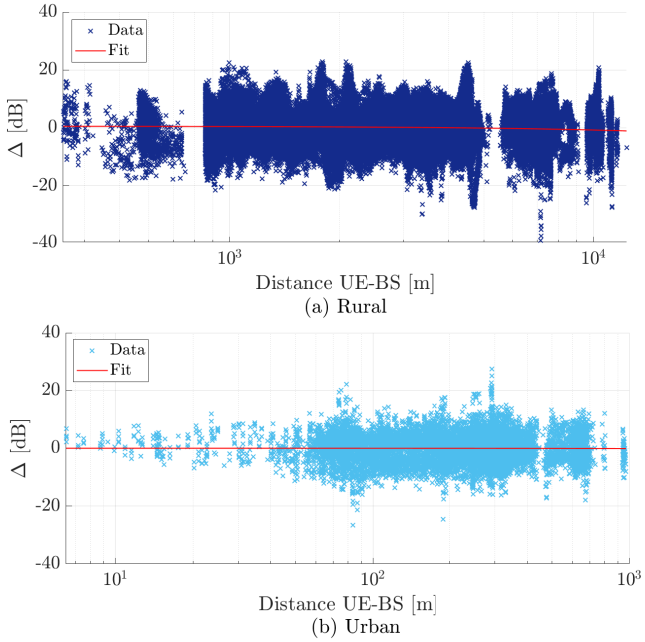

Fig. B.6: Estimation error versus UE-BS distance for the different scenarios: (a) rural and (b) urban.

and re-selection processes, which tend to minimize this effect. There is a high spread of the estimation error values regardless of the distance in both rural and urban scenarios.

In practice, the proposed data-driven approach requires measurement gathering from different users, which could be achieved through MDT. The accuracy of the estimations would be subject to factors such as Global Positioning System (GPS) inaccuracy, environment changes, or measurement system differences. While GPS inaccuracies are reduced by averaging every 10 m, but not otherwise considered in our analysis, measurement system differences are considered by including UE heterogeneity. Similarly, we include the unpredictable environment changes in the estimations by performing several different measurement rounds during the campaign. Additionally, keeping updated estimations and error distributions will require large database storage.

4.1 Estimation Accuracy and Performance Comparison

To evaluate the performance of the RSRP estimation algorithm, we compare the estimations to those obtained using empirical models and ray-tracing.

Table B.3: Data-driven estimation errors based on UEs (before and after MIO correction) and scanner data.

	Rural Δ [dB]	**Urban Δ** [dB]
Before MIO Correction	6.3	4.9
After MIO Correction	4.9	3.6
Scanner	3.6	3.2

Only urban environment data is used for the comparison due to the unavailability of 3D models and terrain elevation maps in the ray-tracing tool for the rural area.

As the performance metric, we use the estimation error calculated for each of the UEs and segments independently. For each UE_i $(i = 1, ..., N)$ the estimation error $\Delta_{UE_{i,seg_j}}$ is calculated segment by segment as the difference between the recorded $RSRP_{UE_{i,seg_j}}$ value and the estimated $\widehat{RSRP_{seg_j}}$ value:

$$\Delta_{UE_{i,seg_j}} = RSRP_{UE_{i,seg_j}} - \widehat{RSRP_{seg_j}} \quad \text{[dB]} \quad \text{(B.2)}$$

As was shown in [7], the distribution of the estimation error is uni-modal and can be well approximated with a Gaussian $\mathcal{N}(0, \sigma)$. This suggests that the results obtained would remain unchanged regardless of the metric used for aggregation (mean, mode or median). Each UE presents an MIO with respect to the overall estimation, which, if corrected, can reduce the estimation error. Table B.3 shows the overall estimation error with and without MIO correction for both urban and rural environments. Later in Section 5.2 we will introduce a technique for MIO correction to actually achieve the approximately 4 dB estimation error shown for MIO correction in Table B.3.

For the comparison with empirical models and ray-tracing, Fig. B.7 shows the recorded RSRP values versus distance to the serving BS together with the estimations based on these traditional approaches. The model parameters have been calibrated using measurement data or environment-specific parameters in each case. The data-driven estimations are not shown since they are cell agnostic and cannot be referenced to a specific site.

Table B.4 shows the estimation error, as per Eq. (B.2), for all the studied techniques. In the case of the empirical and ray-tracing estimations, the estimated value is obtained for the corresponding Physical Cell ID (PCI) recorded by the UE during the measurement campaign, sample by sample. These estimations are then averaged on a segment basis to obtain a serving RSRP estimation at each segment. Further details on the respective approaches are:

Empirical Models

Two empirical models have been used for comparison: Okumura-Hata and 3rd Generation Partnership Project (3GPP) TR 38.901 for Urban Macro (UMa) environments. The operator provided network information (BS location, BS height, and BS radiated power), which was used to calculate the corresponding UE-BS distance for the specific serving cell and other relevant parameters for these empirical models. The UE assumed height is 1.5 m, and the center frequency is 1.8 GHz.

The Okumura-Hata Model [24] was developed using the results of very extensive measurements performed in different environments (urban and suburban). It is typically used by operators, which apply the necessary corrections to fine-tune the model to the specific physical environment under evaluation.

The 3GPP TR 38.901 standardized path loss model for the 3D Urban Macro (UMa) Line-Of-Sight (LOS) and Non-Line-Of-Sight (NLOS) scenarios [25] is also used for comparison. The visibility conditions (LOS/NLOS) between the UE and the BS have been determined using the ray-tracing tool, and the corresponding equation from [25] is applied for each case.

By observing Fig. B.7 it can be seen that for a particular UE-BS distance the spread of the recorded measurements is high. The value estimated by the empirical models, which depends on the distance to the BS and visibility conditions, may not represent the signal level expected in a particular location. This is consistent with what is observed in Table B.4, where the highest estimation errors are observed for the two empirical models. Both show estimation errors 4-6 dB higher than the observed when using the data-driven approach.

Ray-Tracing

A ray-tracing tool is used to obtain predictions for comparison with the data-driven approach [26]. The Dominant Path Model (DPM) is selected to compute the estimations, which calculates the dominant path between the transmitter and the receiver [27]. The 3D maps used in the tool have a 2.5 m spatial resolution. The predictions are further averaged on a 10 m radius in order to compare them with the other two approaches properly. The same is applied for the LOS/NLOS predictions, which are estimated every 2.5 m, and settled using a majority vote of LOS/NLOS conditions within a 10 m radius.

As observed in Fig. B.7, ray-tracing shows more accurate estimations than the empirical models since it accounts for the specific physical environment surrounding the UE and not only the average area characteristics. This is also reflected in Table B.4, where an 7.6 dB estimation error is observed. While this value is 2-4 dB lower than the one observed with the empirical techniques, it

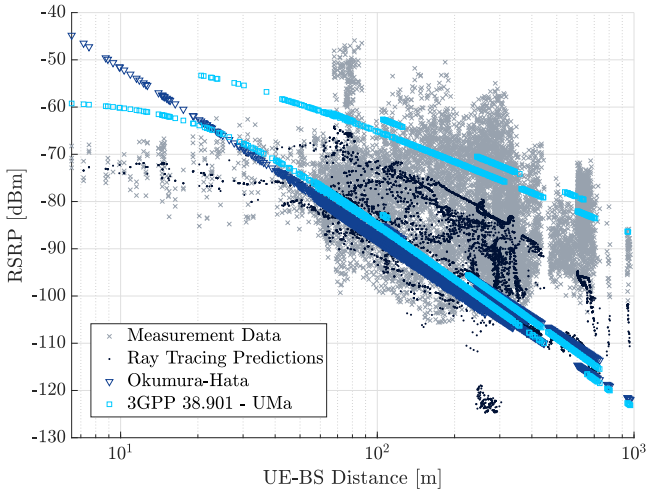

Fig. B.7: Comparison of measurement data with traditional estimation approaches in the urban scenario. LOS/NLOS conditions are considered.

Table B.4: Comparison of data-driven approach estimation error with traditional techniques using urban scenario data.

Estimation Technique	**Estimation Error** [dB]
Data-Driven	4.9
Okumura-Hata	11.1
3GPP 38.901 UMa	9.3
Ray-Tracing	7.6

is still high.

The studied traditional techniques show worse performance than the data-driven approach. The data-driven estimation is based on real location-specific data and, therefore, provides a more accurate estimation than the traditional techniques of the signal level that the UE will perceive when driving along a route. However, a single estimated value is not representative enough, and each UE will observe a certain MIO with respect to the overall mean estimation. In the following sections, we study how the MIO can be predicted, corrected, and used to improve the accuracy of the estimation.

5 Mean Individual Offset Correction

5.1 Pre-service

Correcting the MIO in the pre-service stage would allow the network to perform more accurate estimations on the potential critical areas before the UE starts moving along the route. For that, the network should be able to predict the UE's MIO using relevant context information such as UE's placement (inside/outside the car), UE's orientation, or UE's pattern type, assuming these can be available.

UE Antenna Orientation

The MIO for each UE in the rural (a) and urban environments (b) is shown in Fig. B.8. As it can be observed, the offset remains constant between different runs or loops for the same phone-setup combination where the device is oriented towards the same direction. However, different offsets are observed between devices that are pointing in different directions. This illustrates the relevance of UE orientation to determine the MIO. A clear distinction can also be made between setups A-B and setup C. The phones were located inside the car in the latter, and the penetration loss due to the vehicle's structure caused the signal level to be much lower (7 dB on average) than the one experienced by the phones located in the car top carrier. This resulted in negative MIOs with respect to the overall estimation for all phones located inside the car. Therefore, it is reasonable to assume that another relevant factor impacting the MIO of a UE is its placement (inside/outside) in the car. However, that information would only allow identifying the sign of the MIO, but not the value of it, which seems to depend mainly on the UE orientation and driving direction (as previously shown in [7]).

UE Antenna Pattern Effects Compensation

The consistency of the offset values observed among loops of each UE Fig. B.8, as well as the different offsets for the multiple UEs, suggest that the orientation of the UE is potentially the main factor impacting the MIO. The signal level reaching the receiver will also be subjected to the device's effective antenna pattern, which is directional for all test phones (see Fig. B.3).

Therefore, compensation for the antenna pattern effect could reduce the estimation error. The approach has been tested for the rural scenario data: the reduced interactions of the received signal with surrounding objects and the dominance of LOS conditions simplifies the antenna pattern compensation in that environment. The angle of incidence α of the transmitted signal (from the BS) in the UE antenna pattern is calculated using the bearing angle of

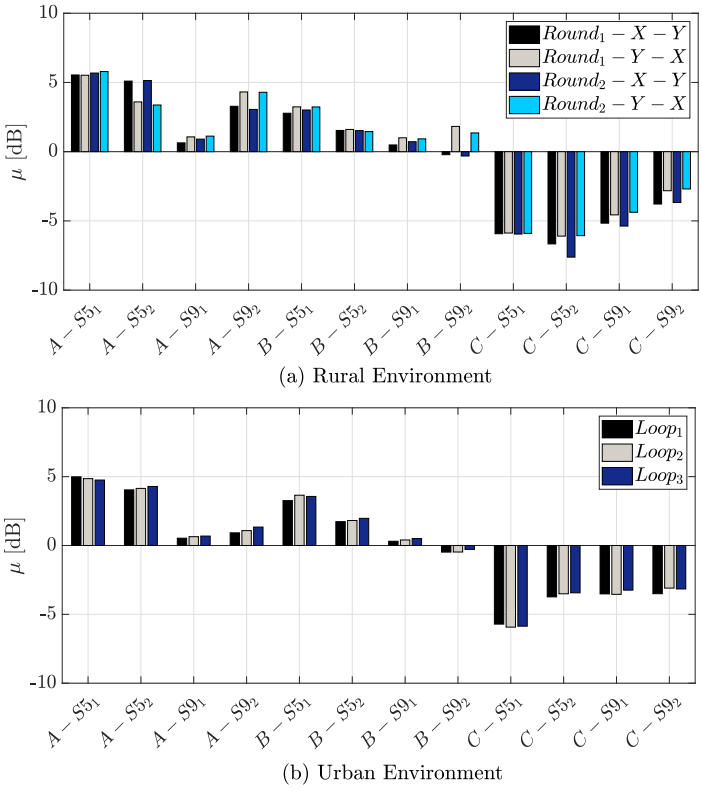

Fig. B.8: MIO with respect to the route estimation. (a) Results for each of the 48 UE traces in the rural environment and (b) for the 36 UE traces in the urban environment.

the serving BS (as recorded by the UE) with respect to the car direction. To account for possible inaccuracies in the calculation of α, the compensation is based on the average relative power shown in Fig. B.3 within a $\pm 15°$ range in both azimuth and elevation directions.

Results in Table B.5 show the overall estimation error Δ for the rural scenario when using setups A and B, before and after pattern compensation. As it can be observed, the antenna pattern compensation has a low impact, resulting in a reduction of 0.4 dB. Setup C is omitted due to the challenge of accounting for the vehicle blockage.

The antenna patterns were measured in an anechoic chamber, where the effects of the car structure or the car top carrier are not considered. Furthermore, the UE-BS distance is considerably high for the rural case, and possible signal interactions with the buildings in the path or ground reflections cannot be accounted for. Although deterministic compensation seems

Table B.5: Effective antenna pattern compensation effects on overall estimation error in the rural scenario.

	Δ [dB]
Before Antenna Pattern Compensation	5.1
After Antenna Pattern Compensation	4.7

intractable, the stability of the estimation error between UEs oriented towards the same direction suggests that the antenna pattern effect is statistically included in the estimation error distribution. In the following section, we study an approach that exploits the stability of the estimation error of the UE traces recorded by devices oriented towards the same direction.

5.2 On-Service

The results in the previous section show that fully correcting the MIO in the pre-service stage is complex. In the following, we present how we use the estimation error characteristics and the observed error based on recorded RSRP during the on-service stage to correct the MIO. The main idea of this approach is to use the most recent information recorded by the UE that is moving along a particular route to predict the MIO that it will observe for the rest of the route.

We use the so-called z-test [28], which is a parametric hypothesis test that can be used to determine whether a set of samples belongs to a certain distribution. The test calculates the probability of observing as extreme a test result as the one observed (p-value), assuming that the null hypothesis is correct.

As shown in Fig. B.9 (using notation $^{(\#)}$) this approach requires to maintain a database where estimation error distributions from previous UEs are stored $^{(1)}$. The distributions from each UE could be approximated by a normal distribution with the corresponding mean and standard deviation. Once the UE starts to move along the route, after a certain number of observed error samples $^{(2)}$, these are checked against the available distributions in the database. The z-test will provide the mean of the best-fit distribution $^{(4)}$ by accepting the distribution with the highest p-value.

To investigate this approach, we store $N - 0.25 * N$ distributions in the estimation error database and use the 25 % of the UE traces (i.e., 9 UE traces in the urban environment) for testing the algorithm. A set of 9 random traces is left out in every iteration until all the UEs have been tested. Fig. B.10 shows the results obtained for urban scenario. The MIOs of the $N = 36$ UEs recorded in the urban environment are shown, as well as the predicted values using the z-test when observing 30 samples (equivalent to an observation distance of d_{obs} = 300 m). The MIO values can generally be accurately predicted.

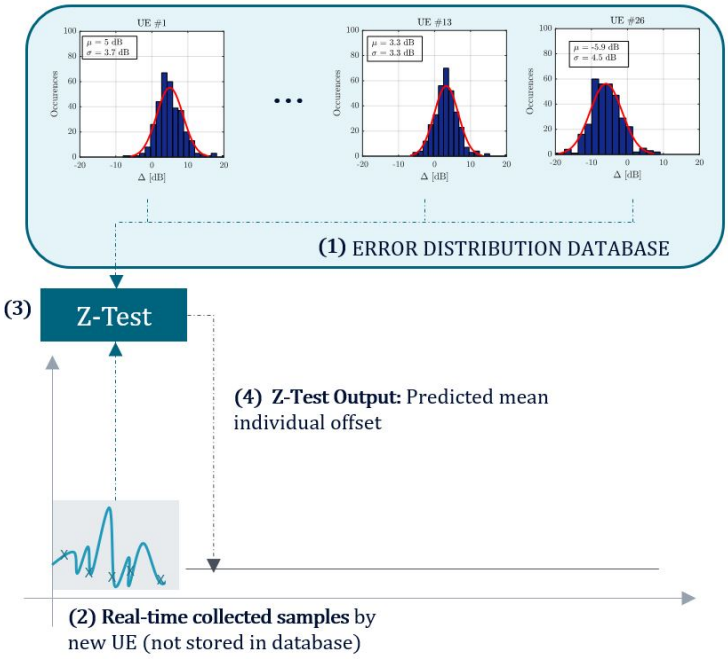

Fig. B.9: MIO correction procedure in the on-service stage. The moving UE estimation error samples are compared to the error distributions stored in the database and provide an estimation of the MIO.

Table B.6 shows a summary of the results obtained for both rural and urban scenarios. The table shows the overall results obtained when the MIO is known and corrected (Target Δ [dB]) and the results obtained when predicting and correcting the MIO using the z-test. The overall results when using the z-test for MIO estimation are reasonably close (maximum 0.2 dB difference) to the values using known offsets. Therefore, the MIO can be corrected using this technique as long as UEs with similar conditions/orientation have previously passed through the same route.

Table B.6 also includes the required observation distance d_{obs}. In the urban environment a d_{obs} of 300 m is required, whereas for the rural scenario a d_{obs} of 100 m is sufficient. In the urban environment, an observation distance of 100 m reduces the overall estimation error from 4.9 dB to 4.1 dB, but a longer observation distance further decreases that value down to 3.7 dB. In the rural case, the error does not decrease regardless of the observation distance. This is most likely due to the stronger signal variations and higher dynamics that were observed in the rural scenario compared to the urban case.

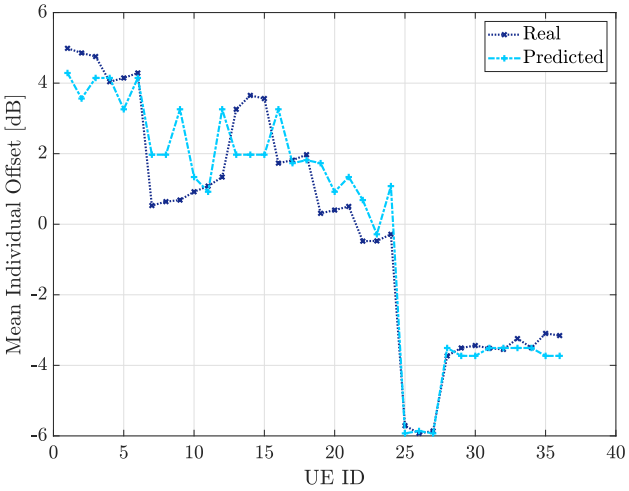

Fig. B.10: Necessary MIO corrections to improve estimation accuracy (light blue) and estimated on-service MIO corrections for all test UE traces in urban scenario (dark blue).

Table B.6: Z-test results comparison with best performance observed in [7].

	Target Δ [dB] **(known MIO)**	**Z-Test**	
		Δ [dB]	d_{obs} [m]
Rural	4.9	5.1	100
Urban	3.6	3.7	300

6 Outage Probability Estimation

As mentioned in Section 2, signal level estimations can be used by the network to obtain information on the potential critical areas along the route, which are defined in terms of expected service availability and reliability. In the following, we further define these QoS metrics and exemplify their use. For a real reference, we focus on the specifications of the V2X services. Although the open literature claims that a requirement of 95 % reliability is enough for a safe communication [29], most of the use cases considered in the V2X 3GPP specifications [30] require a 99.99 % reliability, and that is the requirement we use for evaluation.

6.1 Service Availability

Service availability estimations are obtained by calculating the probability $P_{out,SA}$ that RSRP will drop below a certain threshold γ_{RSRP} along the route.

Table B.7: Average performance metrics for RSRP-based service availability estimations.

		TPR (Hit Rate) [%]	TNR (Specificity) [%]	FNR (Miss Rate) [%]	FPR (Fall-out) [%]
Rural γ_{RSRP} = -115 dBm	**Data-Driven** *Pre-Service*	85.2	95.7	14.8	4.3
	Data-Driven *On-Service*	74.3	97.1	25.7	2.9
Urban γ_{RSRP} = -100 dBm	**Okumura-Hata**	100	4.3	0	95.7
	3GPP 38.901	70	62.4	30	37.6
	Ray-Tracing	63.1	69.4	36.9	30.6
	Data-Driven *Pre-Service*	93.8	83.8	6.2	16.2
	Data-Driven *On-Service*	99.5	89.5	0.5	10.5

For each segment, we provide an estimate of the average RSRP, $\widehat{RSRP}$. We know from Eq. (B.2) that the difference to the actual RSRP value, $RSRP - \widehat{RSRP}$, is Gaussian distributed with standard deviation sigma. Hence assuming, or conditioned on, $\widehat{RSRP}$ being the average RSRP, we calculate the outage probability as the one-sided p-value of the Gaussian distribution at the threshold value, i.e.:

$$\begin{aligned} P_{out,SA} &= P(RSRP < \gamma_{RSRP} | \overline{RSRP} = \widehat{RSRP}) \\ &= \Phi\left(\frac{\gamma_{RSRP} - \widehat{RSRP}}{\sigma}\right) \end{aligned} \tag{B.3}$$

where Φ is the cumulative distribution function of the standard normal distribution.

In Fig. B.11 we show the availability estimation results along the rural route for a $\gamma_{RSRP} = -115$ dBm. This threshold is selected based on the observed intra-frequency mobility thresholds configured by the operator (which range between -115 dBm and -100 dBm in the 1800 MHz band). Fig. B.11a shows the 48 recorded serving RSRP traces, while Fig. B.11b presents the estimated availability for that route, where $P(RSRP > -115 \text{ dBm})$, i.e. $1 - P(RSRP < -115 \text{ dBm})$ is shown such that a 99.99 % threshold is used as a reference to declare a critical area for the selected use case. As it can be seen, the estimated potential critical areas visually match with the ones actually experienced by the UEs. Table B.7 shows a summary of the service availability estimations performance. Service availability is evaluated for each segment in the distance grid. For the RSRP traces recorded by the different UEs, outage is declared in a grid segment if the recorded RSRP value in that segment is below γ_{RSRP}. For the estimated service availability, outage is declared in a grid segment if $P(RSRP > \gamma_{RSRP}) < 99.99$ % in that segment. Performance

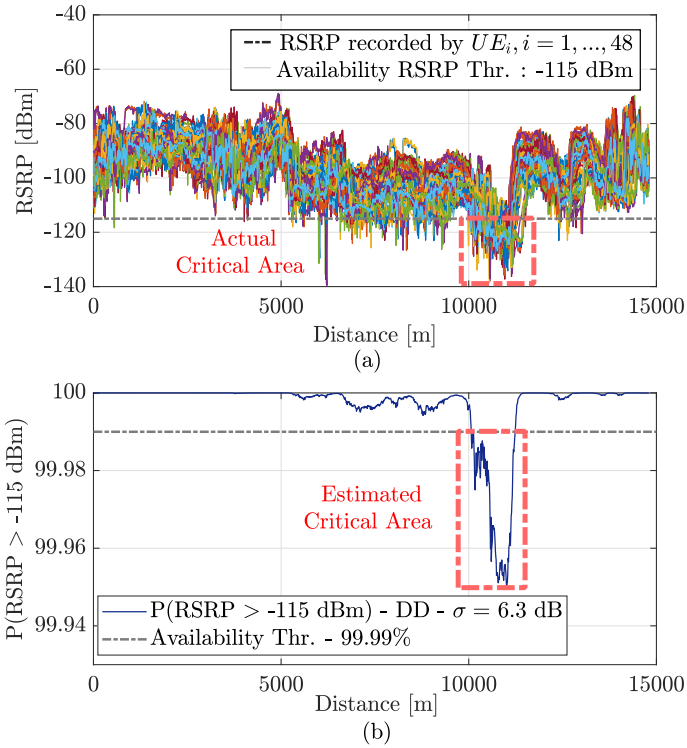

Fig. B.11: Service availability estimation example with rural environment data. (a) Actual RSRP values recorded by all 48 UEs used to build the estimation and (b) $P(RSRP > -115$ dBm) along the route, calculated based on the serving cell RSRP estimation.

of service availability estimations is evaluated using the average over all UE traces of the following metrics [31]:

- **True Positive Rate (TPR)** or Hit Rate: Percentage of correctly estimated service availability outage segments in the grid. It is calculated as the number of correctly estimated outage segments - True Positives (TP) - over the number of actual outage segments (P).

$$TPR = \frac{TP}{P} \qquad [\%] \quad \text{(B.4)}$$

- **True Negative Rate (TNR)** or Specificity: Percentage of correctly estimated service availability "safe" (non-outage) segments in the grid. It is calculated as the number of correctly estimated non-outage segments - True Negatives (TN) - over the number of actual non-outage segments

(N).

$$TNR = \frac{TN}{N} \quad [\%] \quad \text{(B.5)}$$

- **False Negative Rate (FNR)** or Miss Rate: Complementary metric for TPR. Represents the number of missed outage areas.

$$FNR = 1 - TPR \quad [\%] \quad \text{(B.6)}$$

- **False Positive Rate (FPR)** or Fall-out: The complementary metric for TNR. Represents the number of "false alarms," i.e., the percentage of cases where a grid segment was incorrectly estimated as outage area. False positives would lead to a situation where countermeasures are initiated to solve a critical situation that does not exist.

$$FPR = 1 - TNR \quad [\%] \quad \text{(B.7)}$$

Other metrics that are typically used to evaluate classification techniques were not included as they were considered to be misleading in the purpose of this context. Accuracy is typically used to summarize the performance of the estimations, as it represents the rate of correct estimations (positive and negative). However, for the case under evaluation, where the number of actual positives is much lower than the number of actual negatives (unbalanced dataset), accuracy presented very high values (above 90 % for the data-driven approach) and was considered to be non-representative of the estimation performance. F1-Score, on the other hand, is typically used for unbalanced datasets and is calculated such that the cost of false positives and false negatives is equally significant for performance evaluation [32]. This metric presented low values (below 65 %) due to the low number of critical areas for some of the UEs.

Results in Table B.7 show the mean value of the metrics in Eqs. (B.4-B.7) over all UEs. For rural environments, the pre-service stage estimations present high TPR and TNR, indicating that most outage and non-outage areas are correctly estimated. A trade-off is observed in the on-service stage, where the MIO corrections cause a decrease in the TPR and an increase in the TNR.

Another example of service availability estimation is shown in Fig. B.12, where urban data is used to compare the estimation of critical areas when using the data-driven approach in comparison to the traditional estimation techniques. To show the accuracy of the estimations, the availability threshold is raised in this scenario to -100 dBm as higher reliability should be considered in higher population density areas. As shown in Fig. B.12b and in Table B.7, the higher the signal level estimation error, the lower is the accuracy of the estimated critical areas. Using the Okumura-Hata model RSRP

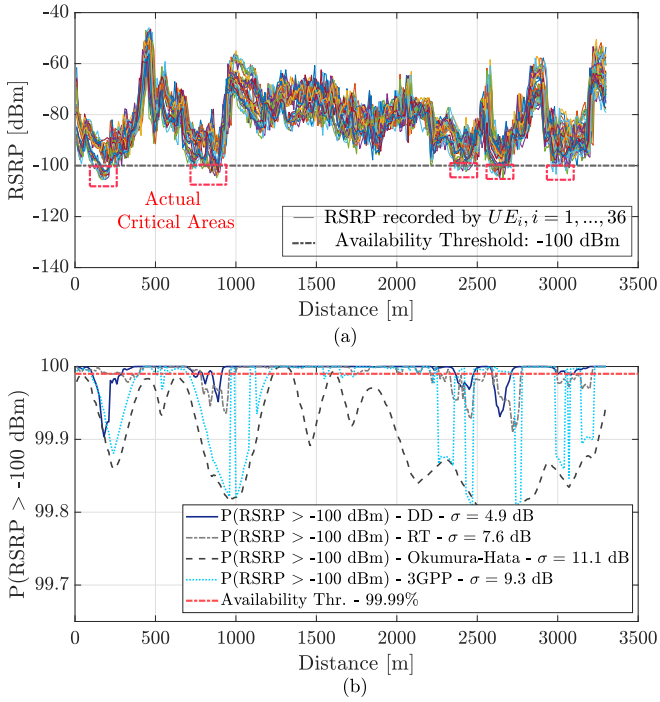

Fig. B.12: Service availability estimation example with urban environment data. (a) Actual RSRP values recorded by all 36 UE traces used to build the estimation and (b) $P(RSRP > -100$ dBm) obtained when using the estimations provided by the different studied RSRP estimation approaches.

estimations results in a very inaccurate estimation of the potential critical areas. Since the full route is declared critical the TPR is 100 %. However, it also presents a very high FPR of 96 %. The 3GPP model estimations show lower FPR than the Okumura-Hata, but still considerably high (38 %). Similar results are observed for the ray-tracing estimations that show a TPR of 63 % and an FPR of 31 %. The data-driven approach provides an average TPR of 94 % in the pre-service stage while maintaining a relatively low FPR (16 %). This shows how the data-driven signal level estimation technique provides better results than traditional techniques when the network aims to obtain in-advance information about the expected service availability along the path.

To further show the benefits of using the data-driven estimations against other traditional techniques, we show in Table B.8 the reliability margin (RM) that needs to be considered to guarantee a certain reliability requirement when using the different estimation techniques. The values in the table show

Table B.8: Reliability margin (RM) for different reliability requirements (with $\gamma_{RSRP} = -100$ dBm).

	90 %	**95** %	**99.99** %
Okumura-Hata	15.2	19.5	27.6
3GPP TR 38.901	12.3	15.7	22.3
Ray-Tracing	10	12.8	18.1
Data-Driven Pre-service	6.2	8	11.3
Data-Driven On-service	4.6	5.9	8.3

that the reliability margin highly decreases when using the data-driven approach. For a 99.99 % reliability requirement, the Okumura-Hata estimations show an RM of almost 28 dB, whereas the data-driven approach reduces the margin to 8 dB in the on-service stage. Higher reliability requirements are not considered in the table as the RM values would be on the limit of what could be practically useful for the purpose of the estimations considered in this article.

In Fig. B.13 we show the effect that MIO correction has on the estimation of critical areas in the on-service stage. Three UEs were used as an example, one from each of the setups. For each UE, the z-test was used to obtain the corresponding MIO estimation. After an observation distance of $d_{obs} = 300$ m, the serving RSRP estimation was corrected according to the estimated MIO, and the probability of RSRP being below -100 dBm was recalculated. In Fig. B.13a the actual serving RSRP traces recorded by each of the three UEs are shown. Fig. B.13b shows $P(RSRP > -100 \text{ dBm})$ in the pre-service stage (valid for any UE planning to move through the same path) and the corrected on-service probability for each of the 3 example UEs (UE-specific estimation). The setup A UE, with positive MIO with respect to the overall estimation, has lower probabilities of dropping below the threshold than initially estimated. There are no critical areas estimated after MIO correction, which matches with the recorded values for that UE (never below -100 dBm). For Setup C UE, with generally lower signal levels due to vehicle blockage, the estimated probabilities of the serving signal level dropping below the threshold are higher than estimated in the pre-service stage, representing well the actual signal levels experienced by that user. The results for on-service stage performance in the urban environment in Table B.7 show that on average, TPR increases to 99 % with respect to 94 % obtained in the pre-service stage, and TNR increases up to 89 % compared to the previous 84 %.

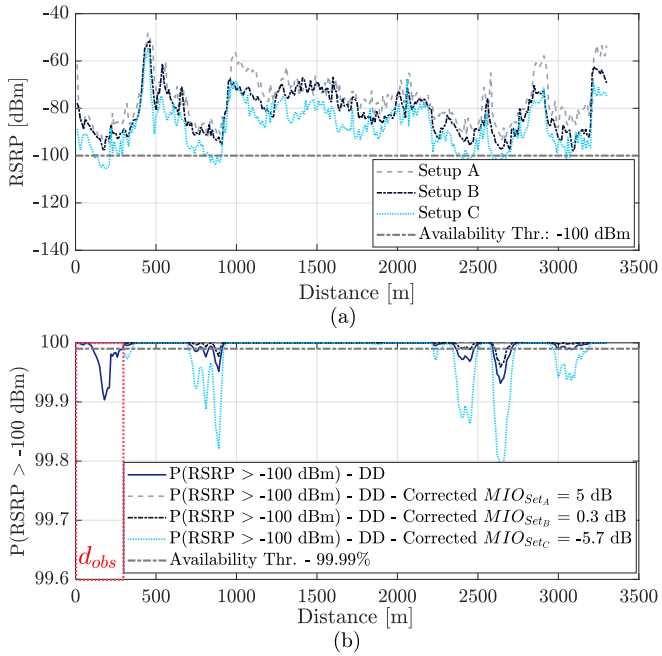

Fig. B.13: Service availability estimation example with urban environment data. (a) Actual RSRP values recorded by 3 example UEs (from setups A, B, C) and (b) $P(RSRP > -100$ dBm$)$ along the route, for the pre-service estimation of all UEs in that path and the on-service estimations for the individual example UEs.

6.2 Service Reliability

To estimate service reliability we first estimate SIR:

$$\widehat{SIR} = \frac{\hat{S}}{\hat{I}} = \frac{\widehat{RSRP_{SC}}}{\sum_{j=1}^{NC} \widehat{RSRP_j} \cdot \delta} \quad \text{[dB]} \qquad \text{(B.8)}$$

$\widehat{RSRP_{SC}}$ is the RSRP estimation of the serving cell, $\widehat{RSRP_j}$ is the estimation of the $j = 1, ..., NC$ neighboring cells and δ is a model for the impact of the traffic load. A maximum of NC = 3 strongest neighbors, when available, are used to calculate SIR.

As in Eq. (B.2), since $RSRP - \widehat{RSRP}$ is Gaussian with zero mean we can view the linear value of the estimator $\widehat{RSRP}$ as a log-normal random variable whose logarithmic mean and standard deviation is respectively the prediction $\widehat{RSRP}$ and σ. This is true for both serving and interfering signals. The interference sum will be approximately log-normal, statistics of which can be calculated numerically by the Schwarz & Yeh algorithm [33]. The same algo-

Table B.9: Average performance metrics for SIR-based service reliability estimations (δ = 30 %).

		TPR (Hit Rate) [%]	**TNR** (Specificity) [%]	**FNR** (Miss Rate) [%]	**FPR** (Fall-out) [%]
Rural γ_{SIR} = -3 dB	**Data-Driven** *Pre-Service*	72.4	62.4	27.6	37.6
	Data-Driven *On-Service*	65	72.3	35	27.7
Urban γ_{SIR} = -3 dB	**Data-Driven** *Pre-Service*	88.2	58.8	11.8	41.2
	Data-Driven *On-Service*	77	68.7	23	31.3

rithm, with some extensions for correlated signals, can be used to calculate the logarithmic mean and standard of the SIR [34] which is also approximately log-normal. Assuming a correlation coefficient of 0.5 [35] between signals of the serving and the interfering cells we use this framework to evaluate the probability $P(SIR < \gamma_{SIR})$.

Fig. B.14b shows the reliability estimation results when considering low, medium and high load (10 %, 30 % and 60 %, respectively) for γ_{SIR} = -3 dB. In Fig. B.14c a color map is used to plot the results for medium load with that same threshold in the urban scenario. The corresponding performance metrics in Table B.9 show a TPR of 88 % and a FPR of 41 %, with a mean F1-score of 16 %. With the on-service stage corrections using MIO correction for the serving cell, results show the same trade-off TPR/TNR above-mentioned. For the rural environment, the values follow the same trend.

The presented results are sensitive to different network traffic load, critical thresholds, and correlation coefficients between the serving cell and the interfering neighbors. For most cases, MIO correction reduces True Positive Rate (TPR) and increases True Negative Rate (TNR), indicating a trade-off between missing outage areas and initiating actions against non-existent ones. Failing to estimate an outage area poses a risk to the service reliability, which is crucial for mission-critical services. On the other hand, estimating non-existent critical areas may lead to a misuse of network resources. On that basis, MIO correction in the on-service stage is beneficial for outage areas estimation. However, initiating MIO correction in the on-service stage may depend on the service priorities, i.e. prioritization of outage area detection or more efficient resource utilization. Furthermore, service reliability could also benefit from the on-service MIO corrections due to the availability of actual load values, which could be adjusted individually for each corresponding neighbor.

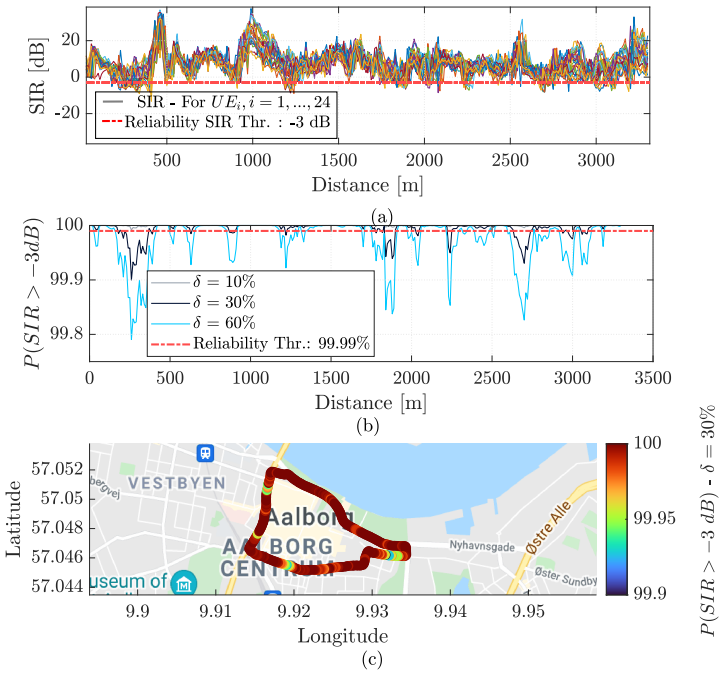

Fig. B.14: Service reliability estimation example with urban environment data. (a) SIR values calculated using recorded RSRP values from serving and neighboring cells for all of the 24 UEs used and assuming average medium load, (b) estimated probability $P(SIR > -3$ dB$)$ for low, medium and high load and (c) same results at medium load in a color map.

7 Conclusion

In this article, we use experimental data recorded during an extensive LTE measurement campaign in rural and urban environments to show that the signal level that a UE will experience along a route can be estimated by aggregating measurements recorded by UEs that have previously passed through that same route.

First, we show how this approach provides an estimation error of 5-6 dB, improving the estimation error obtained using traditional estimation techniques such as empirical models or ray-tracing by 3-6 dB. We show how identifying the MIO of each UE with respect to the overall estimation, using a technique that exploits the estimation error experienced by previous UEs, further reduces the overall RSRP estimation error to approximately 4 dB.

Lastly, we use the signal level estimations to calculate service outage probability in terms of availability (RSRP-based) and reliability (SIR-based). The data-driven approach shows improved accuracy in outage areas estimation

with respect to traditional techniques, detecting a minimum of 70 % of the outage areas with less than 30 % of false alarms. This approach allows providing the network with in-advance information on the expected service conditions in a specific route where the UE is planning to move and can be used by the network to make a decision of whether it is safe for the UE to start the service or it should re-plan the route when possible. Furthermore, we show how using context information during the service can improve the overall accuracy of the service availability and reliability estimations, which the network may use to take in-advance countermeasures for upcoming signal and QoS drops, respectively.

References

[1] 3GPP, "Management and orchestration; 5G end to end Key Performance Indicators (KPI) (Release 17)," Tech. Rep. 28.554 V17.4.0, Sep. 2021.

[2] J. Riihijarvi and P. Mahonen, "Machine learning for performance prediction in mobile cellular networks," *IEEE Computational Intelligence Magazine*, vol. 13, no. 1, pp. 51–60, 2018.

[3] L. Alho, A. Burian, J. Helenius, and J. Pajarinen, "Machine Learning Based Mobile Network Throughput Classification," in *2021 IEEE Wireless Communications and Networking Conference (WCNC)*. IEEE, 2021, pp. 1–6.

[4] 5G Automotive Association, " Making 5G proactive and predictive for the automotive industry," Tech. Rep. White Paper, Jan. 2020.

[5] ACJA, GSMA and GUTMA, "Interface for Data Exchange between MNOs and the UTM Ecosystem: Network Coverage Service Definition, v1.00." Feb. 2021.

[6] 3GPP, "Physical layer; Measurements (Release 16)," Tech. Rep. 36.214 V16.2.0, Mar. 2021.

[7] M. Lopéz, T. B. Sørensen, I. Z. Kovács, J. Wigard, and P. Mogensen, "Experimental evaluation of data-driven signal level estimation in cellular networks," in *2021 IEEE 94th Vehicular Technology Conference (VTC2021-Fall)*. IEEE, 2021, pp. 1–6.

[8] V. Raida, P. Svoboda, M. Koglbauer, and M. Rupp, "On the Stability of RSRP and Variability of Other KPIs in LTE Downlink-An Open Dataset," in *GLOBECOM 2020-2020 IEEE Global Communications Conference*. IEEE, 2020, pp. 1–6.

[9] J. Walfisch and H. L. Bertoni, "A theoretical model of uhf propagation in urban environments," *IEEE Transactions on antennas and propagation*, vol. 36, no. 12, pp. 1788–1796, 1988.

[10] I. Data, "Prediction methods for the terrestrial land-mobile service using the frequency range 30 mhz to 3 ghz'," *CCIR Report*, pp. 567–4.

[11] Z. Yun and M. F. Iskander, "Ray tracing for radio propagation modeling: Principles and applications," *IEEE Access*, vol. 3, pp. 1089–1100, 2015.

[12] M. Toril, V. Wille, S. Luna-Ramírez, M. Fernández-Navarro, and F. Ruiz-Vega, "Characterization of Radio Signal Strength Fluctuations in Road Scenarios for Cellular Vehicular Network Planning in LTE," *IEEE Access*, vol. 9, pp. 33 120–33 131, 2021.

[13] F. Sohrabi and E. Kuehn, "Construction of the rsrp map using sparse mdt measurements by regression clustering," in *2017 IEEE international conference on communications (ICC)*. IEEE, 2017, pp. 1–6.

[14] A. Ghasemi, "Data-driven prediction of cellular networks coverage: An interpretable machine-learning model," in *2018 IEEE Global Conference on Signal and Information Processing (GlobalSIP)*. IEEE, 2018, pp. 604–608.

[15] J. Thrane, B. Sliwa, C. Wietfeld, and H. L. Christiansen, "Deep learning-based signal strength prediction using geographical images and expert knowledge," in *GLOBECOM 2020-2020 IEEE Global Communications Conference*. IEEE, 2020, pp. 1–6.

[16] S. I. Popoola, E. Adetiba, A. A. Atayero, N. Faruk, and C. T. Calafate, "Optimal model for path loss predictions using feed-forward neural networks," *Cogent Engineering*, vol. 5, no. 1, p. 1444345, 2018.

[17] M. Ayadi, A. B. Zineb, and S. Tabbane, "A UHF path loss model using learning machine for heterogeneous networks," *IEEE Transactions on Antennas and Propagation*, vol. 65, no. 7, pp. 3675–3683, 2017.

[18] E. Ostlin, H.-J. Zepernick, and H. Suzuki, "Macrocell path-loss prediction using artificial neural networks," *IEEE Transactions on Vehicular Technology*, vol. 59, no. 6, pp. 2735–2747, 2010.

[19] 3GPP, "Architecture enhancements for 5G System (5GS) to support network data analytics services," Tech. Rep. 23.288 V17.0.0, Mar. 2021.

[20] Rohde & Schwarz, "R&S Test Equipment Information," 2020, https://www.rohde-schwarz.com/dk/products/, Last accessed on 2021-12-21.

[21] Satimo - Microwave Vision Group, "StarGate 24 anechoic chamber," 2020, https://www.mvg-world.com/en/products/antenna-measurement/multi-probe-systems/sg-24, Last accessed on 2021-12-21.

[22] 3GPP, "Radio measurement collection for Minimization of Drive Tests (MDT); Overall description; Stage 2," Tech. Rep. 37.320 V10.1.0, Mar. 2011.

[23] W. Lee and Y. Yeh, "On the estimation of the second-order statistics of log normal fading in mobile radio environment," *IEEE Transactions on Communications*, vol. 22, no. 6, pp. 869–873, 1974.

[24] O. Hata, "Propagation prediction model for uhf range in the prediction methods for the terrestrial land mobile service in the vhf and uhf bands," *ITU-R Recommendation P. 529-2, Geneva: ITU*, pp. 5–7, 1995.

[25] 3GPP, "Study on channel model for frequencies from 0.5 to 100 GHz. (Release 16)," Tech. Rep. 38.901 V16.1.0, Dec. 2019.

[26] Altair Hyperworks, "Winprop Manual," version 2018.1.2.

[27] R. Wahl, G. Wölfle, P. Wertz, P. Wildbolz, and F. Landstorfer, "Dominant path prediction model for urban scenarios," *14th IST Mobile and Wireless Communications Summit, Dresden (Germany)*, 2005.

[28] L. J. Kitchens, *Basic Statistics and Data Analysis*. Thomson/Brooks/Cole, 2002.

[29] G. Pocovi, M. Lauridsen, B. Soret, K. I. Pedersen, and P. Mogensen, "Automation for on-road vehicles: Use cases and requirements for radio design," in *2015 IEEE 82nd Vehicular Technology Conference (VTC2015-Fall)*. IEEE, 2015, pp. 1–5.

[30] 3GPP, "Study on enhancement of 3GPP Support for 5G V2X Services (Release 16)," Tech. Rep. 22.886 V16.2.0, Dec. 2018.

[31] C. Ferri, J. Hernández-Orallo, and R. Modroiu, "An experimental comparison of performance measures for classification," *Pattern Recognition Letters*, vol. 30, no. 1, pp. 27–38, 2009.

[32] J. Brownlee, *Imbalanced classification with Python: better metrics, balance skewed classes, cost-sensitive learning*. Machine Learning Mastery, 2020.

[33] S. C. Schwartz and Y.-S. Yeh, "On the distribution function and moments of power sums with log-normal components," *Bell System Technical Journal*, vol. 61, no. 7, pp. 1441–1462, 1982.

[34] T. B. Sørensen, "Intelligent distributed antenna systems (idas): Assessment by measurement and simulation," 2002.

[35] T. Sorensen, "Slow fading cross-correlation against azimuth separation of base stations," *Electronics Letters*, vol. 35, no. 2, pp. 127–129, 1999.

Paper C

Shadow Fading Spatial Correlation Analysis for Aerial Vehicles: Ray tracing vs. Measurements

Melisa López, Troels B. Sørensen, Preben Mogensen, Jeroen Wigard and István Z. Kovács

The paper has been published in the
IEEE 90th Vehicular Technology Conference (VTC-Fall 2019).

The layout has been revised.

Abstract

Although the use of cellular networks to serve drones has been investigated in several recent works, the path loss or shadowing variation is still relatively unexplored. The variation and its dynamic behaviour is of importance in characterizing the reliability of the drone communication link, but difficult to assess by experimental means on a large scale. The main goal of this paper is to study the feasibility of ray tracing models to accurately predict shadow fading variations at different heights, so that the shadow fading correlation distances for the Unmanned Aerial Vehicles (UAV) channel can be found in both vertical and horizontal directions, without the need of performing extensive field measurement campaigns. For that, predictions obtained through a ray tracing tool are compared to field measurements in an urban scenario. Our results show that with accurate 3D maps, the tool is useful for predicting the dynamics of the UAV propagation channel, and therefore can be used partly as a substitute for field measurements.

1 Introduction

The 5th Generation (5G) New Radio (NR) cellular system is expected to serve a wide range of services. Mission-critical communications, where reliability and a short-time response of the system is needed typically for safety reasons [1], is expected to be one of those services. Some examples would include Vehicle-To-Everything (V2X) communications, railway communications or the Command and Control (C2) link for Unmanned Aerial Vehicles (UAV). All the three examples are characterized by high mobility. Long Term Evolution (LTE) and 5G networks investigations for meeting the requirements of such type of communication [2–4] have been carried out.

The application of interest in this paper is the use of LTE/5G for serving the control link of UAVs. There are multiple UAV uses such as transport of medical goods, rescue services, inspection of telecommunications infrastructure, to name a few [5]. All the mentioned use cases are more attractive if a UAV can fly Beyond Visual Line-of-Sight (BVLOS) of the controller, i.e., allowing the UAV to be controlled from a remote pilot location. For public safety reasons, it is expected that reliability will be a major requirement for BVLOS operation. One of the consequences of this requirement is that the drones, as they are also commonly known, need to be connected to a flight control unit, through the C2 link, which carries mainly flight-related information. The existing cellular networks are a potential option to provide such communication, since their coverage is ubiquitous, and they are already serving many cellular network users, and therefore provide a cost-efficient option. Connection reliability in cellular networks is impacted not only by the coverage provided, but also by the dynamic behaviour of the coverage,

for what concerns both desired and interfering signals. The dynamics impact for example the radio mobility which determines cell selection, reporting and handovers.

There are already several publications such as [6–8] where the radio performance of drones when using cellular networks for the C2 link and some potential interference mitigation schemes are studied. A path loss model for the radio channel between the UAV and cellular networks is proposed in [6], [8], [9]. This height dependent model, based on measurements, suggests a path loss exponent and shadowing which decrease as the UAV height increases. Whereas path loss characterises the (static) large-scale effect, it is also important to consider and model the temporal and/or spatial dynamic effects in propagation, to realistically evaluate connection reliability when the drone moves through airspace. These dynamic effects are typically characterised by the standard deviation, and the correlation properties of shadow fading. There is a need to have more empirical evidence for the study of correlation properties of the radio channel in aerial scenarios. However, achieving this purely by experimental procedure is difficult, given the practicalities in conducting drone flights, particularly in urban environments.

In this paper, we present a large-scale study at different heights, with a multiple transmitters scenario, on the accuracy of the ray tracing tool when predicting shadowing variations by comparing it to field measurements.

The paper is organized as follows: Section 2 introduces the ray tracing models analysed in this study, the measurement setup and the scenario. Results, discussion and conclusions are followed, respectively, in Sections 3, 4 and 5.

2 Methodology

2.1 Field Measurements

To be able to compare ray-tracing predictions with real channel measurement samples, field measurements were required. Two measurement campaigns were performed in a live LTE network in the 1800 MHz frequency band: a drive test campaign at ground level and an airborne campaign with a drone at different heights. Both campaigns were performed in a small area of approximately 0.25 km^2 in the city center of Aarhus, in Denmark, where 17 different locations where measured. The studied area is hilly, and the terrain elevation in the topographic maps varies between 0 m and 27 m. As it is show in Fig. C.1, the network in this area consists of 23 tri-sectorial sites with heights between 15 m and 60 m and average Inter-Site Distance (ISD) of 470 m. Full information of the cells including antenna tilt, orientation, etc., provided by the network operator was used for the study.

Fig. C.1: Measurement route (in green) in Aarhus (Denmark), including LTE network sites location provided by a local operator.

In both measurement campaigns, the car and the drone were equipped with the Rohde & Schwarz FreeRider system [10]. The scanner was equipped with an external omnidirectional antenna, mounted on the rooftop of the car, and respectively, extending about 50 cm above the drone fuselage and rotor plane, as it is shown in Fig. C.2. The GPS position was logged for each measured Reference Signal Received Power (RSRP) sample.

2.2 Ray Tracing Model

Two different propagation models available in the AWE WinProp tool are studied: the Dominant Path Model (DPM) and the Intelligent Ray Tracing (IRT). The authors in [11] describe the algorithm of DPM for an urban scenario, which consists of the determination of the dominant path contributing to the power reaching the receiver. They present the general performance of DPM at ground level and compare it with IRT, which considers all significant possible contributions of the different rays reaching the receiver [12]. It is a one-transmitter study, where results show that DPM considerably reduces computation time respect to IRT, and that mean value and standard deviation of the difference between measurements and predictions is not only equal but sometimes better with DPM.

For this analysis we used average signal power predictions from WinProp, which mainly depend on the propagation exponents settings: before

Fig. C.2: Measurement set up for the drone campaign.

and after breakpoint Line-Of-Sight (LOS) and Obstructed-LOS (OLOS). Since WinProp offers the possibility to tune these parameters by using field measurements, those obtained from the campaigns mentioned in Section 2.1 were used to calibrate the models. The 3D maps (including building shapes and terrain topography of the area) used in the ray tracing tool to perform this study cover an area of 8.5 km^2 with 5m resolution around the campaign area. The building database includes 10019 buildings, where the minimum height is 43 m and the maximum height is 146 m. First, calibration of the propagation exponents was performed for ground level and all the different heights, separately. Calibration in WinProp is a standard procedure and it is performed automatically [13]. It calculates the Minimum Mean Squared Error (MMSE) of the difference between measurements and predictions. The scanner samples were converted from RSRP to signal power and further averaged over 5 m, to match with the 3D maps resolution.

We show in Table C.1 the 50%-ile value of the signal power distributions of measurements and predictions before and after calibration for the ground level case. For both cases, the models provide a better estimation of the signal

Table C.1: 50 %-ile of signal power distributions for measurements and predictions - DPM and IRT models before/after calibration

	Before Calibration	***After Calibration***
Measurements	-72.1	
DPM	-84.9	-72.1
IRT	-66.3	-72.2

Table C.2: Propagation exponents for DPM/IRT predictions

	Ground Level		**10 m, 15 m, 30 m**
	DPM	***IRT***	***DPM/IRT***
LOS exp.	2.6	2.8	2.2
OLOS exp.	2.7	2.9	2.4
LOS exp. after breakpoint	3.5	3	3.3
OLOS exp. after breakpoint	4	3	3.3

power after calibration.

Calibration was performed for both DPM and IRT models, and the results for both models were analysed before and after calibration. For IRT, we first ran predictions using the default WinProp values for ground level. As the difference between calibrated DPM and default WinProp IRT propagation exponents for the ground level case was minimum, we decided to use the calibrated DPM propagation exponents to run IRT predictions at different heights. Results after calibration improved slightly only for the ground level case, whereas for the different heights the results worsened. For this reason, IRT propagation exponents shown in Table C.2 are the calibrated values for ground level case only. For the different heights, the parameters used for IRT were the same as for DPM corresponding to the same height.

The factor for breakpoint distance determination was set to 2π as it is recommended in [13] for the urban case. The initial value for the breakpoint distance is calculated using the heights of the transmitter and receiver, and the wavelength [13]. The exponents after breakpoint distance were not determined during calibration for above ground, and therefore they were set to the default value set in the tool.

A summary of the overall standard deviation of the difference between measurements and predictions for the different heights after DPM calibration is presented in Table C.3. As it can be observed, the overall (including all transmitters) standard deviation of the difference between measurements and predictions is high compared to results in [11] even after calibration. To explain that, we present in Table C.4 a per transmitter analysis, where only some of the transmitters used for calibration of DPM at ground level are shown. The results in Table C.4 are obtained by subtracting, pixel by pixel, measurements to predictions for each transmitter independently. It can be noticed that, per transmitter, there is a considerable spread of the mean values, between -6.1 dB to +14.5 dB, which contributes to the overall high standard deviation of the difference. This will be further discussed in Section 4.

Table C.3: Std. dev. of the overall difference between measurements and predictions after calibration for the different heights

Height	# of transmitters used for calibration	Std. Dev. [dB]
Ground Level	14	10.62
10	16	12.96
15	17	11.66
30	28	8.03

Table C.4: Per-transmitter statistics of the difference between measurements and predictions @ Ground Level

Tramsmitter ID	Mean Value [dB]	Std. Dev. [dB]
A	3.5	6.5
B	10.7	7.8
C	-0.1	5.0
D	14.5	4.7
E	-11.5	5.7
F	5.5	5.1
G	-6.1	5.0

2.3 Shadow Fading Estimation

Once calibration was performed, we ran new predictions with the optimal propagation exponents. The results obtained from those predictions were used for the analysis presented in Section 3.

To analyse shadow fading, distance-dependency was removed from both measurements and predictions. The values were subsequently de-trended per transmitter prediction, so that only the variation in the local mean power level remained. Processed like this, the resulting values are therefore proportional to the shadowing in large-scale propagation.

To measure the accuracy of the predictions, we performed cross-correlation of time sequence samples between measurements and predictions. The cross-correlation coefficient, r_{y1y2}, used for this analysis is presented in Eq. (C.1), where c_{y1y2} represents the cross-covariance, defined in Eq. (C.2), of the time series $y1$ and $y2$, and $s1$ and $s2$ are the sample standard deviation of the time series $y1$ and $y2$, respectively, as it is shown in Eq. (C.3).

$$r_{y1y2} = \frac{c_{y1y2}(k)}{s_{y1}s_{y2}}; k = 0, \pm 1 \tag{C.1}$$

$$c_{y1y2}(k) = \frac{1}{T}\sum_{t=1}^{T-k}(y_{1,t} - \overline{y_1})(y_{2,t+k} - \overline{y_2}); k = 0, \pm 1 \quad \text{(C.2)}$$

$$s_i = \sqrt{c_{y_i y_i}(0)} = \sqrt{Var(y_i)} \quad \text{(C.3)}$$

The cross-correlation was performed for lags $k = 0, \pm 1$, where a lag corresponds to a pixel position (5 m). This was done to take into account that measurement positioning can be off by some meters, and therefore misalign samples in the comparison. For the results, the maximum value among the cases with $k = 0, \pm 1$ was chosen.

3 Results

3.1 Correlation Coefficients between measurements and predictions

The correlation analysis was applied per street and transmitter to get a measure for the accuracy in the prediction of the shadowing. We consider a prediction to be sufficiently accurate when the value obtained from cross-correlation in Eq. (C.1) is higher than 0.6. We present two examples of the measurements and predictions along a street in Figs. C.3 and C.4. For these cases, cross-correlation coefficients (CC) are 0.5457 and 0.8803, respectively. As it can be seen in Fig. C.3, with a correlation value close to the limit we established (0.6), shadow fading is well predicted since the strongest variations are seen in predictions as well as in measurements and the correlation is high in the first stretch of the street.

Figure C.5 shows the CDF of the correlation coefficients of the different combinations of street-transmitter for the whole set of measurement data, for both DPM and IRT. Results are presented for four different heights: ground level (1.5 m), 10 m, 15 m and 30 m. IRT performance is better than DPM in predicting the behaviour of the measurements, as the percentile of correlation coefficients above 0.6 is higher. Prediction accuracy in terms of correlation behaviour, deteriorates with height.

3.2 Shadowing distribution

Figure C.6 shows examples of the Shadow Fading (SF) distributions of both measurements and IRT predictions at ground level. They both adhere reasonably to the log-normal model with zero mean. The best-fit Gaussian is also shown for comparison. The standard deviation of the SF predictions (4.2 dB) is lower than for the measurements (6.2 dB). This is also the observation at

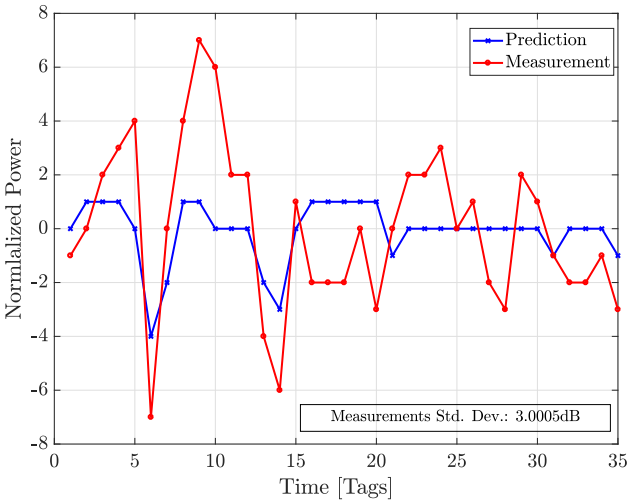

Fig. C.3: Example (I) of comparison of measurement and prediction along the route. CC = 0.5457.

increased height, as shown in Fig. C.7 where the mean SF standard deviation is shown versus height the different models analysed.

Fig. C.7 indicates that the mean standard deviation increases up to about the rooftop level, approx. at 10m, where after it decreases due to the radio path clearance [14]. The same trend is captured by the ray tracing predictions, and therefore seems to suggest that propagation paths in the transition zone at rooftop level, are more diverse and dynamic than below and above rooftop. While at ground level, the dominant paths are mostly "street-guided", and above rooftop level they are predominantly free-space, the high standard deviation at 10 m (i.e., transition zone) suggests that there might be overlapping of "street-guided", over-rooftop and free-space contributions.

4 Discussion

Two factors impact our results. Accurate predictions naturally require maps which are representative. We found inaccuracies in our 3D maps that suggest local changes in some parts of the city in the map areas considered with respect to real layout at the time of measurements. Inaccuracies were identified in four different locations within the map, and the worst case example is shown in Fig. C.8. At ground level, all the predictions with correlations lower than 0.6 have been proven to be close to areas where there are map inaccuracies. However, the same study is difficult to carry out for the dif-

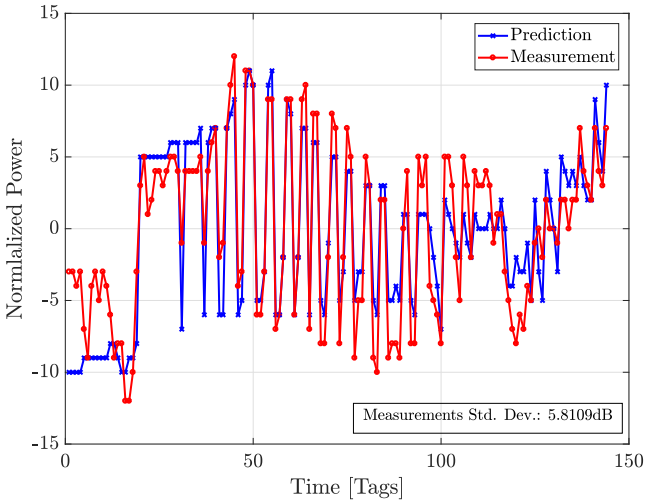

Fig. C.4: Example (II) of comparison of measurement and prediction along the route. CC = 0.8803.

ferent heights, as the transmitters observed by the drone are sometimes far away [6].

On the other hand, there is a limited accuracy on the building data bases [11]. The buildings are modelled as a polygonal cylinder of uniform height, where the rooftop shape is not being considered. This is surely affecting the above-rooftop predictions and explains why some of the transmitters present high mean value and standard deviation on the difference between measurements and predictions, as it is shown in Table C.4. For the same reason, shadowing variation is slightly lower for the predictions than for the measurements, but it can be seen in Figs. C.6 and C.7 that they follow the same trend.

Despite the maps inaccuracies, results show that predictions using IRT and DPM show about the same standard deviation versus height, but IRT is better in capturing the temporal dynamics of the SF process. The cost of using the IRT model is computation time, which is considerably higher than for DPM [11].

5 Conclusion

This paper studies, by comparing with field measurements, the feasibility of ray tracing predictions and models to accurately predict shadowing variations at different heights.

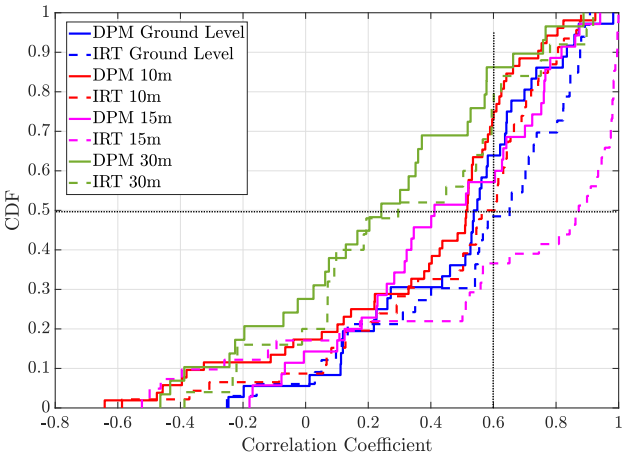

Fig. C.5: CDF of cross-correlation coefficients between measurements and predictions for all measurement locations and transmitters.

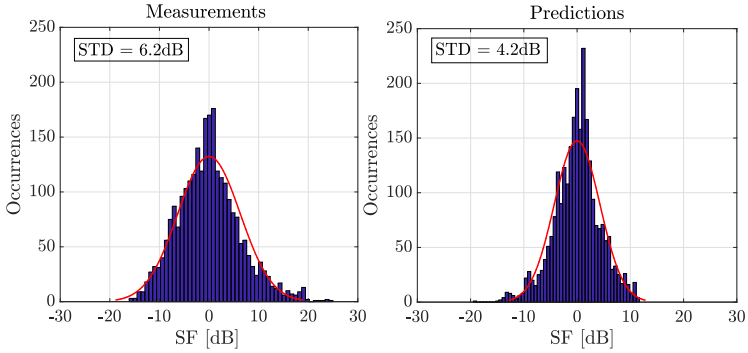

Fig. C.6: SF distribution for ground level measurements and IRT predictions.

From analysis and comparison of standard deviation and correlation properties, there is a good match between predictions and measurement data, the latter covering a set of different propagation conditions in an urban environment.

Overall, our study confirms that ray tracing tools can be used to obtain more empirical evidence and a better knowledge of the UAV radio channel, including shadow fading correlation properties, which play a key role in the mobility management algorithms, such as handover.

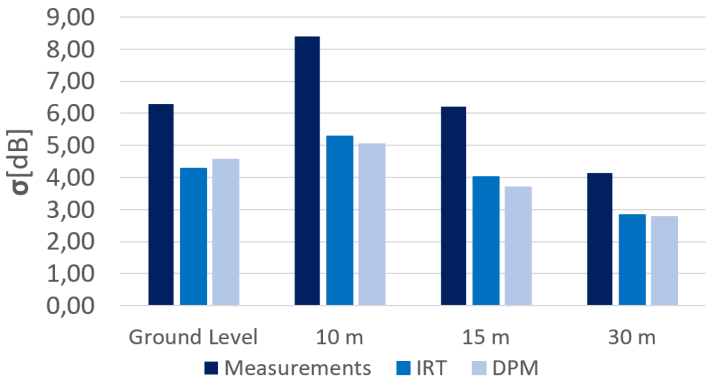

Fig. C.7: Average SF standard deviation values over all transmitter-street combinations.

Acknowledgment

This research has received funding from the SESAR Joint Undertaking under the European Union's Horizon 2020 research and innovation programme, grant agreement No 763601. The research is conducted as part of the DroC2om project.

References

[1] G. P. Fettweis, "The tactile internet: Applications and challenges," *IEEE Vehicular Technology Magazine*, vol. 9, no. 1, pp. 64–70, 2014.

[2] T. Doumi, M. F. Dolan, S. Tatesh, A. Casati, G. Tsirtsis, K. Anchan, and D. Flore, "LTE for public safety networks," *IEEE Communications Magazine*, vol. 51, no. 2, pp. 106–112, 2013.

[3] S. Mukherjee and C. Beard, "A framework for ultra-reliable low latency mission-critical communication," in *2017 Wireless Telecommunications Symposium (WTS)*. IEEE, 2017, pp. 1–5.

[4] R. Ferrus and O. Sallent, "Extending the LTE/LTE-A Business Case: Mission-and Business-Critical Mobile Broadband Communications," *IEEE Vehicular Technology Magazine*, vol. 9, no. 3, pp. 47–55, 2014.

[5] M. Mazur, A. Wisniewski, J. McMillan *et al.*, "Clarity from above: Pwc global report on the commercial applications of drone technology," *Warsaw: Drone Powered Solutions, PriceWater house Coopers*, 2016.

[6] R. Amorim, H. Nguyen, P. Mogensen, I. Z. Kovács, J. Wigard, and T. B. Sørensen, "Radio channel modeling for uav communication over cellular

Fig. C.8: Portion of the studied area: actual maps (top) and 3D database (bottom).

networks," *IEEE Wireless Communications Letters*, vol. 6, no. 4, pp. 514–517, 2017.

[7] I. Kovacs, R. Amorim, H. C. Nguyen, J. Wigard, and P. Mogensen, "Interference analysis for UAV connectivity over LTE using aerial radio measurements," in *2017 IEEE 86th Vehicular Technology Conference (VTC-Fall)*. IEEE, 2017, pp. 1–6.

[8] W. Khawaja, O. Ozdemir, and I. Guvenc, "Uav air-to-ground channel characterization for mmwave systems," in *2017 IEEE 86th Vehicular Technology Conference (VTC-Fall)*. IEEE, 2017, pp. 1–5.

[9] 3GPP, "Study on Enhanced LTE Support for Aerial Vehicles (Release 15)," Tech. Rep. 36.777 V0.3.1, Oct. 2017.

[10] Rohde & Schwarz, "R&S Test Equipment Information," 2020, https://www.rohde-schwarz.com/dk/products/, Last accessed on 2021-12-21.

[11] R. Wahl, G. Wölfle, P. Wertz, P. Wildbolz, and F. Landstorfer, "Dominant path prediction model for urban scenarios," *14th IST Mobile and Wireless Communications Summit, Dresden (Germany)*, 2005.

[12] R. Hoppe, G. Wolfle, and F. Landstorfer, "Accelerated ray optical propagation modeling for the planning of wireless communication networks," in *RAWCON 99. 1999 IEEE Radio and Wireless Conference (Cat. No. 99EX292)*. IEEE, 1999, pp. 159–162.

[13] Altair Hyperworks, "Winprop Manual," version 2018.1.2.

[14] B. Van der Bergh, A. Chiumento, and S. Pollin, "LTE in the sky: Trading off propagation benefits with interference costs for aerial nodes," *IEEE Communications Magazine*, vol. 54, no. 5, pp. 44–50, 2016.

Paper D

Service Outage Estimation for Unmanned Aerial Vehicles: A Measurement-Based Approach

Melisa López, Troels B. Sørensen, Jeroen Wigard, István Z. Kovács and Preben Mogensen

The paper has been accepted for publication in the
Wireless Communications and Networking Conference 2022.

The layout has been revised.

Abstract

One of the key enablers for the use of cellular networks to provide connectivity to UAV is reliability assurance. Estimating accurately the expected service availability and reliability that a UAV will experience along a planned route, helps to avoid critical situations. In this paper, we evaluate the use of a data-driven approach to estimate the expected serving signal level of a UAV planning to fly along a specific path. The estimation approach, presented in a previous study for the ground-level case, is based on the aggregation of measurements of UAV that have previously been flying along the same route. Using this approach we achieve an estimation error as low as 2.7 dB*. Based on the estimations we calculate the expected outage probability in terms of service availability and reliability and provide estimations of the expected critical areas along the route. Results show that 90 % of the availability and 65 % of the reliability critical areas in the route can be accurately estimated.*

1 Introduction

The market potential for commercial applications which make use of Unmanned Aerial Vehicles (UAV), or drones, is rapidly increasing [1]. Most of these applications require the operation of drones Beyond Visual Line-of-Sight (BVLOS). Ubiquitous cellular networks are considered to be one of the main candidates to provide this service. Strict regulatory requirements enforced in standardization [2] have led to extensive research efforts to ensure that the network can provide reliable communication between the drone and its controller.

The existing literature focuses on pointing out the challenges of UAV communications over cellular networks and proposing techniques to overcome them [3]. Studies such as [4] and [5] point out the key role of interference in the performance of UAV communications. Potential solutions such as beamforming, are shown to be a good candidate to improve service reliability in [6]. In [7] and [8], the authors present the benefits of using a dual-operator hybrid access scheme to avoid outages caused by latency. Although there are solutions to improve UAV communications, the use of them is mostly based on reactive schemes. It would be beneficial for the service if the network could foresee the critical situation and proactively act against it. The Aerial Connectivity Joint Activity (ACJA) initiative proposes in [9] a two-phase operational context for UAVs. In the planning phase, RF conditions for the planned path are estimated, and in the flight phase, real-time radio Key Performance Indicators (KPI) are monitored and used to estimate upcoming critical situations. Having beforehand information of a potential drop in the serving signal level or the Signal-To-Interference Ratio (SIR) could contribute to more efficient management of the network resources as well as

more reliable User Equipment (UE) mobility and experienced Quality of Service (QoS) [10]. The most basic approach to obtain this information is to estimate, as accurately as possible, the Reference Signal Received Power (RSRP) that a UE will experience along a route that it is planning to fly through. There are well-known methods to estimate the radio coverage based on empirical and deterministic models such as ray-tracing. However, the estimation accuracy provided by these methods is poor [11].

In this paper, we present an outage estimation method that provides the network with in-advance information on the expected service availability and reliability along a route that a UAV is planning to fly. First, we evaluate the performance of a data-driven approach for serving signal level estimation, which was previously presented in [12] for ground-level scenarios. The estimation is evaluated using real Long Term Evolution (LTE) measurements and consists of the aggregation of RSRP samples recorded by UEs that have previously passed through the same location, regardless of the cell that they are connected to (i.e. *pre-service* estimation). We show how the estimations can be further corrected using RSRP recorded by the UE during the flight phase (i.e. *on-service* estimation). Furthermore, we use the serving RSRP estimations to obtain the expected service availability and reliability. With this information, the network can proactively act against upcoming areas where the signal level or the SIR are likely to drop (*critical areas*).

The paper is organized as follows: in Section 2 we include the description of the UAV radio measurements. In Section 3 we briefly describe the estimation approach. Results and conclusions are included in Sections 4 and 5, respectively.

2 UAV Radio Measurements

To evaluate the performance of the data-driven estimation approach we performed field UAV measurements at 50 m height in a rural scenario nearby the city of Aalborg in Denmark. The measurement route, as depicted in Fig.D.1, covered the last 5 km of a 15 km path (from X to Y) that was previously measured at ground-level [12]. In total, we performed eight round-trips in the 5 km route. The radio environment is characterized by scattered buildings with average heights below 10 m and a terrain profile with variation below 7 m. The measurements, which were conducted in a sparsely coveraged LTE network, are in the 1800 MHz band. The average inter-site distance of 8.3 km, base station heights range from 20 m to 39 m and down-tilts between 3 and 6 degrees.

The measurements were recorded using four commercial smartphones (2 Samsung Galaxy S5 and 2 Samsung Galaxy S9) with the QualiPoc© test firmware [13]. All of them were mounted underneath a drone, with each of

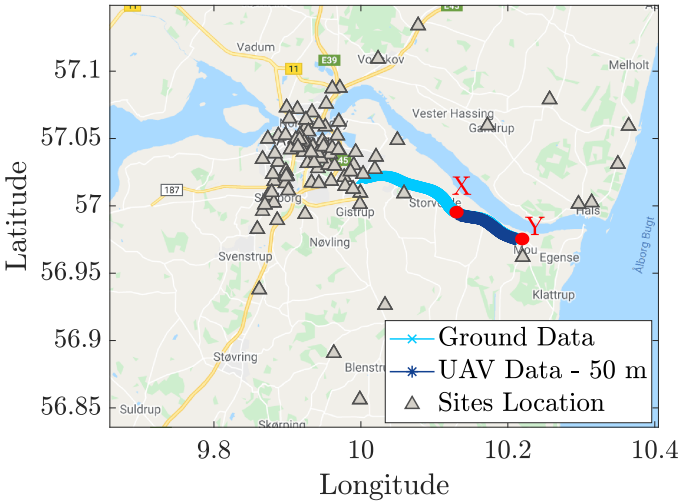

Fig. D.1: Measurement routes and LTE base station sites in Aalborg, Denmark. X and Y mark the beginning and end of the UAV route, respectively.

the UEs oriented towards one of the four main compass directions, as shown in Fig. D.2. The UEs recorded mainly the RSRP of the serving cell, and, in the case of the S5 model, also of the neighbors. An average number of 4 samples were recorded every 10 m.

3 Signal Level and Outage Estimations

The estimation approach used in this paper was previously presented in [12] for ground-level measurements. The serving RSRP values recorded by different UEs in a certain location are averaged (in dB scale) such that an estimation of the mean serving signal level that a UE is going to experience in that same location can be obtained. The estimation is location-based and should be valid for any UE regardless of the cell that it is connected to.

To evaluate this approach, the traces recorded by the UEs were organized along a 10-meter distance grid in $j = 1, ..., J$ segments. With a 5 km flight route, this led to a total of J = 500 segments. The mean value of all the measurements recorded by a UE in a certain grid segment j (4 samples on average, as mentioned in Section 2) is used as the RSRP value recorded by that UE in segment j ($RSRP_{i,seg_j}$ in dB).

For every segment, the mean (in dBm) of all the serving RSRP values recorded by all the different UEs is used as the estimated value in that segment, i.e. the estimation in segment j is defined as:

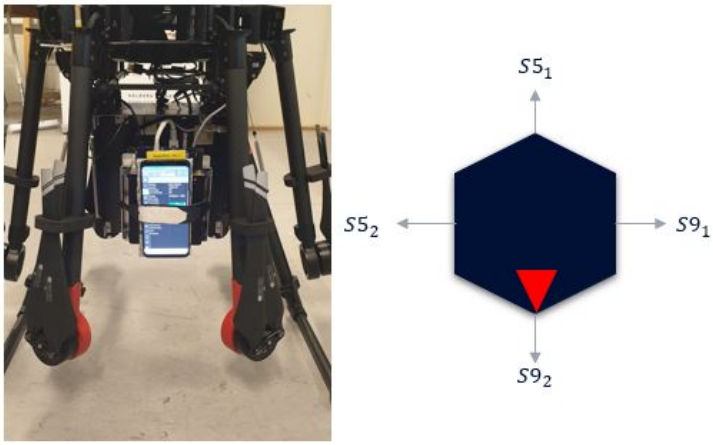

Fig. D.2: Measurement setup (left) - DJI Matrice 600 drone front picture with one of the QualiPoc smartphones visible and (right) orientation scheme of UE positions where the red arrow indicates the drone flight direction.

$$\widehat{RSRP_{seg_j}} = \frac{1}{N}\sum_{i=1}^{N} RSRP_{i,seg_j} \qquad \text{[dBm]} \quad \text{(D.1)}$$

The traces recorded by the UEs in opposite flying directions (X to Y and vice-versa) were considered as traces recorded by different UEs. With 4 measuring UEs and a total of 8 round-trips, the number of samples used to obtain the estimation in Eq. (D.1) equals N=32.

The precision of the signal level estimation is obtained by calculating, in each segment, the difference (in dB scale) between the estimation in that segment and each of the $N = 32$ actual recorded values. The distribution of this difference can be well approximated by a Gaussian distribution $\mathcal{N}(0, \sigma)$, where σ is the standard deviation of the estimation error (referred to as Δ).

3.1 Individual Offset Correction

To improve the performance of the estimation, we propose a method to correct the individual offset that a certain UE is observing with respect to the pre-service estimation in Eq. (D.1). To do this, we use real-time samples that the UAV is experiencing during the service (on-service estimation), as well as error distributions based on individual UEs that have previously passed through that same route. As for the aggregate distribution discussed above, the individual error distributions also have good approximation to a Gaussian with same standard deviation but different Mean Individual Offset (MIO) relative to the aggregate distribution mean. We use the z-test [14] as a

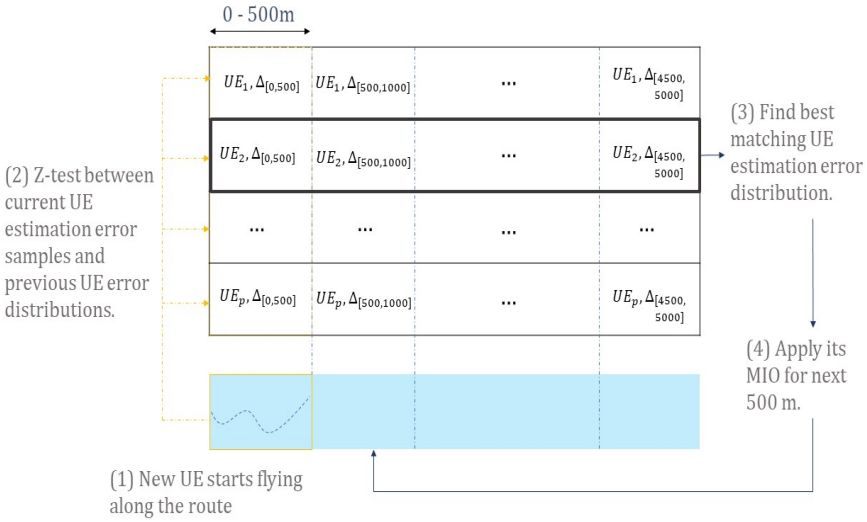

Fig. D.3: Mean individual offset correction procedure.

parametric hypothesis test to determine whether a set of samples is likely to come from one of the individual error distributions.

Compared to the ground-level study case, where the MIO was stable along the route [12] and only a few samples at the beginning of the route allowed for *full-route* MIO correction, we observed that in the UAV case there is a need for updating the correction as the UAV moves along the route. This difference is most likely due to the higher impact of the directional antenna patterns of the UEs in the air compared to the ground. At a 50 m height and with good Line-Of-Sight (LOS) conditions, the number of cells that the UEs can observe is higher than at 1.5 m. Therefore, UEs in the same location but with different orientations in the air have higher probability to be connected to different cells and observe different signal levels.

To compensate for the variation of the MIO along the route, we update the offset estimation every d_{upd} = 500 m (*sliding window* MIO correction). We show in Fig. D.3 the procedure for MIO correction, where the steps 1-4 indicate the order of the steps. When a UAV starts flying along the route (step 1), the samples observed within the first d_{upd} meters are tested against the stored distributions of each of the p UEs that have previously passed through that area (step 2).

The UE distribution with the highest p-value is selected (step 3) based on the z-test, and its MIO is used as a correction factor for the estimation in Eq.

(D.1) (step 4). The hypothesis is tested every d_{upd} meters and the offset is corrected based on the latest observed samples.

3.2 Service Outage Probability

Since an accurate estimation error is observed after correcting the MIO of a MIO, the serving RSRP estimations are further used to estimate the service availability and reliability that can be experienced along the route.

For *service availability*, we calculate the outage probability $P_{out,SA}$ that RSRP will drop below the availability threshold γ_{RSRP}. The probability is calculated as:

$$\begin{aligned} P_{out,SA} &= P(RSRP < \gamma_{RSRP} | \widehat{RSRP} = \widehat{RSRP}) \\ &= \Phi\left(\frac{\gamma_{RSRP} - \widehat{RSRP}}{\sigma}\right) \end{aligned} \tag{D.2}$$

Φ is the cumulative distribution function of the standard normal distribution and σ is the known standard deviation of that distribution. This equation follows from the observation that the estimation error distribution can be well approximated with a Gaussian.

For the *service reliability* estimations, we first estimate the SIR:

$$\widehat{SIR} = \frac{\hat{S}}{\hat{I}} = \frac{\widehat{RSRP_{SC}}}{\sum_{k=1}^{NC} \widehat{RSRP_k} \cdot \delta} \quad \text{[dB]} \tag{D.3}$$

$\widehat{RSRP_{SC}}$ is the serving cell signal level estimation, $\widehat{RSRP_k}$ the estimation of the $k = 1, ..., NC$ neighboring cells (NC = 5 strongest neighbors if available) and δ a fixed constant accounting for the impact of the traffic load.

The outage probability $P_{out,SR}$ that the SIR drops below a certain threshold γ_{SIR} is calculated following the same procedure from Eq. (D.2). Given the Gaussian shape of the estimation error, the linear value of the estimator $\widehat{RSRP}$ can be seen as a log-normal random variable with mean $\widehat{RSRP}$ and standard deviation σ. This is valid for both serving and interfering signals. The interference sum in the denominator of Eq. (D.3) will be approximately log-normal, as will the SIR ratio. Their statistics in the form of logarithmic mean and standard deviation can be calculated numerically by an extended version of the Schwarz & Yeh algorithm with account for correlated signals [15]. We calculate $P(SIR < \gamma_{SIR})$ assuming a correlation coefficient of 0.3 between the serving and interfering signals.

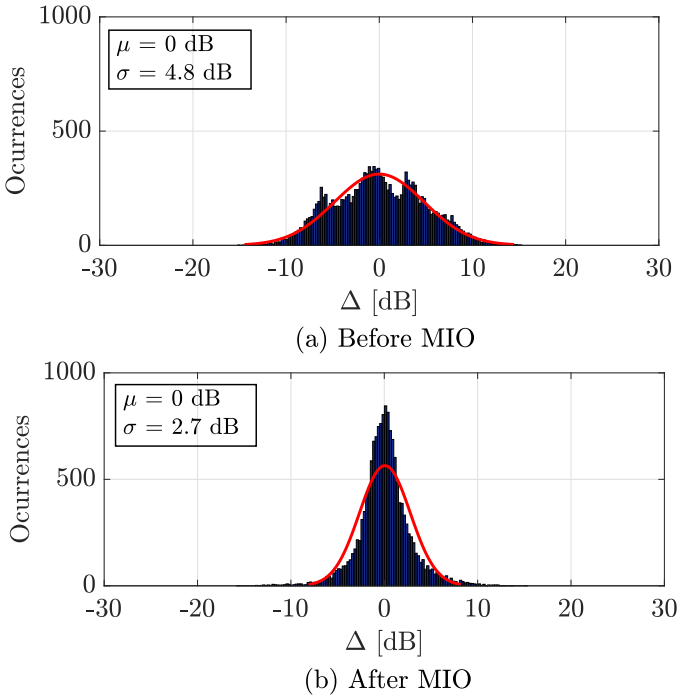

Fig. D.4: Data-driven approach estimation error Δ [dB] before (a) and after (b) MIO correction.

4 Results

We first show the results obtained for the serving RSRP estimations using the data-driven approach. We aggregate the samples of $N = 32$ UE traces recorded to obtain an estimation that, as shown in Fig. D.4a, presents an overall estimation error of 4.9 dB for the pre-service stage. We compare these results with the ones observed in the ground-level case in Table D.1. For reference, we also include the shadow fading values at area level. Since the estimations obtained with the data-driven approach are location-based, the estimation accuracy is below the shadow fading in the area. Due to the improved visibility conditions of the drone, and the lack of obstacles between the transmitter and the receiver, shadow fading for the UE (4.3 dB) is almost 3 dB lower than at ground-level (7.2 dB).

Results in [12] show an overall estimation error of 6.3 dB at ground-level. The fit in the UAV case is not so obvious as the error distribution seems to present multiple modes, which are most likely caused by the different signal levels experienced by UEs oriented towards different directions. This

Table D.1: Results Summary: Ground Level vs. UAV

	Ground Level	**UAV**
Data-Driven Δ [dB] *Before MIO Correction*	6.3	4.8
Data-Driven Δ [dB] *Full-route MIO Correction*	5.1	-
Data-Driven Δ [dB] *Sliding Window MIO Correction*	4.8	2.7
Shadow Fading [dB] *(Areal Level)*	7.2	4.3

leads to differences when correcting the MIO in the air. At ground-level, the stability of the offset for a specific UE oriented towards a certain direction allowed for the correction to be performed at the beginning of the route and be valid for the rest of it (*full-route* MIO correction). This method is not valid in the UAV case as the MIO of the whole route varies along the route and the samples observed for the z-test are not able to find a matching error distribution to the ones stored in the database (from UEs that have previously passed through the same route). Therefore, as explained in Section 3.1, MIO correction needs to be updated along the route. For the results presented here, $p = N * 0.75$, i.e. 25 % (eight) of the available traces were used for testing the correction approach, with eight random traces in every testing round until all of them were tested. Results in Fig. D.4b show that not only the standard deviation of the estimation error is reduced to 2.7 dB, but also the distribution is uni-modal and symmetric now that the offsets due to directivity have been removed. Although the distribution is clearly more peaked than a Gaussian, we keep that assumption for simplicity in the sequel. We also include in Table D.1 the results for *sliding window* MIO correction at ground-level. The difference when using the *full-route* correction is 0.3 dB (5.1 dB vs 4.8 dB). This indicates that the sliding window approach has a low impact as the error is stable along the whole route.

4.1 Service Outage Estimation

Achieving a high accuracy of 2.7 dB allows us to further use the serving RSRP estimations to estimate the expected service availability and reliability as per (D.2) and (D.3). Fig. D.6 shows the results for service availability when using γ_{RSRP} = -100 dBm. For reference, we include in Fig. D.5 the 32 serving RSRP traces recorded in the 5 km route along with the estimation and the threshold. In Fig. D.6a, we choose three example UEs pointing towards different directions (and with different MIOs) to show the effects of

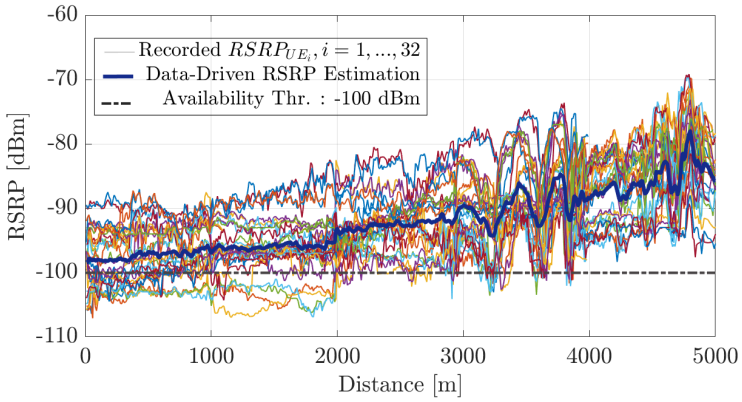

Fig. D.5: N = 32 recorded traces and data-driven serving RSRP estimation.

Table D.2: Accuracy of service availability and reliability outage areas estimation.

	TPR [%] (Hit Rate)	**TNR** [%] (Specificity)	**FNR** [%] (Miss Rate)	**FPR** [%] (Fall-Out)
Availability *Pre-service*	81.1	49.9	18.9	50.1
Availability *On-service*	88.4	76.6	11.6	23.4
Reliability *Pre-service*	68.8	71.5	31.2	28.5
Reliability *On-service*	66.9	76.8	33.1	23.2

MIO correction. As it can be seen, the corrected estimation traces in the on-service stage follow the trend of the actual ones better than the pre-service estimation. This is also observed in Fig. D.6b, where the outage probability for service availability is shown. If we choose UE A as a reference, we observe that the actual recorded RSRP level is below -100 dBm up to approximately two kilometers, in agreement with the estimated outage probability. For UE C, on the other hand, the actual trace is shown to be above the threshold along the whole route. Contrary to what was initially estimated in the pre-service stage, where almost half of the route would be declared critical, the on-service stage estimates a very low service availability outage probability for UE C.

To evaluate the performance of the outage probability estimations, we classify the segments into critical (true positive or critical area) and non-critical (true negative or non-critical area). We use True Positive Rate (TPR),

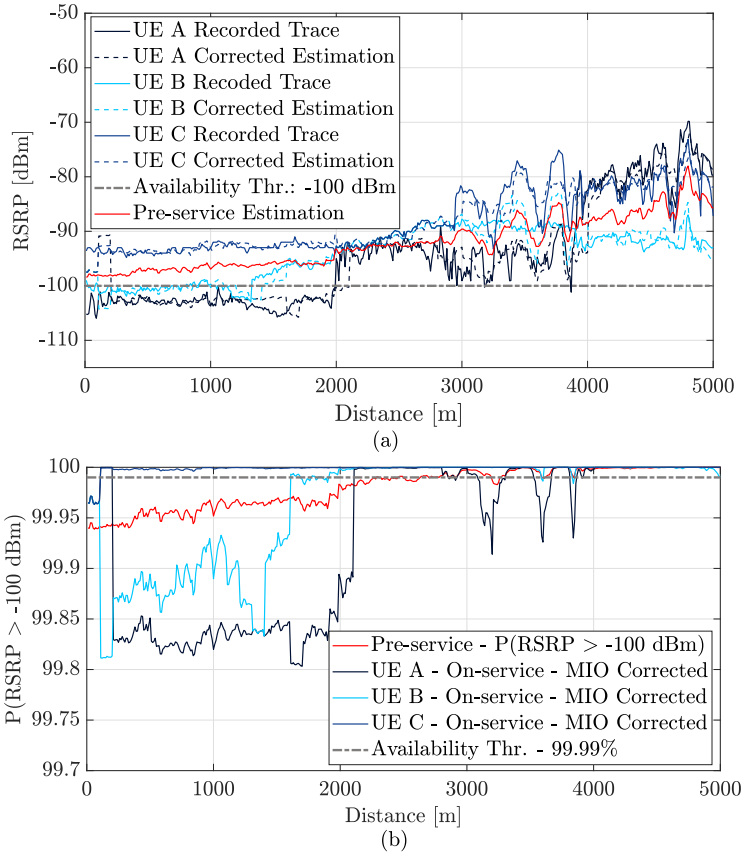

Fig. D.6: Service Availability: (a) real and estimated traces of three example UEs and (b) outage probability estimations based on pre-service and on-service estimations for the three example UEs.

True Negative Rate (TNR), False Negative Rate (FNR), and False Positive Rate (FPR) for evaluation, as these metrics are typically used for classification methods [16]. Other metrics such as accuracy and F1-score have not been included as they were considered to be misleading for the purpose of our evaluation due to the low number of critical areas (unbalanced dataset). Our main objective is to obtain the highest TPR possible, which indicates the number of positives that are correctly classified, i.e. the number of critical areas that are correctly estimated since both service availability and reliability outages would be very critical for UAV communication. However, we would also like to reduce as much as possible the FPR, i.e. the number of incorrectly classified critical areas (false alarms), since that may lead to inef-

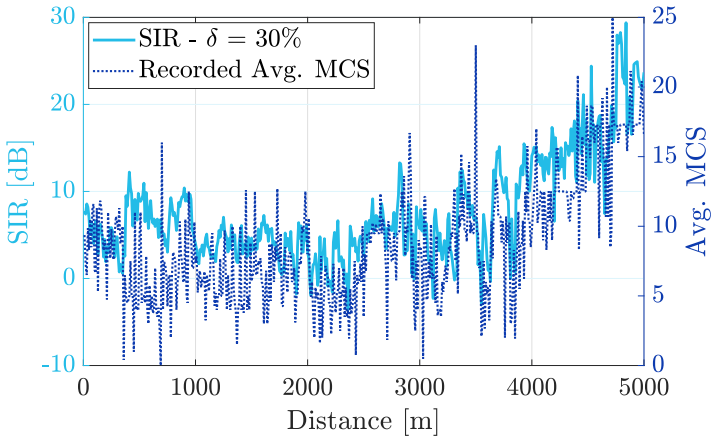

Fig. D.7: Comparison of estimated SIR with δ = 30% with the recorded Avg. Modulation and Coding Scheme (MCS) trends(example UE).

ficient resource management (e.g. unnecessary resource reservation). Results are shown in Table D.2. Service availability estimations show an 81 % TPR and a high FPR of 50 % in the pre-service stage. However, in the on-service stage, almost 90 % of the service availability critical areas can be estimated while observing only 20 % of false alarms. As observed in Fig. D.5, the number of samples dropping below the threshold is small (approximately 10 %) compared to the total number of samples

For the service reliability estimations we first calculate, following Eq. (D.3), the SIR for each of the 16 UE traces at which the strongest neighbors RSRP were also recorded (*S*5 smartphones). The SIR is calculated using an estimation of low, medium, and high load values (10 %, 30 %, and 60 %, respectively). Fig. D.8a shows the resulting SIR traces for δ = 30 % and the corresponding threshold γ_{SIR} = -3 dB. The SIR is obtained by estimating the same load for all neighboring cells. To show that this is a fair representation of the actual quality experienced by the UAV, we include Fig. D.7. We compare an example UE trace of the calculated SIR (with δ = 30 %) and the corresponding recorded average MCS which the is selected by the UE proportionally to the data channel SIR. As it can be observed, the trends observed in the average MCS trace are also followed by the calculated SIR. On that basis, we calculate the service reliability outage probability using the approach explained in Section 3.2. Results in Fig. D.8b show that the outage probability increases with the load in the network. It can also be observed how the δ = 30 % outage probability estimation matches best the SIR calculated traces in Fig. D.8a. As previously done for service availability, the performance of the estimations is shown using the classification metrics. Table D.2 shows that 69

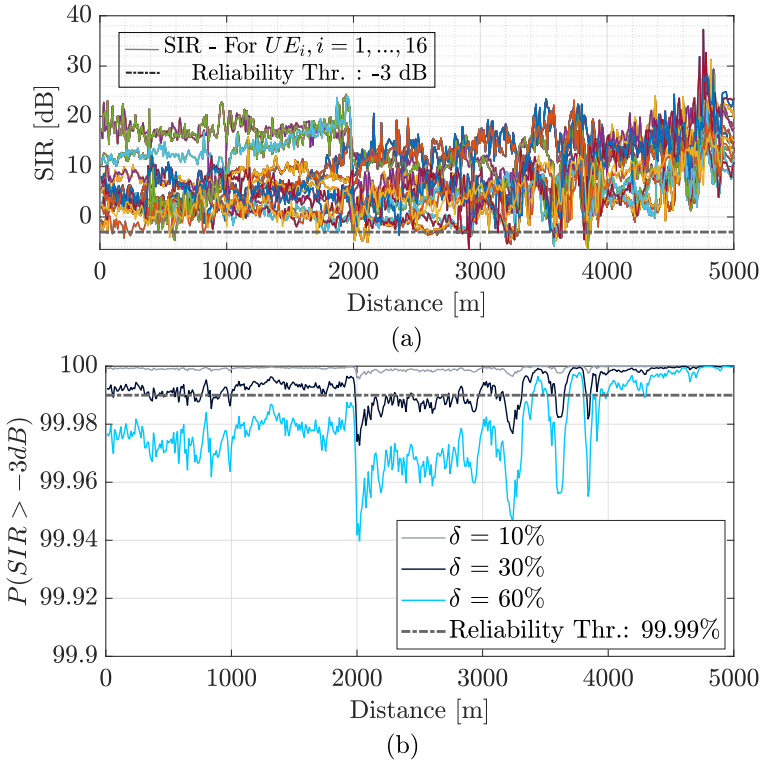

Fig. D.8: Service Reliability: (a) N = 16 SIR traces estimated based on actual values and (b) outage probability estimation based on pre-service estimation.

% of the critical areas are correctly estimated in the pre-service stage with an FPR of 28 %. The TPR slightly decreases to 67 % in the on-service stage, but so does the FPR to 23 %. The benefits of MIO correction are not so obvious for the service reliability estimations as the MIO correction is only performed for the serving cell. MIO correction was not possible for the neighbors due to the very different error distributions observed from previous UEs (high number of cells observed).

5 Discussion and Conclusions

The estimation results shown in Section 4 contribute to ensuring reliable communication between the UAV and its controller. Seen in the ACJA operational context to ensure reliable communication, the network can consider the pre-service estimations to decide whether the UAV can start the service or it

should re-plan the route. Furthermore, the on-service estimations can contribute to more proactive and seamless UE mobility and QoS management. Decisions such as activating dual connectivity or an interference mitigation technique can be made in advance, i.e., before the signal level or the quality of service is degraded.

In this paper, we discuss the use of a data-driven approach to estimate the expected serving signal level of a UAV along a planned path. The data-driven estimation consists of aggregating measurements from UEs that have previously passed through the same location. The method provides an overall accuracy of 4.9 dB.

The error can be further reduced to 2.7 dB by proactively correcting the MIO of the flying UAV with respect to the overall estimation. The correction is done using error distributions from previous UEs and updated based on observations of the most recent samples. The data-driven estimation approach and the MIO correction procedure require data from previous UEs to be available, limiting the use of these approaches.

With an accurate estimation of the serving RSRP, the network is able to calculate the expected service outage probability in terms of availability and reliability. The estimations show that almost 90 % of the expected critical areas along the route in terms of availability can be detected in advance, showing only 20 % of false alarms. For service reliability, the network would be able to detect almost 70 % of the critical areas, maintaining the fall-out rate below 25 %.

Acknowledgement

The authors would like to thank Telenor (Denmark) for supporting this work by sharing the network information. We would also like to express gratitude to Steffen Hansen, our drone pilot, and other colleagues at Aalborg University for the help provided during the measurement campaign.

References

[1] L. Godage, "Global unmanned aerial vehicle market (uav) industry analysis and forecast (2018–2026)," *Montana Ledger: Boston, MA, USA*, 2019.

[2] 3GPP, "Study on Enhanced LTE Support for Aerial Vehicles (Release 15)," Tech. Rep. 36.777 V0.3.1, Oct. 2017.

[3] A. Fotouhi, H. Qiang, M. Ding, M. Hassan, L. G. Giordano, A. Garcia-Rodriguez, and J. Yuan, "Survey on uav cellular communications: Practical aspects, standardization advancements, regulation, and security

challenges," *IEEE Communications Surveys & Tutorials*, vol. 21, no. 4, pp. 3417–3442, 2019.

[4] H. C. Nguyen, R. Amorim, J. Wigard, I. Z. Kovács, T. B. Sørensen, and P. E. Mogensen, "How to ensure reliable connectivity for aerial vehicles over cellular networks," *Ieee Access*, vol. 6, pp. 12 304–12 317, 2018.

[5] H. Marques, P. Marques, J. Ribeiro, T. Alves, and L. Pereira, "Experimental evaluation of cellular networks for uav operation and services," in *2019 IEEE 24th International Workshop on Computer Aided Modeling and Design of Communication Links and Networks (CAMAD)*. IEEE, 2019, pp. 1–6.

[6] T. Izydorczyk, M. Bucur, F. M. Tavares, G. Berardinelli, and P. Mogensen, "Experimental evaluation of multi-antenna receivers for uav communication in live lte networks," in *2018 IEEE Globecom Workshops (GC Wkshps)*. IEEE, 2018, pp. 1–6.

[7] R. Amorim, I. Z. Kovacs, J. Wigard, G. Pocovi, T. B. Sorensen, and P. Mogensen, "Improving drone's command and control link reliability through dual-network connectivity," in *2019 IEEE 89th Vehicular Technology Conference (VTC2019-Spring)*. IEEE, 2019, pp. 1–6.

[8] J. Güldenring, P. Gorczak, F. Eckermann, M. Patchou, J. Tiemann, F. Kurtz, and C. Wietfeld, "Reliable long-range multi-link communication for unmanned search and rescue aircraft systems in beyond visual line of sight operation," *Drones*, vol. 4, no. 2, p. 16, 2020.

[9] ACJA, GSMA and GUTMA, "Interface for Data Exchange between MNOs and the UTM Ecosystem: Network Coverage Service Definition, v1.00." Feb. 2021.

[10] N. Bui, "Prediction-based techniques for the optimization of mobile networks," 2017.

[11] J. Thrane, D. Zibar, and H. L. Christiansen, "Comparison of empirical and ray-tracing models for mobile communication systems at 2.6 ghz," in *2019 IEEE 90th Vehicular Technology Conference (VTC2019-Fall)*. IEEE, 2019, pp. 1–5.

[12] M. Lopéz, T. B. Sørensen, I. Z. Kovács, J. Wigard, and P. Mogensen, "Experimental evaluation of data-driven signal level estimation in cellular networks," in *2021 IEEE 94th Vehicular Technology Conference (VTC2021-Fall)*. IEEE, 2021, pp. 1–6.

[13] Rohde & Schwarz, "R&S Test Equipment Information," 2020, https://www.rohde-schwarz.com/dk/products/, Last accessed on 2021-12-21.

[14] L. J. Kitchens, *Basic Statistics and Data Analysis*. Thomson/Brooks/Cole, 2002.

[15] T. B. Sørensen, "Intelligent distributed antenna systems (idas): Assessment by measurement and simulation," 2002.

[16] M. Hossin and M. N. Sulaiman, "A review on evaluation metrics for data classification evaluations," *International journal of data mining & knowledge management process*, vol. 5, no. 2, p. 1, 2015.

ISSN (online): 2446-1628
ISBN (online): 978-87-7573-941-7

AALBORG UNIVERSITY PRESS